AN EXPERIMENTAL STUDY OF WING FLUTTER

A DISSERTATION
SUBMITTED TO THE FACULTY OF
UNIVERSITY OF MINNESOTA
BY

SALMAN AMSARI ALFIFI

IN PARTIAL FULFILLMENT OF THE REQUIREMENTS
FOR THE DEGREE OF
DOCTOR OF PHILOSOPHY

WILLIAM GARRARD

MAY 2017

Acknowledgements

First and foremost I offer my sincerest gratitude to my advisor, professor William Garrard, who has supported me throughout my thesis with his help, generous support, valuable suggestions and timely advice. He was always kind, understanding and sympathetic to me. One simply could not wish for a better or friendlier advisor.

Many thanks and appreciation to my committee members, Dr. Joseph Nichols, Dr. Ted Higman and Dr. Tom Shield, for their valuable help and advice.

I would like to thank the department lab engineer, Mr. Kale Hedstrom for his valuable advice and help in arranging the lab for my experiments throughout this work. My thanks to his assistant, Gabriel Dreisbach, for his great help and assistance in using the laser cutter.

My sincere and heartfelt appreciations are dedicated to my parents, my wife, my kids, my brother, sisters and all my relatives. My deep gratitude is towards my parents and wife, for their incessant prayers, moral support, guidance encouragement and patience during the course of my studies. They are the source of power, inspiration and confidence in me.

Dedication

This dissertation is dedicated to my beloved parents, wife, kids, brother and sisters

Abstract

While many experimental studies use springs to model the bending and torsional motions of a fluttered wing in wind tunnel experiments, the mass of the spring is often neglected in flutter calculation. In large test facilities, the spring mass is usually small compared to the mass of the wing. For smaller wind tunnels, however, the mass of the springs is larger relative to the mass of the test wing, and so perhaps should not be neglected.

The purpose of this dissertation is to determine the sensitivity of flutter measurements to non-negligible spring mass effects, and thereby qualify a source of uncertainty present in a wide range of flutter experiments reported in the literature.

For this purpose of research, two sets of experimental apparatus were designed and built to demonstrate classical two-degree of freedom flutter in open-return, low-speed wind tunnel in the Aerospace and Engineering Mechanics Department at university of Minnesota. In the first set-up, torsion and tension springs were used to provide the pitch and plunge motions, while in the second set-up, tension springs only were used. This apparatus was used to experimentally determine flutter speed for a range of supporting springs. Classical aerodynamic theory was used to calculate flutter speeds to determine how to model added mass due to supporting springs so as to make theory and experiment agree.

Table of Contents

List of Tables

List of Figures

NOMENCLATURE

c	chord length of airfoil (m)
b	half-length of chord (m)
L	wing span (m)
α	angle of attack (pitching motion) (radian)
t	time (s)
τ	dimensionless time
δ	downwash
S	firs moment of wing about elastic axis (kg.m)
Q_h	applied force (N)
Q_h	moment about the elastic axis (N.m)
m	wing mass (kg)
I_{CG}	mass moment of inertia about center of gravity (kg.m^2)
I_α	mass moment of inertia about elastic axis (kg.m^2)
d	distance between center of gravity and elastic axis (m)
h	distance in vertical motion (m)
k_h	tension spring constant that resists vertical motion (N/m)
k_α	torsion spring constant that resists pitching motion (N.m)
K_h	total tension spring constant (N/m)
K_α	total torsion spring constant (N.m)
ω	frequency (rad/s)
ω_h	uncoupled natural frequency of vertical motion (rad/s)

ω_α	uncoupled natural frequency of the pitching motion (rad/s)
X_{CG}	distance from leading edge to location of center of gravity (m)
X_e	distance from leading edge to location of elastic axis (m)
r_α	non-dimensional radius of gyration about elastic axis
μ	mass ratio between wing mass and mass of air around the wing
x_α	non-dimensional distance of the wing center of gravity aft of the elastic axis in semichords
a_h	non-dimensional distance from center of chord to elastic axis
g_h , g_α	damping coefficients
k	reduced frequency (non-dimensional)
ρ	density (kg/m^3)
$C(k)$	Theodorsen's Function
F	real part of Theodorsen's Function
G	imaginary part of Theodorsen's Function
Φ	Wagner's Function
H_0, H_1	Hänkel Functions
K_0, K_1	modified Bessel functions
U	flow velocity (m/s)
U_F	flutter speed (m/s)
ε	dummy variable
AC	aerodynamic center
CG	center of gravity

LE	leading edge
TE	trailing edge

CHAPTER 1

Introduction:

1.1 Fundamental Concept of Flutter

Flutter is a dangerous phenomenon encountered in flexible structures subjected to aerodynamic forces. Flutter can be encountered in aircraft, buildings, bridges, and even in smaller structures like street signs. Flutter can lead to structural fatigue and even catastrophic failure [1].

Flutter occurs in a structure because of interactions between aerodynamic, structural, and inertial forces as shown in figure 1.1 [2].

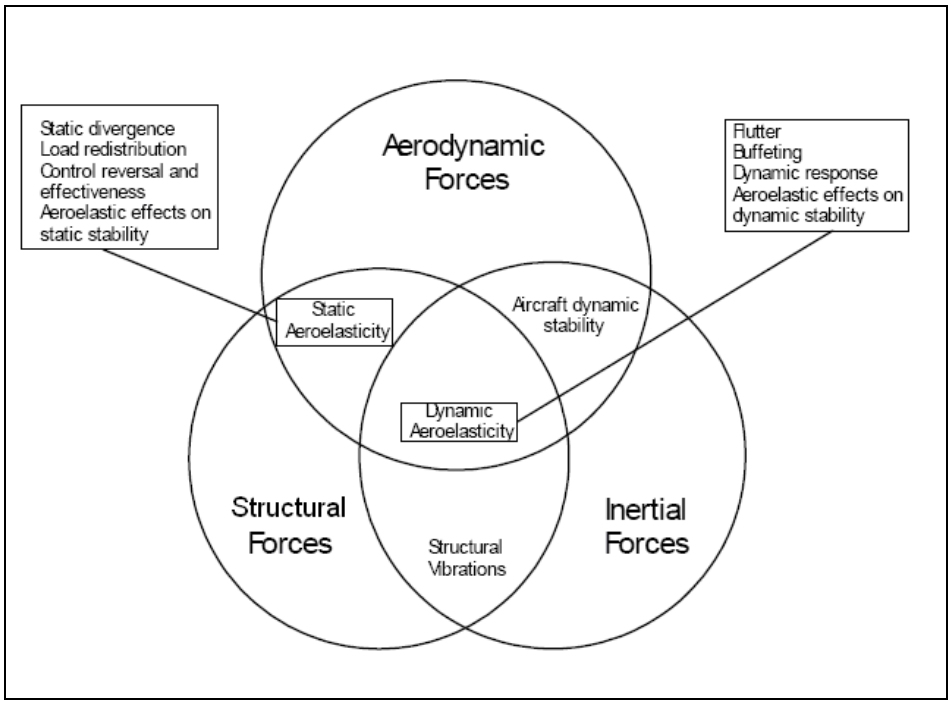

Figure 1.1 Interaction between aerodynamics, stiffness, and inertial forces (reproduced from ref. 2)

The most famous example of flutter occurred when the Tacoma Narrows Bridge was destroyed on November 7, 1940. At fairly constant wind speed and based on its aerodynamic design, the bridge began to flutter based on its aerodynamic and experienced violent, growing oscillations before collapsing.

Flutter is an aeroelasticity phenomenon whereby the inertia forces can modify the behavior of a flexible, stable system to an unstable system due to extracting energy from the incoming flow. When the airspeed is great enough, this results in complex interactions between aerodynamic, structural and inertial forces, leading to a continuous oscillation that can increase to the point where failure occurs [3].

In aircraft, flutter can create devastating damage to different components such as wings, flaps, ailerons, rudders, engine plates or any part that has the shape of an airfoil as shown in figure 1.2 [4]. All of these components must be tested under a wide range of flow conditions to ensure that flutter does not occur.

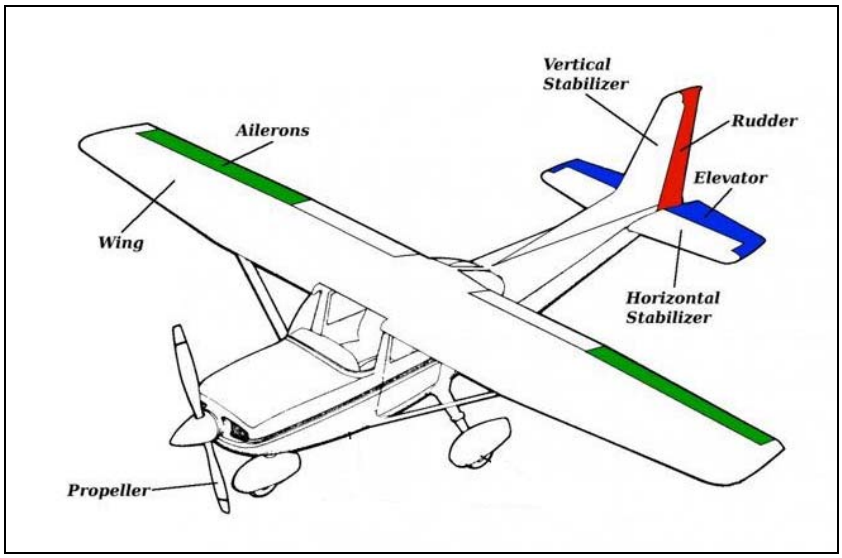

Figure 1.2 Aircraft control surfaces exposed to flutter

1.1.1 A physical explanation of wing flutter

In modern aircraft, wings are usually very flexible. When the aircraft is flying at cruise, the lift equals the weight of the aircraft, and each wing supports half the weight of the aircraft. Both wings are bent upwards. When wind speed increases suddenly, the aircraft is shaken, and the wings are flapped up and down due to inertia reaction. If the aircraft is not subjected to flutter, then the vertical vibration of the wings is damped out and does not amplify. However, if the wind has a frequency that matches the natural structural frequency of the wing, the wing would enter resonance and the up and down deflection of the wing would increase, amplify, and eventually lead to destruction of the wing.

In fact, when the wind speed increases suddenly as in the case of a wind gust, a change in the pressure around the wing occurs and causes the wing tip to move down, a vertical relative airflow hits the lower surface of the wing, increasing its angle of attack, increasing the upwards aerodynamic reaction, causing an extra lift on the wing tip. When the wing tip reaches its lowest point, the extra lift generated combined with the elasticity of the structure pushes the tip upwards. Now, a similar situation happens in the return journey, while the wing tip goes upwards, there is a downwards relative airflow on the tip which decreases the angle of attack of the wing tip, thus decreasing the lift. When the tip reaches its highest point, the lift is low or even directed downwards (negative lift). The wing is now pushed downwards again. If the frequency of the wind matches the natural

structural frequency of the wing, this process of motion would continue. In this case, aeroelastic flutter takes place.

1.1.2 Illustration of phasing for flutter

When a wing enters the mode of flutter, a phase shift between the bending and torsion motions occurs, the phase shift between the bending and torsion enables their corresponding lift components to extract energy from the incoming airflow. A simple illustration is shown in figure 1.3. In the upper plot, the motions of bending and torsion are in-phase with each other, and the maximum and minimum values of the resulting lift are 90^o out-of-phase, which means that the two lift components subtract each other, no flutter in this case. However, in the lower plot, the motions of bending and torsion are 90^o out-of-phase, and thus the maximum and minimum lift components are in-phase, which means that an extra lift is generated, flutter occurs in this case [5].

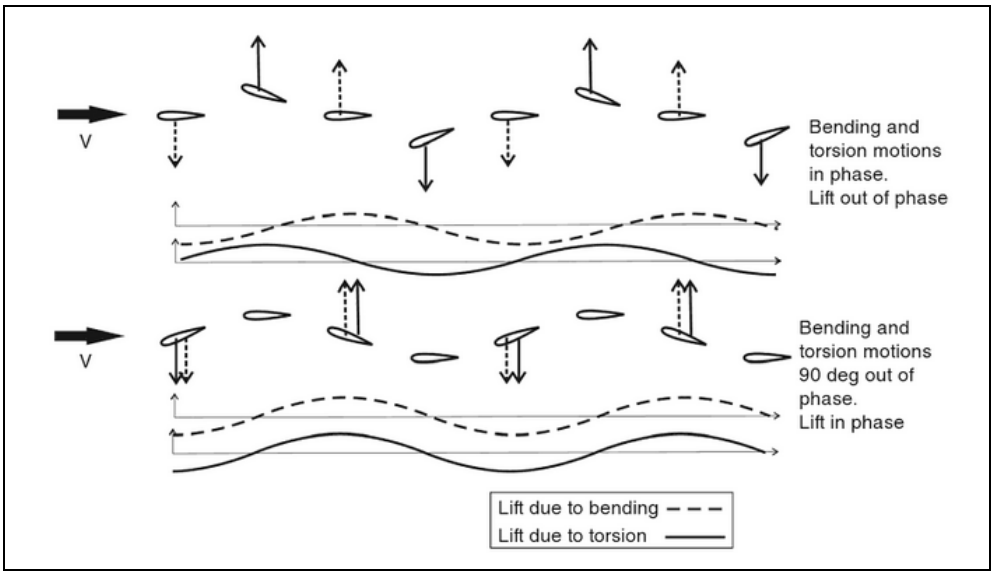

Figure 1.3 Lift due to bending and torsion components of the wing with different phasing between motions (reproduced from ref. 5)

1.2 Background

Aeroelasticity, and in particular flutter, has influenced the evolution of aircraft since the earliest days of flight. Research in flutter has been pursued in many countries. From a review of the historical facts, it is notable that the evolution of flutter has manifested itself in several lifting structures in the aircraft. The first documented flutter incident was in 1916 on a Handley Page O/400 bomber aircraft. The tail experienced a violent oscillation [6].

In the early years of aviation, flutter testing of full-scaled aircraft was not possible due to the lack of proper instrumentation. Only which the aircraft was flown to its maximum speed to ensure that the aircraft is free from flutter within the flight envelope was carried out [7].

The German von Schlippe was documented as the first person who carried out a flight-testing of flutter in 1935 [8]. In examining the historical progression of flutter research, substantial work and experimentation occurred from the years 1920 onward. Increased research has been done since then based on the recognition of the extent of the threats that the flutter posed to the aviation industry's success. From 1930-1940 was a period that was characterized by an increased development in flight-testing techniques as well as the development of flutter theory. At this time, two-dimensional flutter theory was developed and applied for unsteady aerodynamics. This is still extensively used today.

The basic flutter theory was devised by Theodore Theodorsen in 1934 [9]. After devising the flutter theory, it became possible to calculate flutter for airfoils and different wing-configuration. Theodorsen obtained a closed-form solution describing the dynamics of an oscillating airfoil-aileron combination mechanism with three degrees of freedom. Theodorsen used springs to represent the stiffness of the airfoil; he only considered the mass of the airfoil in his calculation, the springs mass was not included.

In 1937, the German scientist Voigt performed wind tunnel experiments to investigate torsional flutter on heavy and light weight wings using springs; the experimental flutter speed agreed well with the theoretical value computed; however, there was no matching in the case of light wings [10].

In 1940, Theodorsen and Garrick conducted large number of experiments using scale-model wing sections in the high-speed wind tunnel at the NACA Langley Memorial Aeronautical Laboratory. The purpose of these experiments was to verify the flutter theory and to study its adaptability to three-dimensional problems [11].

Despite there being increased advancements made in previous years for both experimental as well as theoretical techniques, numerous occurrences of flutter were being reported and this again substantiated the need for the development of means for flutter prevention. After 1940, as World War II drew closer, there were many new developments in aircraft capabilities and in aviation technology as the nations at war desired to have aircraft superiority [7]. The invention of jets, which could reach

supersonic speeds, was initiated and this led to the drive for more experimental and theoretical research in flutter.

In the following years, Theodorsen, Garrick, Fung [12] and others mainly worked simplification of the dynamic system mathematical model using linearizing assumptions, which provided good matching with the experiments [13].

More wind tunnel and flight test techniques for flutter were investigated numerical methods to simulate flutter using computers were developed. Some developments include instrumentation, excitation systems, control surfaces pulses, oscillating control surfaces, inertial exciters, thrusters, and aerodynamic vanes [14, 15, 16, 17, 18, 19, 20, 21, 22].

Moreover, much experimental work has been done from 1960 until today to investigate flutter on different aircraft models. In many experiments, the models were fixed inside test sections of wind tunnels or attached using supporting cables. This type of testing is not considered in this study. The focus and interest of this research is only to track the progression of work that has been done on wind tunnel experiments of wing flutter using tension springs.

Huttsell, Noll and Holsapple performed an experimental and analytical study to establish the flutter trends of a highly swept wing-tail configuration in the low supersonic regime [23]. Their model was tested in the Arnold Engineering Development Center (AEDC). The flutter occurred at Mach number of 1.2, analytical comparison agreed very well with the experimental flutter speed. A small spring was used to provide roll stiffness.

Fazle Ali [24] carried out experiments on NACA 0015 airfoil at the University of Minnesota wind tunnel to investigate the flutter speed and frequency. He used two torsion

springs and four tension springs to achieve flutter. He used Theodorsen's mathematical model to calculate the flutter speed and frequency to be compared with measured values. Ali did not include the tension springs mass in the calculation, there was an error difference up to 15.6% in flutter frequency and 6.6% in flutter speed.

In 1991, Jennifer Heeg carried out an analytical and experimental study on flutter suppression employing piezometric actuators. She used a 4-inch span wing model; the mount system provided the plunge and the pitch motion via springs. There was about 7.6% difference between the analytical and the measured values of flutter speed [25].

In 2010, Jieun Song, Seung Jin Song and Taehyoun Kim performed an experimental study to determine unsteady aerodynamic coefficients and flutter behavior of a rigid wing using a novel semi-experimental method [26]. The experiment was conducted in a low speed, subsonic wind tunnel at Seoul National University; springs were used to provide both the plunge and pitch motions. The spring mass was not included in the calculations. Good agreement between experiment and theory was achieved with this method; however, in some cases, 25% error in the flutter speed was noted as the reference speed was lowered.

In the above literature review, researchers did not include the mass of spring to their calculations when comparing calculations to the flutter experimental results. The purpose of this research is to focus on investigating the effect of spring mass on flutter speed.

There are two motions for fluttering wing, the vertical motion, which is called heave or plunge motion, and the rotational motion, which is called pitch motion. The pitch and plunge can be achieved by combination of torsion and tension springs as it exists in

typical flutter model case. We pursue this approach in the current investigation as well as pioneer an approach based only on tension springs.

Experiments in this research were conducted in open-return, low-speed wind tunnel in the Aerospace and Engineering Mechanics Department at the University of Minnesota. Speeds obtainable in this wind tunnel were low enough to require light-weight airfoils. The weight of the supporting springs was comparable to that of the airfoil and could not be ignored. The current study investigates in detail the effect of spring mass attached to the wing model in a flutter experiment. The outcomes from this study may be important in subsequent flutter research.

1.3 Objective of the Study and Problem Definition

While many experimental studies use springs to model the bending and torsional motions of a fluttered wing, the mass of the spring is often neglected. In large test facilities, the spring mass is usually small compared to the mass of the airfoil because large wing sections can be used. For smaller wind tunnels, however, the mass of the springs is larger relative to the mass of the test wing, and so perhaps should not be neglected.

The purpose of this dissertation is to determine the sensitivity of flutter measurements and calculations to non-negligible spring mass effects, and thereby qualify a source of uncertainty present in a wide range of flutter experiments reported in the literature.

Determining the effect of spring mass on flutter speed became a primary concern after finding a hypothesis in vibration claiming that mass of spring is not trivial component to the attached body and has to be included in the calculation [27]. A standard approach for including the mass of springs is as follows:

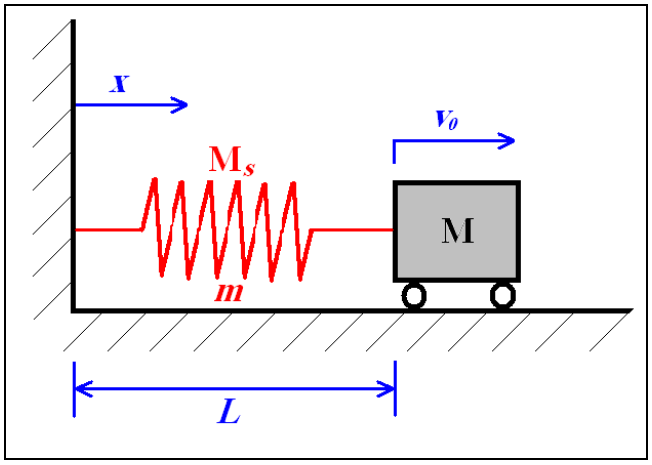

Figure 1.4 Diagram of body mass attached to a spring

Where v_0 is the velocity of the body mass, M is the mass of the body, m is the mass per unit length of the spring, M_s is the mass of the spring ($M_s = m\ L$) and k_s is the spring constant.

Assuming that the spring has a linear velocity profile as illustrated in figure 1.5

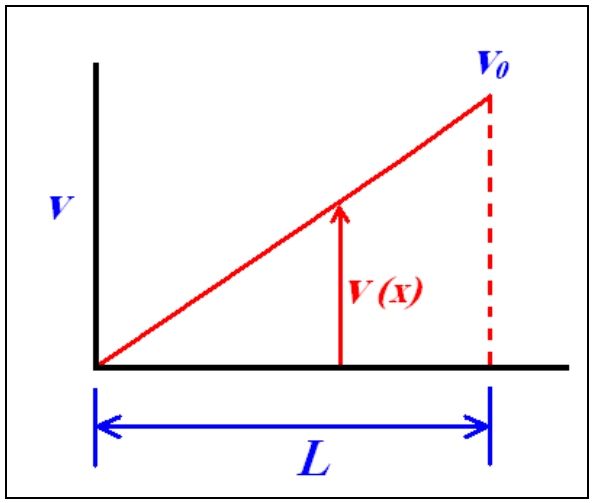

Figure 1.5 Velocity profile of the spring

$$v(x) = v_0 \frac{x}{L} \tag{1.1}$$

Then the kinetic energy at a section of spring loaded at x with a length of dx is:

$$dT_s = \frac{1}{2} m v^2\, dx \tag{1.2}$$

Substituting equation (1.1) into equation (1.2), we get:

$$dT_s = \frac{1}{2} m \left(v_0 \frac{x}{L} \right)^2 dx \tag{1.3}$$

$$dT_s = \frac{1}{2} m \frac{{v_0}^2}{L^2} x^2 \, dx \tag{1.4}$$

The total kinetic energy of the spring, T_s, is:

$$T_s = \int_0^L dT_s = \int_0^L \frac{1}{2} m \frac{{v_0}^2}{L^2} x^2 \, dx \tag{1.5}$$

$$T_s = \frac{1}{2} m \frac{{v_0}^2}{L^2} \int_0^L x^2 \, dx = \frac{1}{2} m \frac{{v_0}^2}{L^2} \left[\frac{x^3}{3} \right]_0^L$$

$$T_s = \frac{1}{2} m \frac{{v_0}^2}{L^2} \left[\frac{L^3}{3} \right]$$

$$T_s = \frac{1}{2} \frac{m}{3} {v_0}^2 L \tag{1.6}$$

Substituting the value of spring mass ($M_s = m\,L$) into equation 1.6, we get:

$$T_s = \frac{1}{2} \left(\frac{M_s}{3} \right) {v_0}^2 \tag{1.7}$$

The total kinetic energy of the system is:

$$T_{total} = T_M + T_s \tag{1.8}$$

$$T_M = \frac{1}{2} M v_0^2 \tag{1.9}$$

Substituting equation (1.7) and equation (1.9) into equation (1.8), we get:

$$T_{total} = \frac{1}{2} M v_0^2 + \frac{1}{2} \left(\frac{M_s}{3} \right) v_0{}^2$$

Thus, it can be concluded that total kinetic energy is:

$$T_{total} = \frac{1}{2} \left(M + \frac{M_s}{3} \right) v_0{}^2 \tag{1.10}$$

Therefore, one third of the mass of the spring should be included in the mass of the system.

Subsequently, the work of this thesis is devoted to examining the effect of spring mass on flutter speed. This is achieved by determining experimentally the flutter speed of a wing inside the wind tunnel for different sets of tension springs with different spring constants and masses. In parallel with the experimental work, the solution of Theodorsen mathematical model is carried out for different cases, the experimental results are compared with calculated values from the Theodorsen solution.

1.4 Organization of Dissertation

Chapter 2 discusses in detail the flutter theory devised by Theodorsen, providing the solution method for finding the flutter speed and frequency of an airfoil.

Chapter 3 provides complete description of experimental set-up and procedure. The description includes the first and second experimental set-ups, describing the manufacturing process and apparatus used. Finally, the mechanism of the experimental procedure for both set-ups is illustrated.

Chapter 4 presents the experimental results of the first experimental set-up, including the Theodorsen solution. Comparison is made between the experimental results of this set-up and Theodorsen solution. Finally, the results are discussed.

Chapter 5 presents the experimental results of the second experimental set-up, including the Theodorsen solution. Comparison is made between the experimental results of this set-up and Theodorsen solution. Finally, the results are discussed.

Chapter 6 is the summary. It includes the conclusions from this study and the contributions this investigation makes to the current understanding of flutter. Finally, directions and recommendations are made for future work.

CHAPTER 2

Theoretical Determination of Flutter Speed Using Theodorsen Approach

Theodore Theodorsen laid the theoretical foundations of flutter analysis by developing a mathematical model in 1935. He made two major assumptions in his approach, the first assumption was that the wing is a flat plate and the second was that of potential flow such that the flow is always attached and the wake is flat. The model is based on elementary solutions of the Laplace equation.

$$\nabla^2 \phi = 0 \tag{2.1}$$

Where ϕ is the velocity potential. Such solutions are the free stream, the source and the sink, the vortex and the doublet. Theodorsen modeled the wing as a circle that can be mapped onto a flat plate though a conformal transformation. He pointed out the singularities as follows:

- The flow has a free stream speed *U* and zero angle of attack.
- Double strength of source (+2σ) on the top surface, balanced by a double strength of source (-2σ) on the lower surface
- A pattern of vortices +ΔΓ on the flat plate, balanced by opposite vortices +ΔΓ on the wake.

After transformation from the circle to a flat plat using Joukowski's conformal transformation, the flow field, which includes the wing and wake, was complete. With the resulting flow field and the assumptions noted at the beginning of this chapter, the

total vorticity is always zero. Theodorsen was able to calculate a closed-form solution that includes the effect of the wake. This solution is called the Theodorsen's Function. Details can be found in his paper [9] and in appendix F.

The equations of motions of a wing in a flow motion are determined in the next section based on Theodorsen approach in which the wing is considered as a flat plate.

2.1 Equations of Motion

Let us consider a typical section of a two-dimensional flat plate airfoil in figure 2.1.

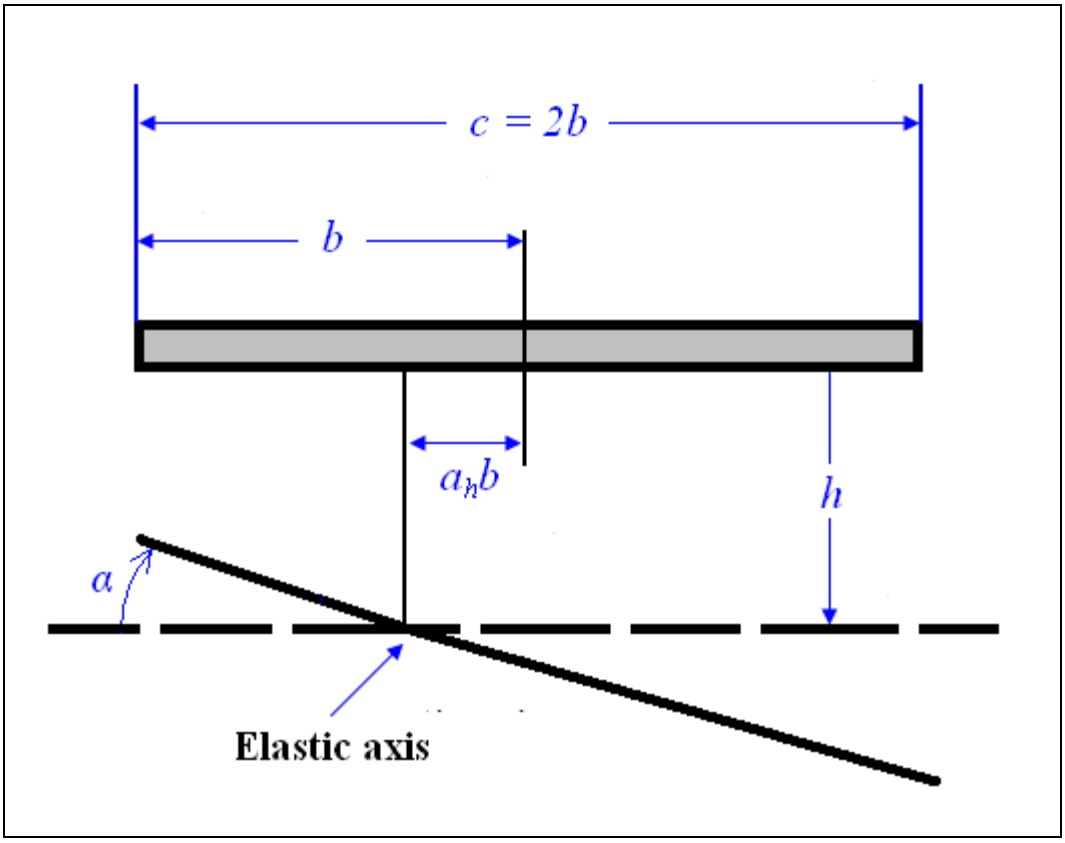

Figure 2.1 Notations of a two-dimensional flat plate airfoil

The positive nose up angle of attack is α, the downward vertical displacement is h and U is the speed of free stream flow.

The equations of motion can be written according to the condition that sum of the inertia and elastic forces and moments must balance the externally applied forces and moments. If Q_h is the applied force and Q_α is the resultant moment about the elastic axis, which includes the aerodynamic forces and other mechanical excitations, then the equations of motion are [12]:

$$m\ddot{h} + S\ddot{\alpha} + k_h h = Q_h \tag{2.2}$$

$$S\ddot{h} + I_\alpha \ddot{\alpha} + k_\alpha \alpha = Q_\alpha \tag{2.3}$$

Where m is the mass of the wing, S is the first moment of the wing about the elastic axis, I_α is the mass moment of inertia about the elastic axis, k_h is the tension spring constant that resists the vertical motion, k_α is the torsion spring constant that resists the pitching motion.

These equations can be written slightly in a different way by expressing the spring constants in terms of frequencies. If the airfoil is considered to be restrained that only one degree of freedom, say h, is permitted, assuming further that no external force is applied, then equation (2.2) becomes:

$$m\ddot{h} + k_h h = 0 \quad , \qquad \text{for } (\alpha = 0 \text{ and } Q_h = 0) \tag{2.4}$$

$$\frac{k_h}{m} = -\frac{\ddot{h}}{h}$$, leading to:

$$\frac{k_h}{m} = \omega_h^2$$

$$\omega_h = \sqrt{\frac{k_h}{m}} \tag{2.5}$$

ω_h represents the uncoupled natural frequency of the vertical motion.

Hence, we may write

$$k_h = m\,\omega_h^2 \tag{2.6}$$

Similarly, if the airfoil is considered to be restrained that only one degree of freedom, say α this time, is permitted, assuming further that no external moments are applied, then equation (2.3) becomes:

$$I_\alpha \ddot{\alpha} + k_\alpha\,\alpha = 0 \ , \qquad \text{for } (h = 0 \text{ and } Q_\alpha = 0) \tag{2.7}$$

$$\frac{k_\alpha}{I_\alpha} = -\frac{\ddot{\alpha}}{\alpha}$$, leading to:

$$\frac{k_\alpha}{I_\alpha} = \omega_\alpha^2$$

$$\omega_\alpha = \sqrt{\frac{k_\alpha}{I_\alpha}} \tag{2.8}$$

ω_α represents the uncoupled natural frequency of the pitching motion.

Hence, we may write

$$k_\alpha = I_\alpha\,\omega_\alpha^2 \tag{2.9}$$

2.2 Aerodynamic Forces

Let us evaluate the aerodynamic forces acting on a two-dimensional airfoil in an incompressible flow.

The chord of the airfoil is *2b* (*c = 2b*) and the angle of attack is α. As shown in figure 2.2, let us consider the growth of circulation about the airfoil that impulsively accelerates to a velocity *U* from rest [24].

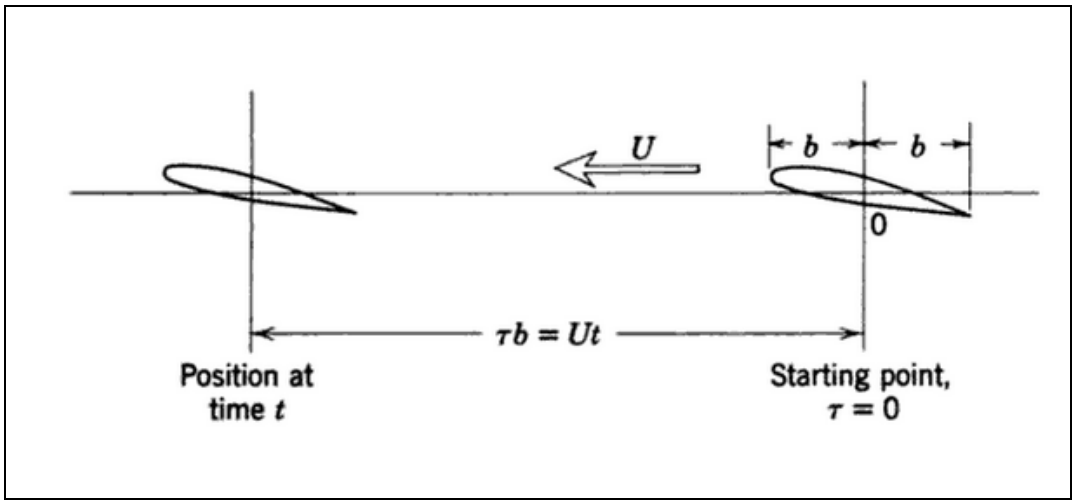

Figure 2.2 Impulsive motion of an airfoil, (reproduced from ref. 24)

If $\tau = 0$ is the time at which the motion is initiated, then the downwash on the airfoil is $\delta = U \sin(\alpha) = U_\alpha$, since the flow is tangential to the airfoil. Let us derive the lift due to the circulation on a strip of unit span assuming that the velocity at the trailing edge is finite (Kutta condition), i.e.

$$L_1(\tau) = 2\pi b \rho U \delta \Phi(\tau), \quad \Phi(\tau) = 0 \text{ if } \tau < 0 \tag{2.10}$$

$$\tau = \frac{U t}{b} \tag{2.11}$$

Where τ is a non-dimensional time

The function $\Phi(\tau)$ is called Wagner's function [28], and is shown in figure 2.3.

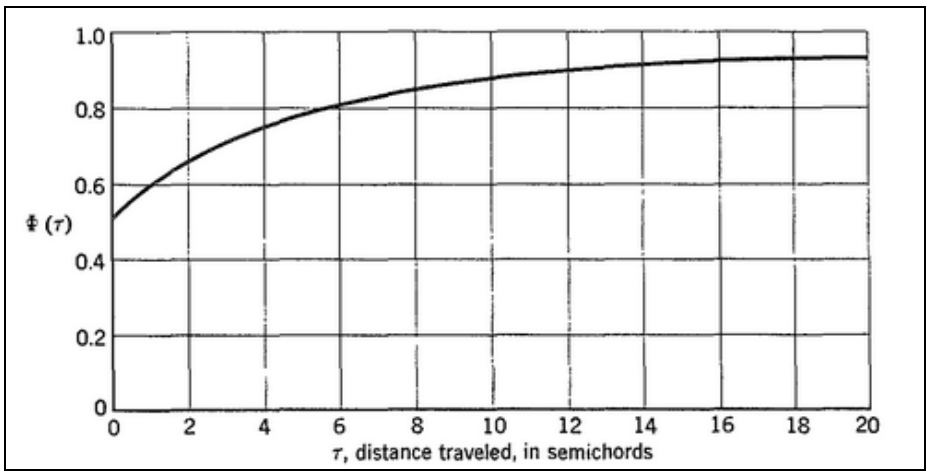

Figure 2.3 Wagner's function for an impulsively started airfoil in an incompressible fluid (reproduced from ref. 12)

The exact form of $\Phi(\tau)$ is:

$$\Phi(\tau) = 1 - \int_0^\infty \left[(K_0 - K_1)^2 + \pi^2 (I_0 - I_1)^2 \right]^{-1} e^{-x\tau} x^{-2} \, dx \tag{2.12}$$

The modified Bessel functions of the second and first kind are the terms K_0, K_1, I_0 and I_1 respectively [12].

For a general motion having the two degrees of freedom h and α, the downwash over the airfoil is not uniform. There is a uniform downwash corresponding to the pitch angle α.

$$\delta_2 = U\sin(\alpha) = U\alpha \tag{2.13}$$

The pitch angle is assumed small so that the sine can be approximated by the angle.

The vertical translation h creates a uniform downwash which written as:

$$\delta_2 = \frac{dh}{d\tau} \bullet \frac{d\tau}{dt} = \frac{Uh'}{b} \tag{2.14}$$

The prime notation denotes differentiation with respect to non-dimensional time (τ) and the dot is with respect to time (t).

There is also a non-uniform downwash due to $\dot{\alpha}$, it is written as:

$$\delta_3 = \left(\frac{1}{2} - a_h\right) b \frac{d\alpha}{dt} = \left(\frac{1}{2} - a_h\right) U\alpha' \tag{2.15}$$

Thus, combining the three components of downwash, we obtain

$$\delta = U\alpha\ (\tau) + \frac{Uh'}{b}\ (\tau) + \left(\frac{1}{2} - a_h\right) U\alpha'\ (\tau) \tag{2.16}$$

When δ remains small, the superposition principle is used to find the circulatory lift per unit span (L_1).

$$L_1(\tau) = 2\pi b \rho U \int_{-\infty}^{\tau} \Phi(\tau - \tau_0) \frac{d\delta}{d\tau_0}(\tau_0) d\tau_0 \tag{2.17}$$

Combining equation (2.17) with equation (2.16), we get:

$$L_1(\tau)=2\pi b\rho U^2\int_{-\infty}^{\tau}\Phi(\tau-\tau_0)\left[\alpha'(\tau_0)+\frac{1}{b}h''(\tau_0)+\left(\frac{1}{2}-a_h\right)\alpha''(\tau_0)\right]d\tau_0 \qquad (2.18)$$

The non-circulatory lift and moment must be added when the airfoil has a general motion. There is a lift force with center of pressure at the mid-chord (L_2), it is equal to the apparent air mass ($\rho\pi b^2$) times the vertical acceleration at the mid-chord point.

$$L_2=\rho\pi b^2\left(\ddot{h}-a_h b\ddot{\alpha}\right)=\rho\pi U^2\left(h''-a_h b\alpha''\right) \qquad (2.19)$$

There is another lift force with center of pressure at 3/4-chord point (L_3), it is equal to the apparent mass ($\rho\pi b^2$) times $\left(U\dot{\alpha}\right)$.

$$L_3=\rho\pi b^2 U\dot{\alpha}=\rho\pi bU^2\alpha' \qquad (2.20)$$

There is a nose-down couple moment (M_α), that is equal to the apparent moment of inertia [$\rho\pi b^2$ ($b^2/8$)] times the angular acceleration $\left(\ddot{\alpha}\right)$.

$$M_\alpha=-\frac{\rho\pi b^4\ddot{\alpha}}{8}=-\frac{\rho\pi b^2U^2}{8}\alpha'' \qquad (2.21)$$

Thus, the total aerodynamic lift and moment per unit span about the elastic axis induced by h and α are:

$$L = L_1+L_2+L_3 \qquad (2.22)$$

$$M=\left(\frac{1}{2}+a_h\right)bL_1+a_h bL_2-\left(\frac{1}{2}-a_h\right)bL_3+M_\alpha \qquad (2.23)$$

Substituting terms in equations (2.22) and (2.23), we obtain:

$$L = 2\pi b \rho U^2 \int_{-\infty}^{\tau} \Phi(\tau - \tau_0) \left[\alpha'(\tau_0) + \frac{1}{b} h''(\tau_0) + \left(\frac{1}{2} - a_h \right) \alpha''(\tau_0) \right] d\tau_0$$
$$+ \rho\pi U^2 \left(h'' - a_h b \alpha'' \right) \tag{2.24}$$
$$+ \rho\pi b U^2 \alpha'$$

$$M = \left(\frac{1}{2} + a_h \right) 2\pi b^2 \rho U^2 \int_{-\infty}^{\tau} \Phi(\tau - \tau_0) \left[\alpha'(\tau_0) + \frac{1}{b} h''(\tau_0) + \left(\frac{1}{2} - a_h \right) \alpha''(\tau_0) \right] d\tau_0$$
$$+ a_h b \rho\pi U^2 \left(h'' - a_h b \alpha'' \right) \tag{2.25}$$
$$- \left(\frac{1}{2} - a_h \right) \rho\pi b^2 U^2 \alpha' - \frac{\rho \pi b^2 U^2}{8} \alpha''$$

Let $P(\tau)$ denote an imaginary applied external force (positive downward) and $Q(\tau)$ an imaginary applied external moment (positive nose up). The equations of motion (2.2) and (2.3) become:

$$m \frac{U^2}{b^2} h'' + S \frac{U^2}{b^2} \alpha'' + m \omega_h^2 h = -L(\tau) + P(\tau) \tag{2.26}$$

$$S \frac{U^2}{b^2} h'' + I_\alpha \frac{U^2}{b^2} \alpha'' + I_\alpha \omega_\alpha^2 \alpha = M(\tau) + Q(\tau) \tag{2.27}$$

Equations (2.26) and (2.27) can be solved by the method of Laplace transformation. However, the steady-state forced oscillation due to a periodic excitation is used here [12]. In this case, the integrals in equation (2.25) can be evaluated explicitly.

2.3 Forced Oscillation

For a two-dimensional airfoil under a harmonic exciting force, the external force and moment per unit span are:

$$P = P_0 e^{i\omega t} \tag{2.28}$$

$$Q = Q_0 e^{i\omega t} \tag{2.29}$$

Where P_0 and Q_0 are complex constants.

The resulting steady state bending and pitching responses are:

$$h = h_0 e^{i\omega t} \tag{2.30}$$

$$\alpha = \alpha_0 e^{i\omega t} \tag{2.31}$$

Since the response has reached a steady state, the motion of the airfoil must be of the same period as the exciting force. h_0 and α_0 are complex constants and their absolute value represent the amplitude of oscillation.

Since $\tau = \frac{U}{b} t$, the equations (2.28), (2.29),(2.30) and (2.31) can be written as:

$$P(\tau) = P_0 e^{ik\tau} \tag{2.32}$$

$$Q(\tau) = Q_0 e^{ik\tau} \tag{2.33}$$

$$h(\tau) = h_0 e^{ik\tau} \tag{2.34}$$

$$\alpha(\tau) = \alpha_0 e^{ik\tau} \tag{2.35}$$

Where k is a non-dimensional number called the reduced frequency.

$$k = \frac{\omega b}{U} \tag{2.36}$$

To avoid the mathematical difficulties in evaluating the integrals at (-∞) in equations (2.24) and (2.25), a convergence factor ($e^{\varepsilon\tau_0}$, ε > 0) is introduced into the integrand and pass the limit (ε → 0) through positive real values.

Let us write:

$$\lim_{\varepsilon\to 0+} ik \int_{-\infty}^{\tau} \Phi(\tau-\tau_0) e^{ik\tau_0+\varepsilon\tau_0}\, d\tau_0 = C(k) e^{ik\tau} \tag{2.37}$$

Therefore, the integrals in equations (2.24) and (2.25) can be evaluated as:

$$\begin{aligned}\lim_{\varepsilon\to 0+} \int_{-\infty}^{\tau} \Phi(\tau-\tau_0)\left[\alpha'(\tau_0)+\frac{1}{b}h''(\tau_0)+\left(\frac{1}{2}-a_h\right)\alpha''(\tau_0)\right] e^{\varepsilon\tau_0}\, d\tau_0 \\ = C(k)\left[\alpha_0+\frac{i}{b}k\,h_0+\left(\frac{1}{2}-a_h\right)ik\alpha_0\right] e^{ik\tau}\end{aligned} \tag{2.38}$$

The complex function $C(k)$ is called Theodorsen's function.

$$C(k) = F(k) + i\,G(k) \tag{2.39}$$

F and G are the standard notations for the real and imaginary parts of $C(k)$ respectively. F and G are tabulated in table 2.1 and shown in figure 2.4.

The exact expression of the Theodorsen's function is:

$$\begin{aligned}C(k) = F(k) + i\,G(k) &= \frac{H_1^{(2)}(k)}{H_1^{(2)}(k) + i\,H_0^{(2)}(k)} \\ &= \frac{K_1(ik)}{K_0(ik) + i\,K_1(ik)}\end{aligned} \tag{2.40}$$

Where H_0, H_1 are Hänkel functions and K_0, K_1 are modified Bessel functions

Approximate expressions for Theodorsen's function are provided by (R. T. Jones) and (W. P. Jones) in equations (2.41) and (2.42).

$$C(k) = 1 - \frac{0.165}{1 - \frac{0.0455}{k} i} - \frac{0.335}{1 - \frac{0.3}{k} i} \tag{2.41}$$

$$C(k) = 1 - \frac{0.165}{1 - \frac{0.041}{k} i} - \frac{0.335}{1 - \frac{0.32}{k} i} \tag{2.42}$$

Table 2.1 Theodorsen's function and related quantities (reproduced from ref. 12)

k	$1/k$	F	$-G$	$-2G/k$	$2F/k^2$
∞	0.000	0.5000	0	0	0
10.00	0.100	0.5006	0.0124	0.00248	0.010012
6.00	0.16667	0.5017	0.0206	0.00686	0.02787
4.00	0.250	0.5037	0.0305	0.01525	0.06296
3.00	0.33333	0.5063	0.0400	0.02667	0.1125
2.00	0.500	0.5129	0.0577	0.0577	0.2565
1.50	0.66667	0.5210	0.0736	0.0948	0.4631
1.20	0.83333	0.5300	0.0877	0.1462	0.7361
1.00	1.000	0.5394	0.1003	0.2006	1.0788
0.80	1.250	0.5541	0.1165	0.2912	1.7316
0.66	1.51516	0.5699	0.1308	0.3964	2.6166
0.60	1.66667	0.5788	0.1378	0.4593	3.2156
0.56	1.78572	0.5857	0.1428	0.5100	3.7353
0.50	2.000	0.5979	0.1507	0.6028	4.7832
0.44	2.27273	0.6130	0.1592	0.7236	6.3326
0.40	2.500	0.6250	0.1650	0.8250	7.8125
0.34	2.94118	0.6469	0.1738	1.022	11.192
0.30	3.33333	0.6650	0.1793	1.195	14.778
0.24	4.16667	0.6989	0.1862	1.552	24.267
0.20	5.000	0.7276	0.1886	1.886	36.380
0.16	6.250	0.7628	0.1876	2.345	59.592
0.12	8.33333	0.8063	0.1801	3.002	111.99
0.10	10.000	0.8320	0.1723	3.446	166.4
0.08	12.500	0.8604	0.1604	4.010	268.9
0.06	16.66667	0.8920	0.1426	4.753	495.6
0.05	20.000	0.9090	0.1305	5.220	727.2
0.04	25.000	0.9267	0.1160	5.800	1158.3
0.025	40.000	0.9545	0.0872	6.976	3054.4
0.01	100.000	0.9824	0.0482	9.640	19648
0	∞	1.000	0	∞	∞

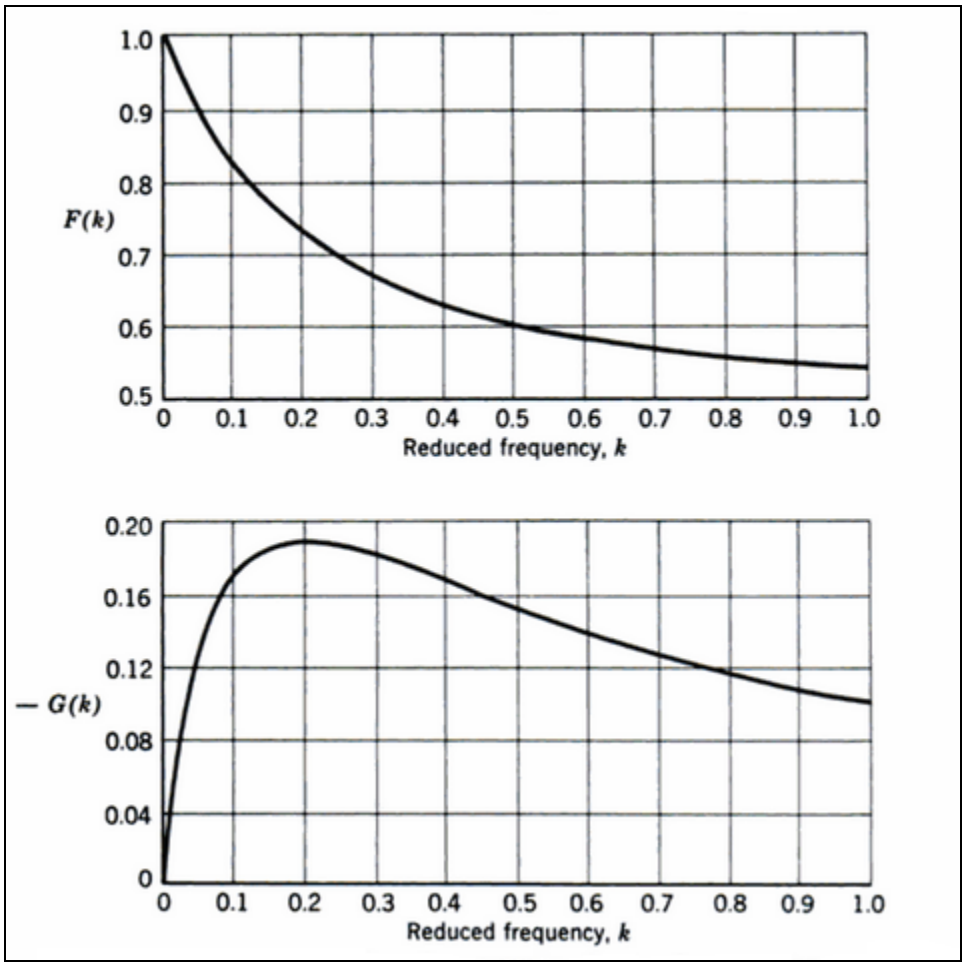

Figure 2.4 The real and imaginary part of Theodorsen's function $F(k)$ and $G(k)$ (reproduced from ref. 12)

Let us introduce three dimensionless coefficients:

- The non-dimensional radius of gyration about the elastic axis (r_α)

$$r_\alpha = \sqrt{\frac{I_\alpha}{m\,b^2}} \tag{2.43}$$

- The non-dimensional mass (μ), μ is the mass ratio between the wing mass and the mass of the air around the wing

$$\mu = \frac{m}{\pi\,\rho_{air}\,b^2\,L}, \text{ } L \text{ is the wing span} \tag{2.44}$$

- The non-dimensional distance of the wing center of gravity aft of the elastic axis in semichords (x_α), it is positive if the location of the elastic axis is in front of the location of center of gravity.

$$x_\alpha = \frac{S}{mb} = \frac{m\left(X_{CG} - X_e\right)}{m\,b} = \frac{2\,d}{c} \tag{2.45}$$

Figure 2.5 provides an illustration of these non-dimensional coefficients.

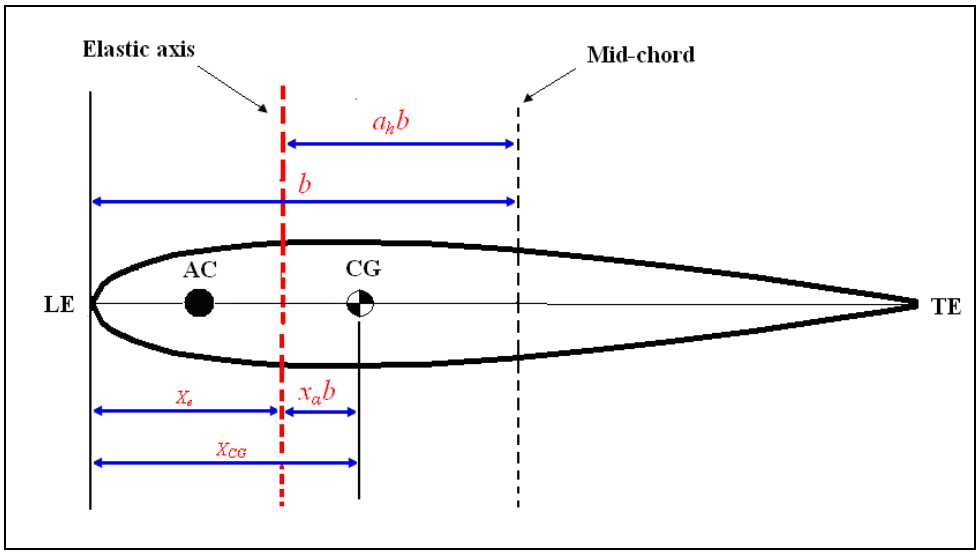

Figure 2.5 Illustration of the non-dimensional coefficients

First we substitute equations (2.32), (2.33), (2.34), (2.35) and (2.38) into equations (2.24) and (2.25). Then we divide equation (2.26) by ($\pi\rho b^3\omega^2$) and equation (2.27) by ($\pi\rho b^4\omega^2$), and omitting the time factor ($e^{ik\tau}$), we get:

$$\begin{aligned} &-\mu\frac{h_0}{b}-\mu x_\alpha\alpha_0+\mu\frac{\omega_h^2}{\omega^2}\frac{h_0}{b}-\frac{h_0}{b}+a_h\alpha_0+\frac{i}{k}\alpha_0 \\ &+2\frac{C(k)}{k^2}\left[\alpha_0+ik\frac{h_0}{b}+\left(\frac{1}{2}-a_h\right)ik\alpha_0\right]=\frac{P_0}{\rho\pi b^3\omega^2} \end{aligned} \tag{2.46}$$

$$\begin{aligned} &-\mu x_\alpha\frac{h_0}{b}-\mu r_\alpha^2\alpha_0+\mu r_\alpha^2\frac{\omega_\alpha^2}{\omega^2}\alpha_0-\frac{h_0}{b}+a_h\left(\frac{h_0}{b}-a_h\alpha_0\right)+i\left(\frac{1}{2}-a_h\right)\frac{1}{k}\alpha_0 \\ &-\frac{1}{8}\alpha_0-\left(\frac{1}{2}+a_h\right)+2\frac{C(k)}{k^2}\left[\alpha_0+ik\frac{h_0}{b}+\left(\frac{1}{2}-a_h\right)ik\alpha_0\right]=\frac{Q_0}{\rho\pi b^4\omega^2} \end{aligned} \tag{2.47}$$

In the above equations, we may wish to include structural damping, which is generally small in aircraft structures. We can assume that the energy dissipation varies with the square of the amplitude of oscillation [12]. Thus, there is a shift of phase angle of the restoring elastic force resulting in a damping force ($- ig_h k_h h_0 e^{ik\tau}$), where

g_h is the damping coefficient.

When:

$$p_0 = \frac{P_0}{\rho \pi b^3 \omega^2} \tag{2.48}$$

$$q_0 = \frac{Q_0}{\rho \pi b^4 \omega^2} \tag{2.49}$$

Equations (2.46) and (2.47) take the form

$$A\frac{h_0}{b} + B\alpha_0 = p_0 \tag{2.50}$$

$$D\frac{h_0}{b} + E\alpha_0 = q_0 \tag{2.51}$$

Where the modifications for the structural damping was made by replacing the restoring force terms ($k_h\ h$) and ($k_\alpha\ \alpha$) by the terms of the form [$k_h\ h\ (1+ig_h)$], [$k_\alpha\ \alpha\ (1+ig_\alpha)$], and equivalently ($\omega_h^2$) and ($\omega_\alpha^2$) are replaced by [$\omega_h^2\ (1+ig_h)$], [$\omega_\alpha^2\ (1+ig_\alpha)$] respectively.

The coefficients A, B, D, and E are therefore functions of k, g_h, g_α, U and ω.

Let us take k and ω as fundamental parameters and let

$$\frac{\omega_\alpha^2}{\omega^2} = x \tag{2.52}$$

Then the coefficients may be written as:

$$A = A_R + iA_I + (1 + ig_h)\,\mu\frac{\omega_h^2}{\omega_\alpha^2}x \tag{2.53}$$

$$B = B_R + iB_I \tag{2.54}$$

$$D = D_R + iD_I \tag{2.55}$$

$$E = E_R + iE_I + (1 + ig_\alpha)\,\mu r_\alpha^2\,x \tag{2.56}$$

Where:

$$A_R = -(\mu + 1) - \frac{2G}{k} \tag{2.57}$$

$$A_I = \frac{2F}{k} \tag{2.58}$$

$$B_R = -(\mu x_\alpha - a_h) + \frac{2F}{k^2} - \left(\frac{1}{2} - a_h\right)\frac{2G}{k} \tag{2.59}$$

$$B_I = \frac{1}{k}\left[1 + \frac{2G}{k} + \left(\frac{1}{2} - a_h\right)2F\right] \tag{2.60}$$

$$D_R = -(\mu x_\alpha - a_h) + \left(\frac{1}{2} + a_h\right)\frac{2G}{k} \tag{2.61}$$

$$D_I = -\left(\frac{1}{2} + a_h\right)\frac{2F}{k} \tag{2.62}$$

$$E_R = -\left(\mu r_\alpha^2 + a_h^2 + \frac{1}{8}\right) + \left(\frac{1}{4} - a_h^2\right)\frac{2G}{k} - \left(\frac{1}{2} + a_h\right)\frac{2F}{k^2} \tag{2.63}$$

$$E_I = \frac{1}{k}\left[\left(\frac{1}{2} - a_h\right) - \left(\frac{1}{2} + a_h\right)\frac{2G}{k} - \left(\frac{1}{4} - a_h^2\right)2F\right] \tag{2.64}$$

The solution of equations (2.50) and (2.51) can be written as:

$$\frac{h_0}{b} = \frac{1}{\Delta}\begin{vmatrix} p_0 & B \\ q_0 & E \end{vmatrix} \tag{2.65}$$

$$\alpha_0 = \frac{1}{\Delta}\begin{vmatrix} A & p_0 \\ D & q_0 \end{vmatrix} \tag{2.66}$$

Where:

$$\Delta = \frac{1}{\Delta}\begin{vmatrix} A & D \\ B & E \end{vmatrix} = \Delta_R + i\Delta_I \tag{2.67}$$

Δ_R and Δ_I are the real and imaginary parts of the determinant Δ. From equations (2.53), (2.54), (2.55) and (2.56), we obtain:

$$\begin{aligned} \Delta_R = {} & \left(1 - g_h g_\alpha\right)\mu^2 r_\alpha^2 \frac{\omega_h^2}{\omega_\alpha^2} x^2 \\ & + \left[\mu \frac{\omega_h^2}{\omega_\alpha^2}\left(E_R - g_h E_I\right) + \mu r_\alpha^2\left(A_R - g_\alpha A_I\right)\right] x \\ & + A_R E_R - B_R D_R - A_I E_I + B_I D_I \end{aligned} \tag{2.68}$$

$$\begin{aligned} \Delta_I = {} & \left(g_h + g_\alpha\right)\mu^2 r_\alpha^2 \frac{\omega_h^2}{\omega_\alpha^2} x^2 \\ & + \left[\mu \frac{\omega_h^2}{\omega_\alpha^2}\left(g_h E_R + E_I\right) + \mu r_\alpha^2\left(A_I + g_\alpha A_R\right)\right] x \\ & + A_I E_R - B_R D_I + A_R E_I - B_I D_R \end{aligned} \tag{2.69}$$

If P_0 and Q_0 are zero for non-forced oscillations, by Cramer's rule, the determinant is equal to zero:

$$\Delta = \Delta_R + i\,\Delta_I = 0 + i\,0$$

2.4 Steps of Solution for Flutter Determinant Using Theodorsen Function

To calculate the flutter speed and frequency, we have to solve the characteristic equation ($\Delta = 0$) for the real variables U and ω. Both the real and imaginary parts of (Δ) vanish, i.e.

$$\Delta_R = 0, \qquad \Delta_I = 0$$

The solution can be achieved in steps as follows:

The first step is to find all quantities needed to evaluate the determinant coefficients A, B, D, E, A_R, A_I, B_R, B_I, D_R, D_I, E_R and E_I. This is achieved as in the following sequence of steps:

1- The wing data are given, the mass (m), the chord length (c) and the span (L)

2- The springs data are given, the spring constant (k_h or k_α), the mass, the dimension (length and diameter)

3- Calculating the location of center of gravity (x_{CG})

4- Calculating the mass moment of inertia about the center of gravity (I_{CG})

5- Determining the location of elastic axis (x_e)

6- Evaluating the distance between the locations of elastic axis and the center of gravity (d)

7- Calculating the mass moment of inertia about the elastic axis (I_α)

8- Calculating the non-dimensional radius of gyration (r_α)

9- Calculating the non-dimensional mass (μ)

10- Calculating the non-dimensional distance of wing center of gravity aft of the elastic axis in semichords (x_α)

11- Calculating the non-dimensional distance from mid-chord to elastic axis (a_h)

12- Evaluating the uncoupled natural frequency in tension (ω_h)

13- Evaluating the uncoupled natural frequency in torsion (ω_α)

14- Picking a series of values of reduced frequency (k) and the related values of the Theodorsen's function F and G

Thus, all coefficients can be calculated as a function of k.

The second step is to substitute these coefficients in equations (2.68) and (2.69). We then get Δ_R and Δ_I as functions of x only, equating Δ_R and Δ_I to zero we obtain two quadratic equations in x.

The third step is to solve for x, since x is a positive quantity from equation (2.52), only the real positive roots are significant. Therefore by using various values of reduced frequency (k), we obtain the corresponding value of x.

The fourth step is to plot curves of ($\frac{1}{k}$ VS $\sqrt{x}$). The points of intersection of the curves determines the values of $\sqrt{x}$ and $\frac{1}{k}$ at which ($\Delta = 0$), i.e. the points at which Δ_R and Δ_I are simultaneously zero. If the curves do not intersect, then there is no flutter.

Since $\sqrt{x} = \frac{\omega_\alpha}{\omega}$, and $\frac{1}{k} = \frac{U}{\omega b}$, then

The flutter speed is given by:

$$U_F = \frac{1}{k_F}\frac{\omega_\alpha b}{\sqrt{x_F}} = \frac{1}{k_F}\frac{\omega_\alpha c}{2\sqrt{x_F}} \tag{2.70}$$

And the flutter frequency is given by:

$$\omega_F = \frac{\omega_\alpha}{\sqrt{x_F}} \tag{2.71}$$

Where x_F is the value of x and k_F is the value of k at which the curves $\Delta_R = 0$ and $\Delta_I = 0$ intersect.

If the intersection of $\Delta_R = 0$ and $\Delta_I = 0$ occurs at more than one point, then each represents a critical condition. The lowest value of flutter speed (U_F) is the most important because it represents a transition speed below which the wing is stable and above which it is unstable.

A sample calculation of flutter speed and related quantities is found in appendix E.

CHAPTER 3

Experimental Set-up and Methodology

In this chapter, a complete description of the experimental set-ups and procedures is provided. The description includes the first and second experimental set-ups and describes the manufacturing process and apparatus used.

3.1 First Experimental Set-up

The first experimental set-up represents the typical flutter model using torsion and tension springs. This model provides a well-defined two-degree of freedom dynamic system in which a rigid wing simulates bending-torsion flutter. The force is provided by the tension spring and the torque is provided by the torsion spring. Two torsion springs are mounted on both sides of the wing while four tension springs are attached to plate supports that connect these springs to the wing. Figure 3.1 shows the basic set-up.

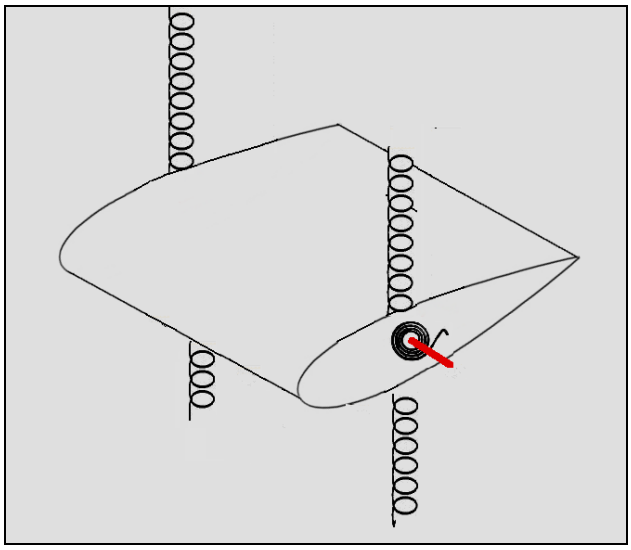

Figure 3.1 The first experimental set-up using torsion and tension springs

The wing model consists of the main airfoil, NACA 0015, two plate supports, two torsion springs and four tension springs.

3.1.1 Manufacturing process of first experimental set-up model

The airfoil is made of foam (XPS 2.3), it has a chord length of 5 inches and a span of 12 inches, and it is denoted here as the Blue wing, due to its color. The airfoil was cut professionally by *FlyingFoam* Company in Fort Collins, Colorado.

The torsion spring was mounted to the wing using a bolt made of nylon fixed from one end; the other end was joined to the support plate using another similar bolt. A hex nut was used to securely join the bolt to the support plate. Figure 3.2 shows these components for one side of the Blue wing.

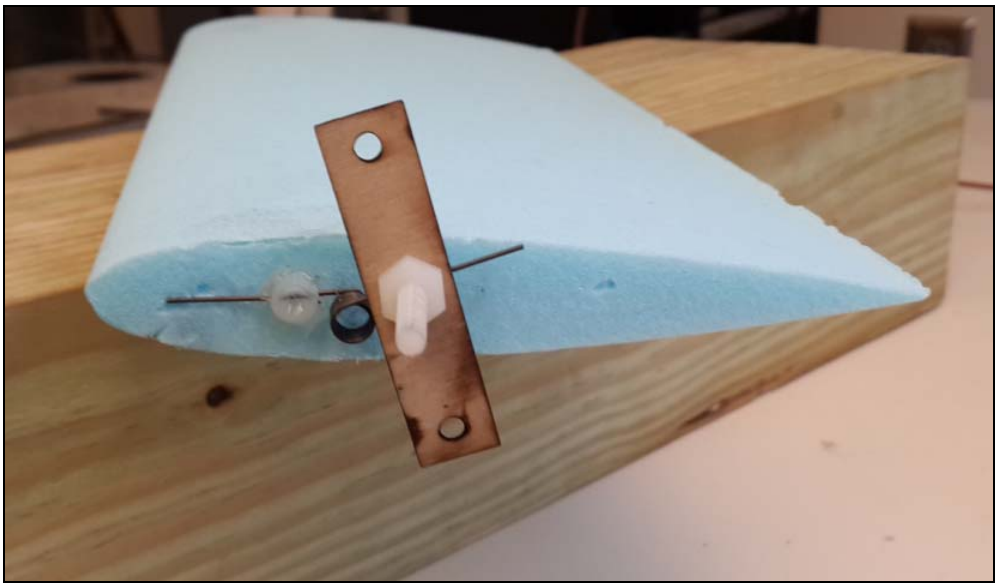

Figure 3.2 One side of the Blue wing

The support plate is made of plywood. It is 2 inches in height, 0.5 inches in length and 0.0625 inches in thickness. It has two holes, one at the top and the other at the bottom, these holes are used to attach the tension spring. The support plates were cut using the laser cutter.

SOLIDWORKS was used to draw the model of the first experimental set-up as shown in figures 3.3 and 3.4.

Dimensions and weights of all components are presented in chapter 4 when related quantities are calculated.

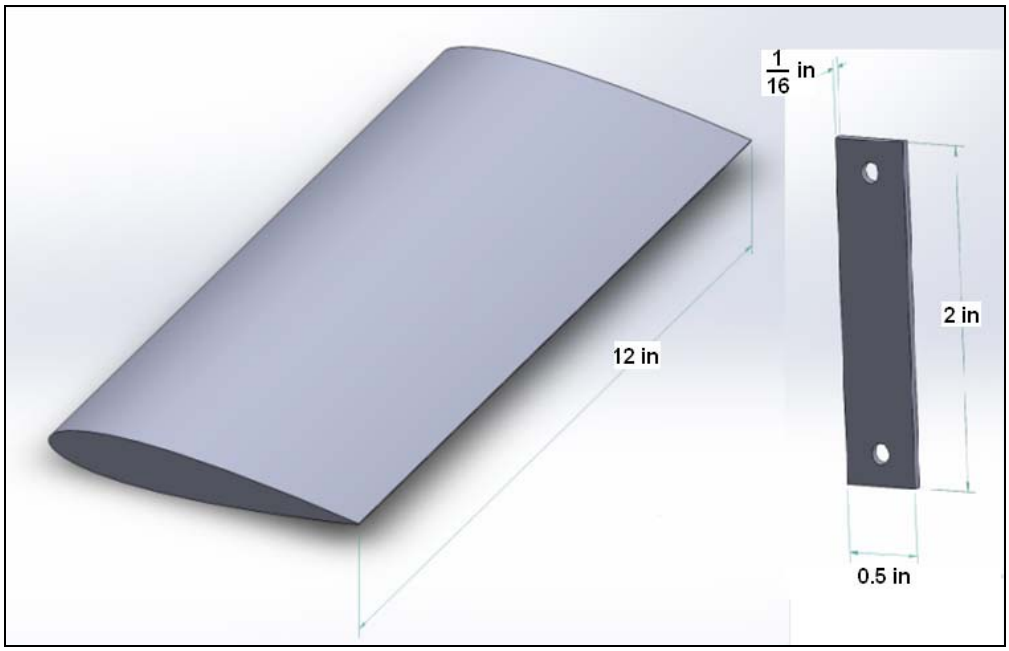

Figure 3.3 SOLIDWORKS drawing of the airfoil and plate support

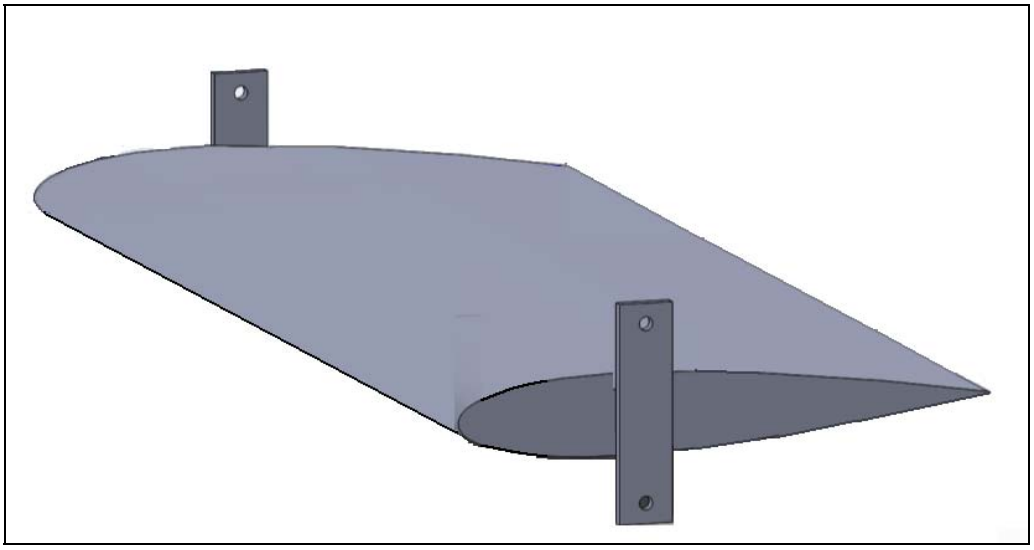

Figure 3.4 SOLIDWORKS assembly drawing of the airfoil and plate support (1^{st} experimental set-up)

3.1.2 Designing and manufacturing of the support fixture for the first experimental set-up

A fixture was designed and built to support the model inside the wind tunnel test section. This fixture consists of two wooden panels. One panel is laid on the bottom of the wind tunnel section while the other panel is attached to the ceiling of the wind tunnel section by supporting rods. Each panel has four small metal fixtures that are used to attach the tension springs. Figure 3.5 shows the fixture.

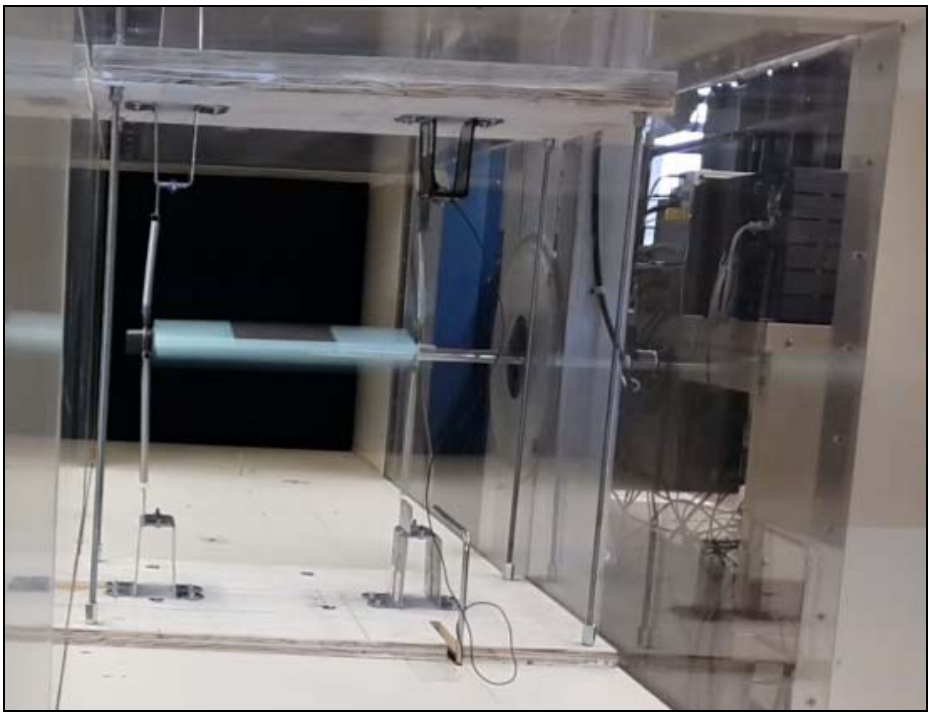

Figure 3.5 The fixture for supporting the wing

The tension springs are attached to the support plates and to the fixture as final step before testing as shown in figure 3.6.

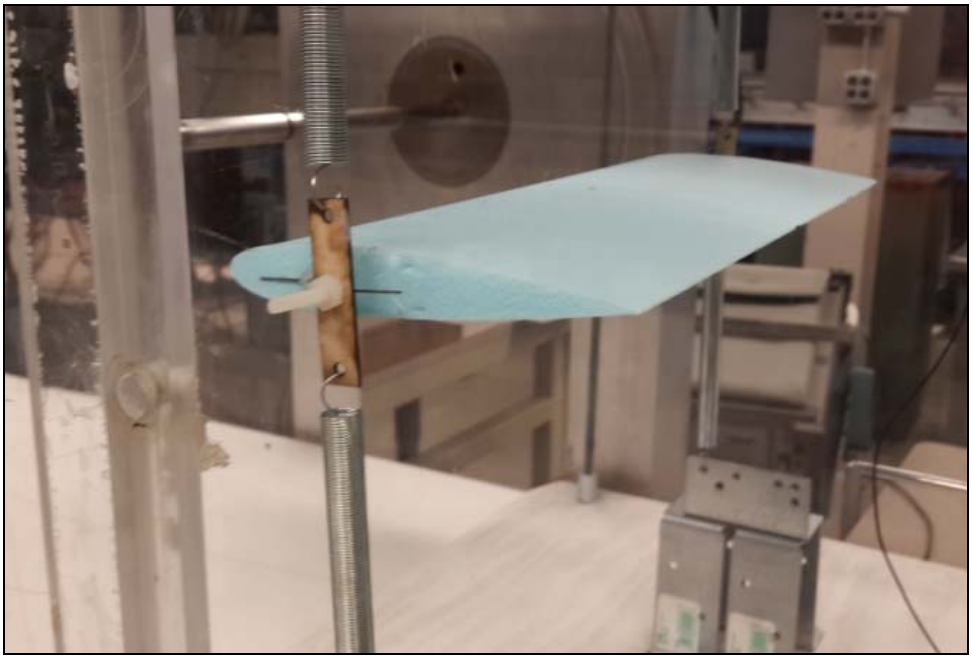

Figure 3.6 Completion of first experimental set-up before testing

3.2 Second Experimental Set-up

The second experimental set-up represents the flutter model using tension springs only. This model can flutter in pitch and plunge with two degrees of freedom. There are eight tension springs attached to plate supports that connect them to the wing. Figure 3.7 shows the basic set-up.

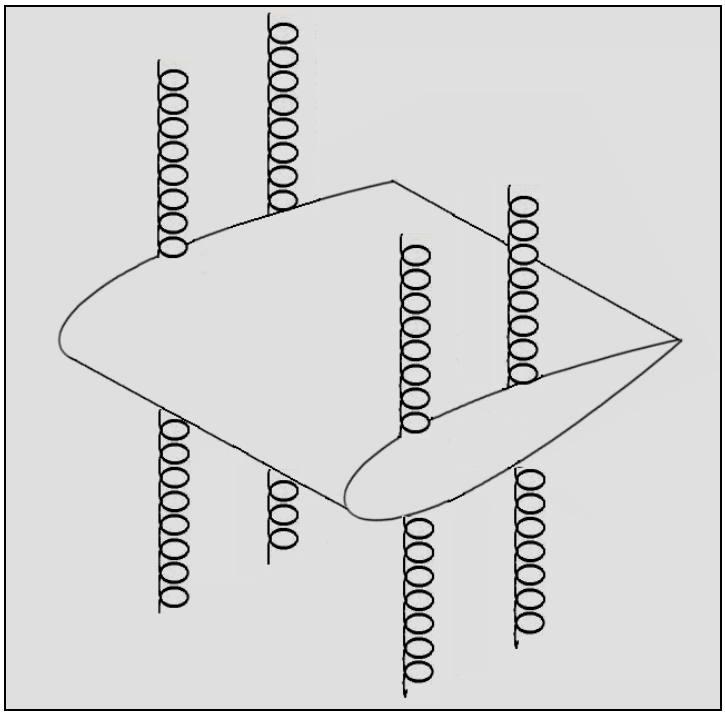

Figure 3.7 The second experimental set-up using tension springs

The wing model consists of the main airfoil, NACA 0015, two wooden cap side airfoils, NACA 0015, four plate supports and eight tension springs.

3.2.1 Manufacturing process of second experimental set-up model

The airfoil is made of foam (EPS 1.5), it has a chord length of 5 inches and a span of 12 inches, and it is denoted here as the Red wing because of its color. The airfoil was cut professionally by *FlyingFoam* Company in Fort Collins, Colorado.

The side cap airfoil is made of plywood; it has a chord length of 5 inches and a span of 0.0625 inches. It is glued to the main airfoil to provide a stronger connection with the support plate. The side cap airfoils were cut using the laser cutter as shown in figure 3.8.

Figure 3.8 The laser cutter used to cut the side cap airfoils and plate supports

The support plate used in this set-up is the same as the one used in the first experimental set-up. Figure 3.9 shows these components for one side of the Red wing.

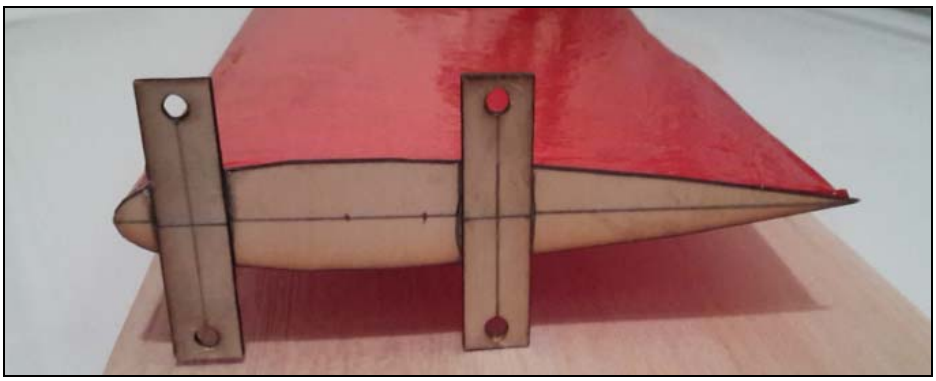

Figure 3.9 One side of the Red wing

SOLIDWORKS was used to draw the model of the second experimental set-up as shown in figure 3.10.

All dimension and weights of all components are presented in chapter 5 when related quantities are calculated.

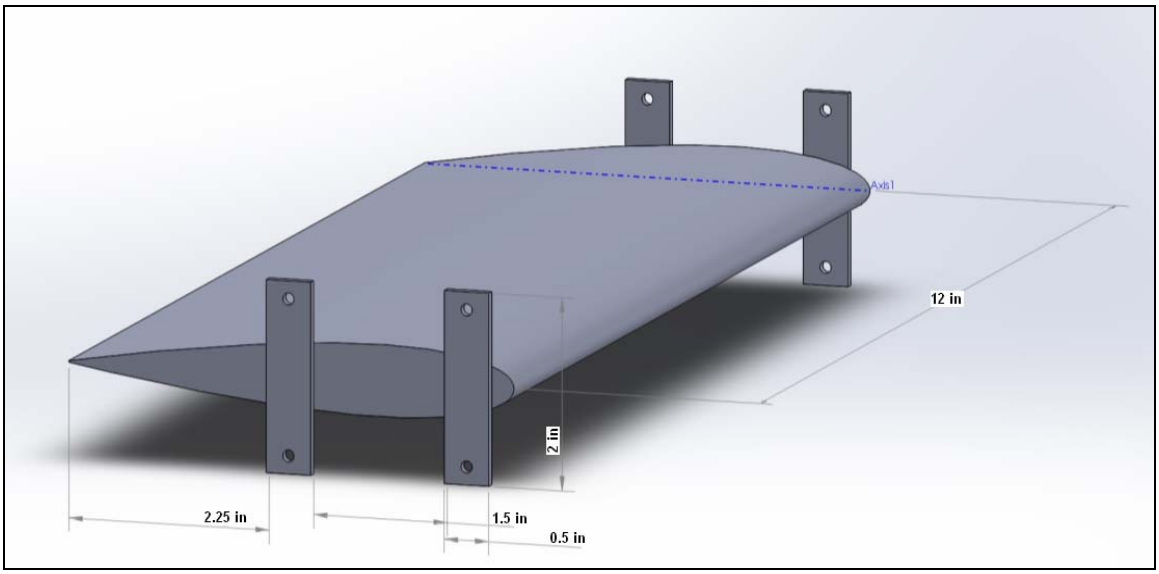

Figure 3.10 SOLIDWORKS assembly drawing of the airfoil and plate support (2^{nd} experimental set-up)

3.2.2 The fixture used for the first experimental set-up

The fixture used in this set-up is the same fixture used in the first experimental set-up (figure 3.5) but with an extra metal fixture to attach the extra tension springs.

The tension springs are attached to the support plates and to the fixture as a final step before testing as shown in figure 3.11.

Figure 3.11 Completion of second experimental set-up before testing

3.3 Experimental Procedure

The first step is to put the wing model inside the wind tunnel and attach the first set of tension springs (spring type # 1).

The second step is to turn on the signal analyzer and adjust it to the proper setting, and set the accelerometer firmly on the wing surface, it is preferred to place it exactly on the location of the wing center of gravity to avoid any possible translation due the mass of the accelerometer. The third step is to run the wind tunnel and gradually increase the speed until the onset of flutter. The fourth step is to take measurements. The flutter speed can be read automatically from the wind tunnel board panel, the frequency can be measured directly by using the stroboscope or by the output of the signal analyzer.

All steps above are repeated for the remaining sets of tension springs for both first experimental set-up and second experimental set-up.

For the first experimental set-up, we only have the Blue wing, however, for the second experimental set-up, we have the Red wing plus another four wings.

3.4 Apparatus Used in the Experiment

- The wind tunnel (figure 3.12)

The wind tunnel used was subsonic, open return tunnel located on the fourth floor of Akerman Hall at the University of Minnesota. The dimensions of the wind tunnel test section are 23.625 inches in width by 23.625 inches in height. The maximum speed is about 50 m/s. the level of noise of this wind tunnel is very low, it was measured up to 40 m/s by the lab engineer Kale Hedstrom during the experiment using a hot wire. The level of noise was small and did not exceed 0.3% of the velocity.

- The accelerometer (figure 3.14)

The accelerometer used is model (PCB Piezotronics 353B16). It has a measurement range of (±4905 m/s² peak), broadband resolution of (0.05 m/s² rms) and a frequency range of (1 to 10000 Hz).

- The signal analyzer (figure 3.15)

The signal analyzer used is a Hewlett Packard model (35670A). It has seven signal sources, and it can provide a resolution of 1600 lines and accuracy of (± 0.15 dB). The frequency rage is 102.4 kHz for one channel, 51.2 kHz for two channel and 25.6 kHz for four channel.

- The stroboscope (figure 3.16)

The stroboscope used is a digital type of model (HHT32). It has a rotary encoder to enable quick and precise frequency setting from 30 to 14,000 flashes per minute. It provides accurate readings to 0.1 RPM.

More pictures of the experimental work for different wings can be found in appendix G.

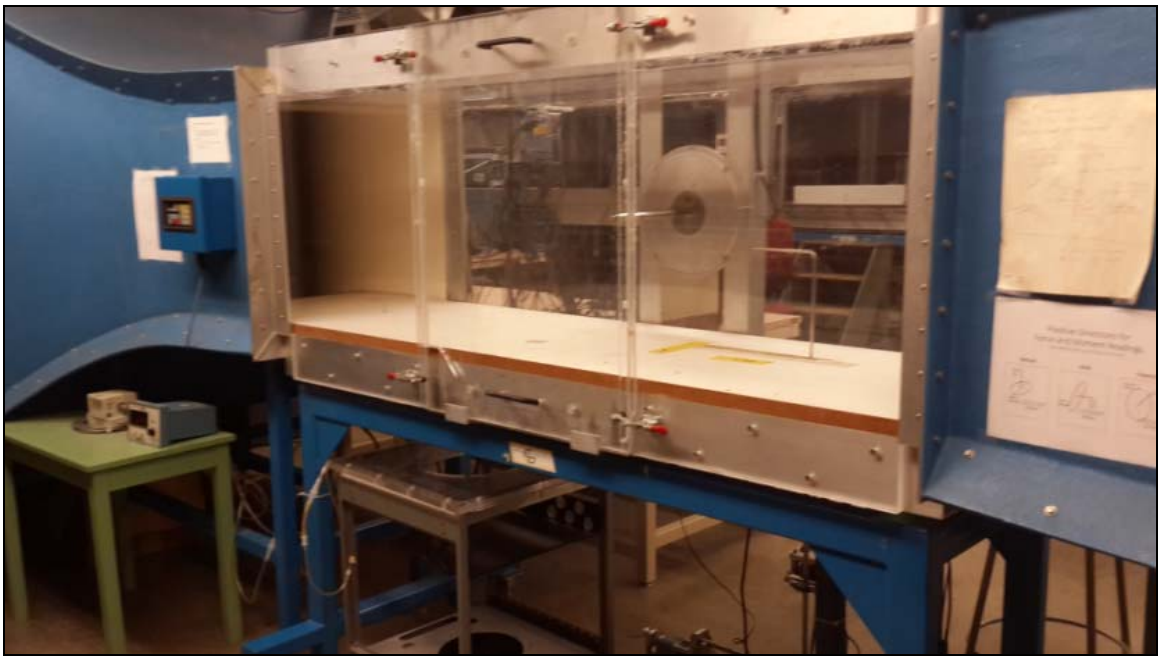

Figure 3.12 The wind tunnel

Figure 3.13 The wind tunnel control board panel

Figure 3.14 The accelerometer (PCB Piezotronics model 353B16)

Figure 3.15 The signal analyzer (Hewlett Packard model 35670A)

Figure 3.16 The stroboscope (VBX model HHT32)

CHAPTER 4

First Experimental Set-up Results and Comparison with Theodorsen Solution

In this chapter, the experimental results for the first experimental set-ups will be tabulated and compared with the calculated values from the Theodorsen Function.

All experimental results belonging to the Blue wing are considered.

4.1 Torsion-Tension spring Set-up (1st Experimental Set-up)

The first experimental flutter model under investigation is a two-dimensional typical airfoil section defined by independent two degrees of freedom, which are selected to be the vertical displacement (plunge), h, and the rotation (pitch), α. The forces and moments on theses two degrees of freedom are produced by two torsion and four tension springs as shown in figure 4.1.

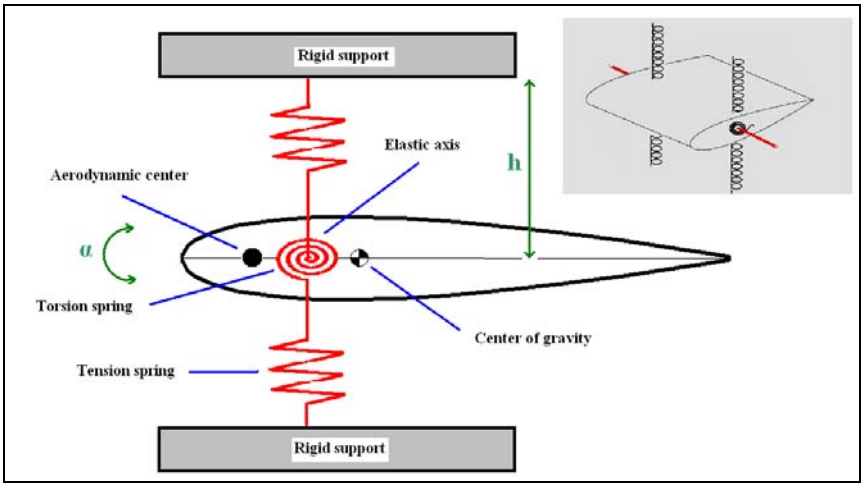

Figure 4.1 A typical airfoil section with two degrees of freedom

The wing and torsion spring technical data are given in table 4.1.

Table 4.1 Blue wing and springs technical data

Airfoil type	NACA 0015 (Blue wing)
Weight of airfoil by itself	18.81×10^{-3} (kg)
Total weight of wing section	23.09×10^{-3} (kg)
Torsion spring constant	(0.552 lbs-in) = 0.0624 (N.m)

Where the weight of wing section includes the weight of all elements mounted into the airfoil as follows:

Original wing (airfoil) = 18.81×10^{-3} kg

- Two plate supports (plywood material) = 2 x (0.6×10^{-3} kg)
- Two torsion springs = 2 x (0.57×10^{-3} kg)
- Four bolts (nylon material) = 4 x (0.4×10^{-3} kg)
- Two hex nuts (nylon material) = 2 x (0.16×10^{-3} kg)

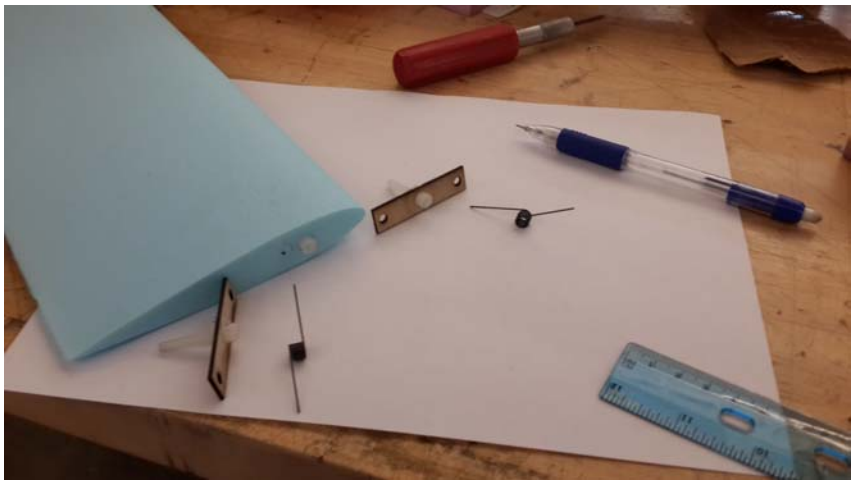

Figure 4.2 Elements mounted in the Blue wing

The Blue wing while being tested in the wind tunnel as shown in figure 4.3.

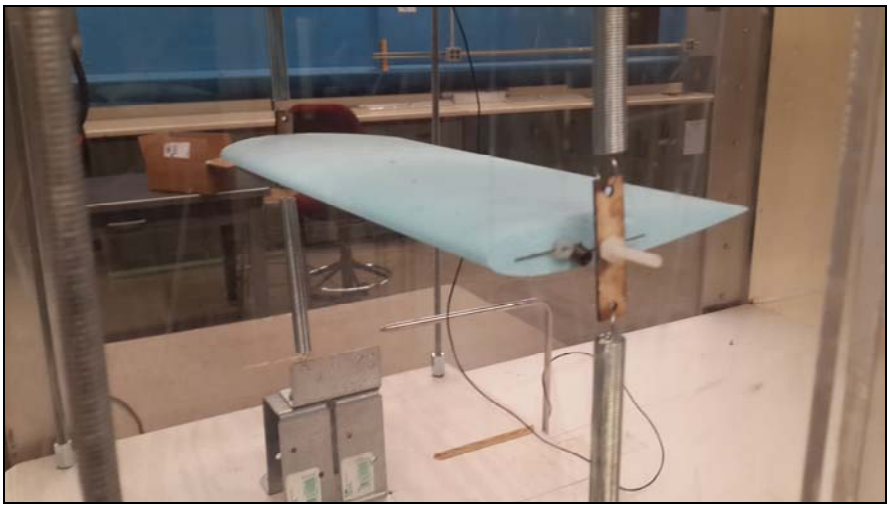

Figure 4.3 Testing the Blue wing in the wind tunnel

The experiment was carried out for six different sets of tension springs. These springs have the same length of 4.5 inches but different weights and outer diameters. The weight of each spring was measured using the electronic scale while the other data was provided by the manufacturer. The technical data of all tension springs is given in table 4.2.

Table 4.2 Tension springs data

Tension spring #	Spring constant K_h (N/m)	Weight (kg)	Outer diameter (m)
# 1	(0.1 lbs/in) = 17.52	13.24×10^{-3}	11.13×10^{-3}
# 2	(0.16 lbs/in) = 28.03	11.34×10^{-3}	9.53×10^{-3}
# 3	(0.27 lbs/in) = 47.3	12.74×10^{-3}	9.53×10^{-3}
# 4	(1.22 lbs/in) = 213.73	44.83×10^{-3}	19.05×10^{-3}
# 5	(2.0 lbs/in) = 350.37	29.2×10^{-3}	12.7×10^{-3}
# 6	(2.3 lbs/in) = 402.93	29.46×10^{-3}	12.7×10^{-3}

The experimental results for the torsion-tension set-up for the six different tension springs are tabulated in table 4.3.

The flutter speed was measured as indicated by the wind tunnel electronic board panel. However, the frequency was measured in two different ways, (1) by using the electronic stroboscope (strobe) and (2) by the accelerometer due the difficulty, in some cases, of determining the values of low frequencies.

It was noticed that there was a small change in the flutter speed when the accelerometer sensor was placed on wing surface in all cases. The flutter speed was increased about 2 m/s in average and that might be due the added weight of the sensor that was measured to be 5.5 x 10^{-3} kg. The frequencies in table 4.3 were all measured by using the accelerometer.

Table 4.3 Torsion-tension set-up experimental results

Tension spring #	# 1	# 2	# 3	# 4	# 5	# 6
Flutter speed (m/s)	10.2	11.5	13	17.2	16	20
Flutter frequency (Hz)	8	8.75	10.5	14.75	22	22.75

The following flutter frequency figures were generated using the signal analyzer, which indicates the accelerometer measurements. The maximum peak occurs at the flutter frequency.

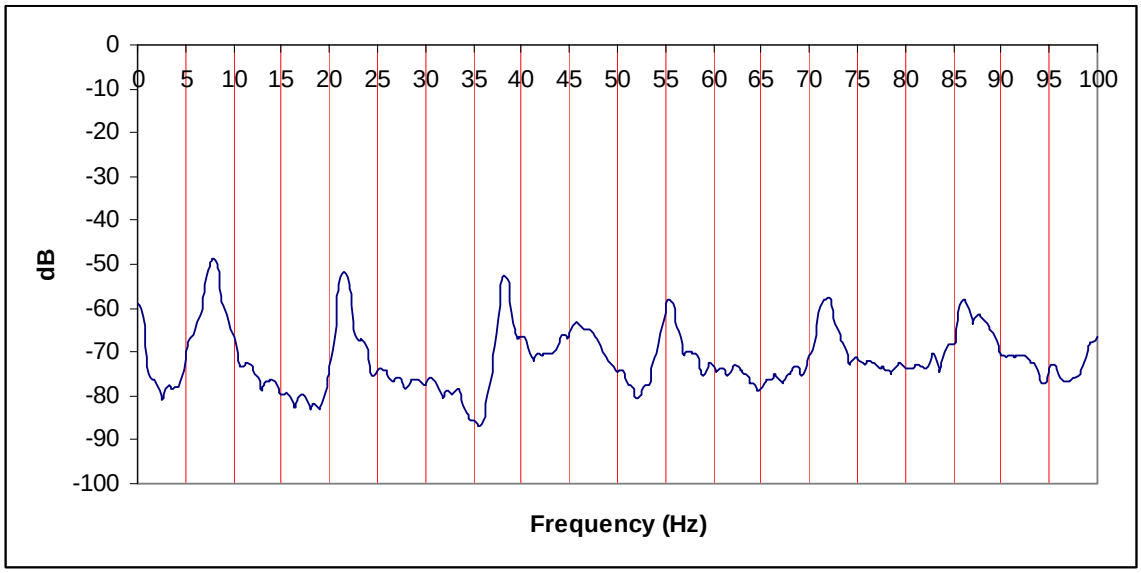

Figure 4.4 Frequency of the Blue wing for tension spring # 1 (1st experimental set-up)

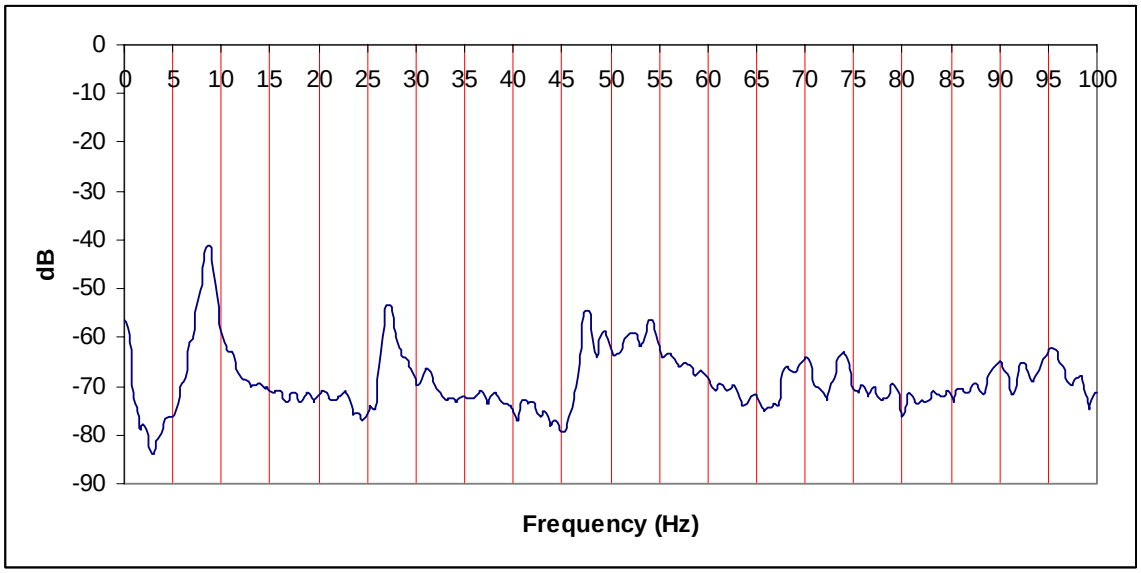

Figure 4.5 Frequency of the Blue wing for tension spring # 2 (1st experimental set-up)

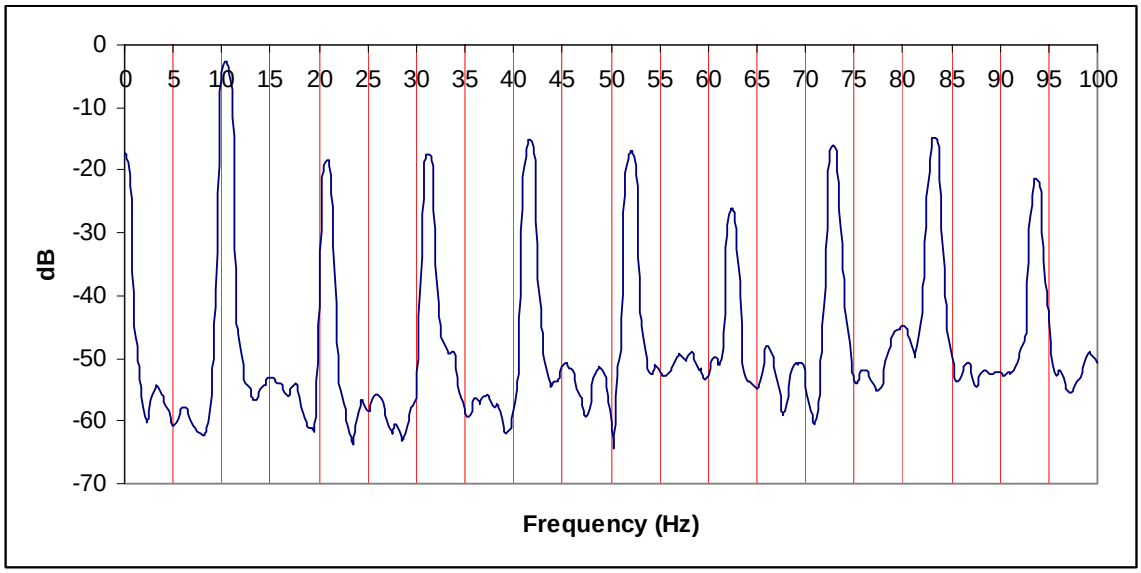

Figure 4.6 Frequency of the Blue wing for tension spring # 3 (1st experimental set-up)

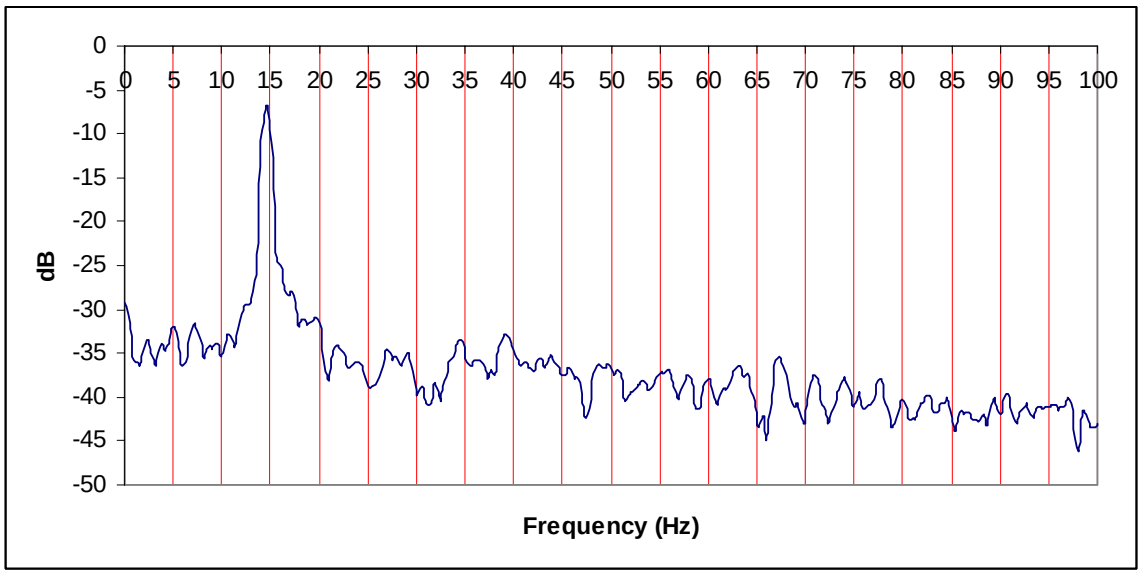

Figure 4.7 Frequency of the Blue wing for tension spring # 4 (1st experimental set-up)

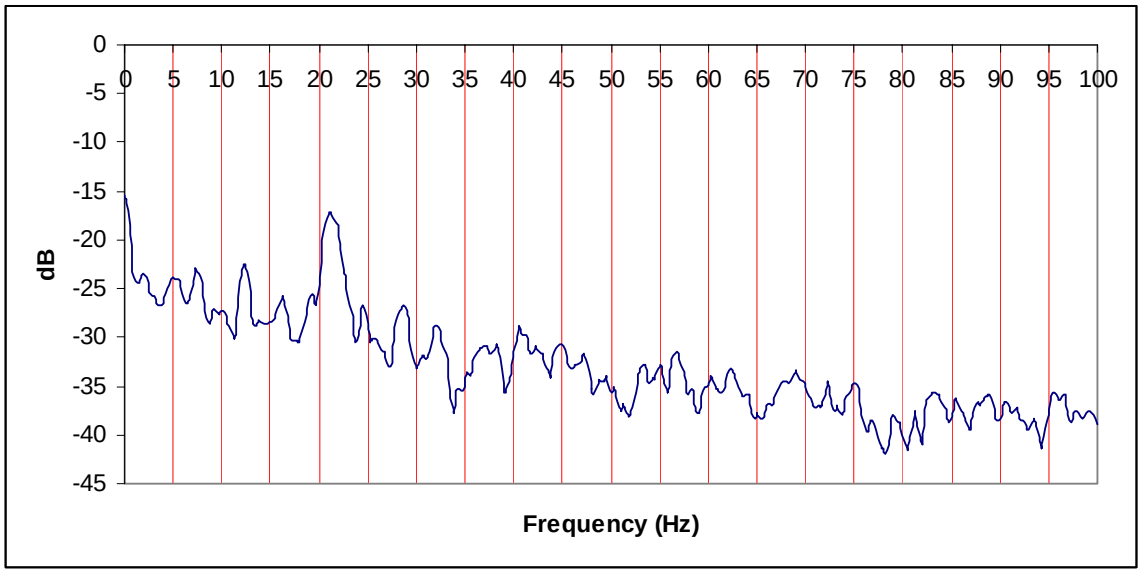

Figure 4.8 Frequency of the Blue wing for tension spring # 5 (1st experimental set-up)

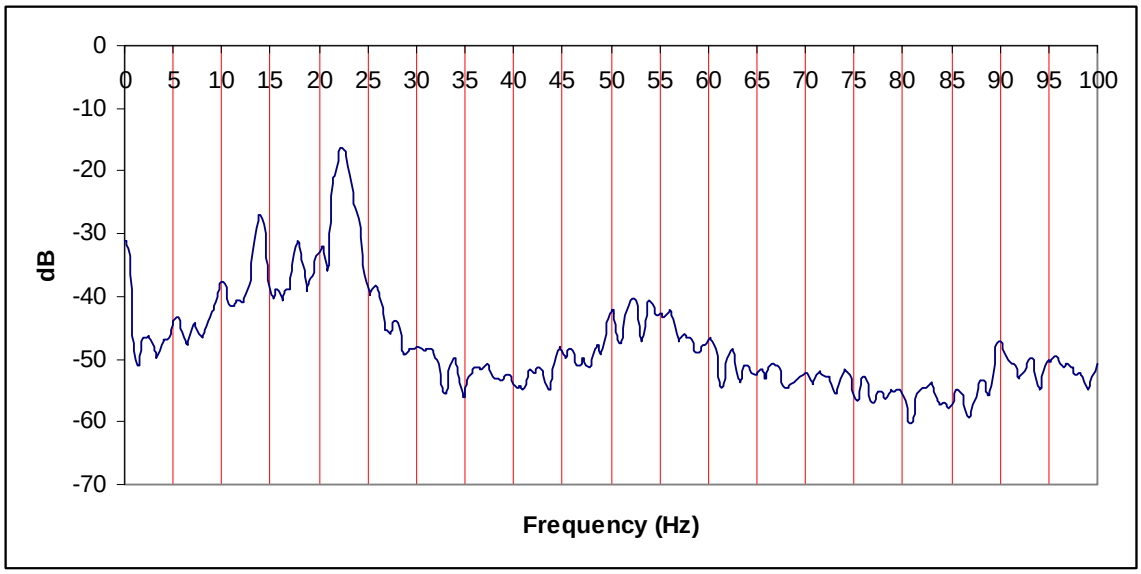

Figure 4.9 Frequency of the Blue wing for tension spring # 6 (1st experimental set-up)

4.1.1 Remarks on the results of Torsion-Tension spring Set-up (1st Experimental Set-up)

The experimental results in table 4.3 show that the flutter speed increased as the spring constant increased which is as expected from theory. It is of interest to investigate the impact of the mass of the spring on the flutter speed. The spring masses for spring #1, #2 and #3 are close to each other and as the spring constants increase, it was expected that the flutter speed would also increase.

Spring #4 has the largest mass of all the spring, with a spring mass of (44.83 x 10^{-3} kg) and a spring constant of (213.73 N/m). If spring #4 is compared with spring #3, which has a mass of (12.74 x 10-3), and a spring constant of (47.3 N/m), it would be expected to have a higher value of flutter speed (17.2 m/s) due to the higher value of spring constant and this is what was observed.

However, if comparison is made between spring #4 and spring #5, which has a higher spring constant (350.37 N/m) but a lower mass (29.2 x 10^{-3}) than spring #4, then we can explain the effect of the spring mass on the flutter speed in both cases. The interesting observation is that in spite of the lower value of stiffness in spring #4 compared to spring #5, the flutter speed is higher in the case of spring #4. This indicates that the spring mass is the responsible parameter that has an important effect on the flutter speed.

The differences in flutter speed were small in all cases due to the low value of the torsion spring constant. This did not give a very clear understanding of the role of the spring mass; however, the second experimental set-up where we eliminate the torsion spring may give a better clarification of that effect.

In the next section, the experimental results of first experimental set-up will be compared with Theodorsen solutions.

4.2 Theodorsen Solution for Torsion-Tension spring Set-up (1st Experimental set-up)

To carry out the Theodorsen solution we need to first calculate related quantities, like center of gravity (CG), the moment of inertia of the complete airfoil section about the center of gravity and about the elastic axis.

Figure 4.10 illustrates the nomenclature of airfoil model parameters.

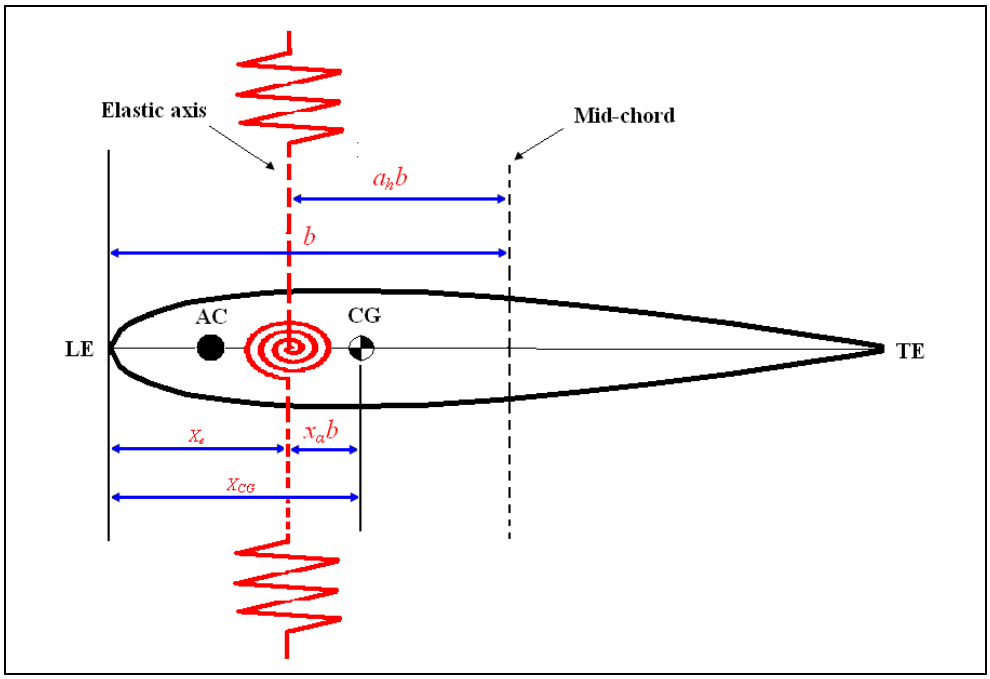

Figure 4.10 Nomenclature of airfoil model parameters of 1st experimental set-up

4.2.1 Center of gravity:

The center of gravity is the point at which the entire weight of a body may be thought of as centered so that if supported at this point the body would balance perfectly.

The center of gravity of different objects is given by:

$$X_{CG} = \frac{W_1 d_1 + W_2 d_2 + W_3 d_3 + ... + W_n d_n}{W} \quad (4.1)$$

Where W_1, W_2, W_3, W_n, d_1, d_2, d_3, d_n represents the weight of each object and distance of that object from a reference point respectively and W represents the total weight of all the objects.

In the first experimental set-up, we have different components as shown in figure 4.11. The weights of different components and distances from leading edge (LE) are tabulated in tables 4.4 and 4.5.

Table 4.4 Weights of airfoil components for 1st experimental set-up

Object	Weight (kg)
Original wing (airfoil)	18.81 x 10^{-3} kg
Two plate supports	2 x (0.6 x 10^{-3} kg)
Two torsion springs	2 x (0.57 x 10^{-3} kg)
Two front bolts	2 x (0.4 x 10^{-3} kg)
Two aft bolts	2 x (0.4 x 10^{-3} kg)
Two hex nuts	2 x (0.16 x 10^{-3} kg)

Table 4.5 Distances from LE of airfoil components for 1st experimental set-up

Object	Distance from LE (m)
Original wing (airfoil)	(2.1 in) = 0.05334
Two plate supports	(1.5 in) = 0.0381
Two torsion springs	(1.5 in) = 0.0381
Two front bolts	(1.19 in) = 0.03023
Two aft bolts	(1.5 in) = 0.0381
Two hex nuts	(1.5 in) = 0.0381

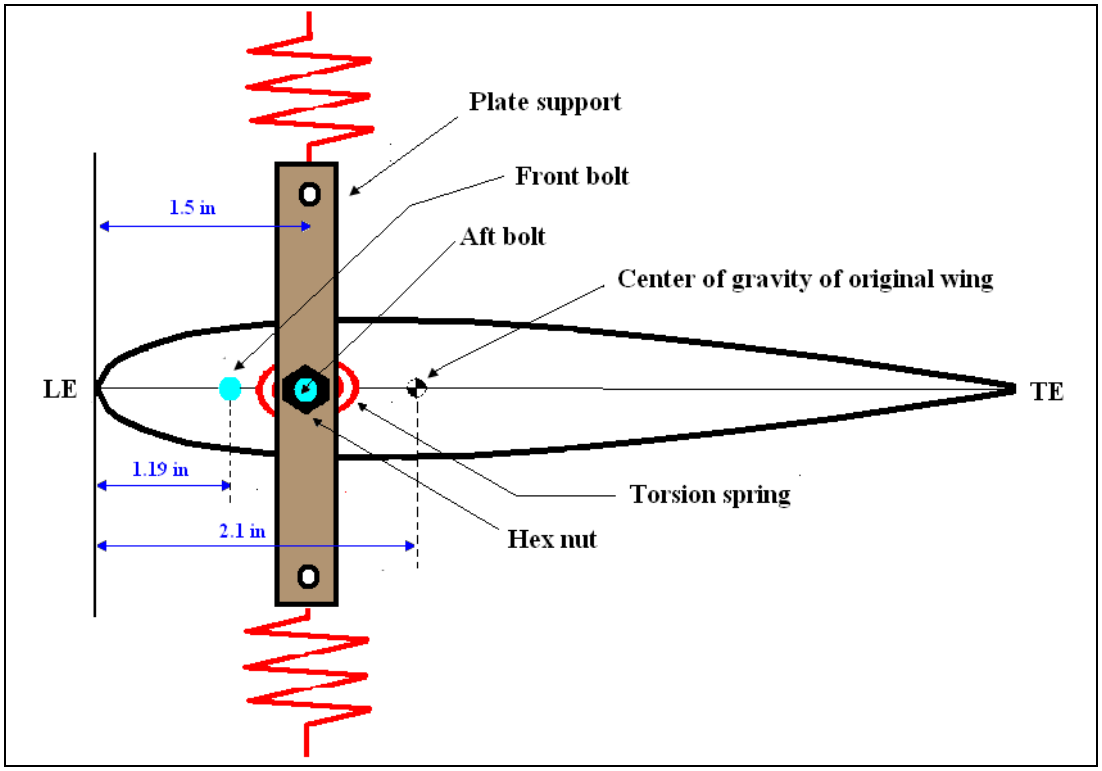

Figure 4.11 Front view of airfoil with different components for 1st experimental set-up

The calculation of the center of the gravity of the original wing itself is not simple as the other regular shaped objects. It is more complicated due the irregular shape of the wing (NACA 0015).

The center of gravity (X_{CG} , Y_{CG}) of any shape with uniform density can be given by:

$$X_{cg} = \frac{1}{A}\int_a^b x\left(f(x) - g(x)\right)dx \tag{4.2}$$

$$Y_{cg} = \frac{1}{A}\int_a^b \frac{1}{2}\left(\left[f(x)\right]^2 - \left[g(x)\right]^2\right)dx \tag{4.3}$$

Where:

- *f(x)* and *g(x)* are the upper and lower function bounding the shape.
- *a* and *b* are the limits.
- *A* is the area of between the two functions

$$A = \int_a^b \left(f(x) - g(x)\right)dx \tag{4.4}$$

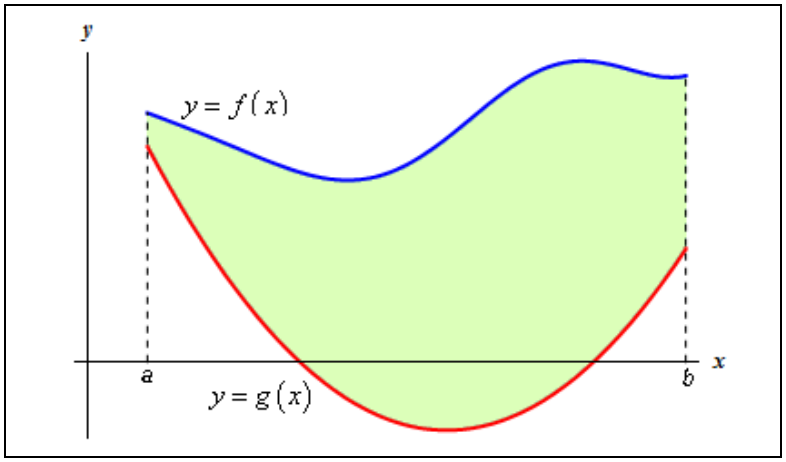

Figure 4.12 Finding center of gravity

Therefore, to find the center of gravity of an airfoil, the upper and lower functions are needed.

The general equation for a symmetrical 4-digit NACA airfoil is given by [29]:

$$y_t = 5t\left[0.2969\sqrt{\frac{x}{c}} - 0.126\left(\frac{x}{c}\right) - 0.3516\left(\frac{x}{c}\right)^2 + 0.2843\left(\frac{x}{c}\right)^3 - 0.1015\left(\frac{x}{c}\right)^4\right] \quad (4.5)$$

Where:

- c is the cord length
- x is the position along the chord from 0 to c
- y_t is the half thickness at a given value of x
- t is the maximum thickness as a fraction of the chord

In our case, the chord length is 5 inches (0.127 m), the thickness of NACA 0015 is calculated as (t = 15*c/100)

The airfoil was generated as shown in figure 4.13 using a MATLAB code in appendix B.

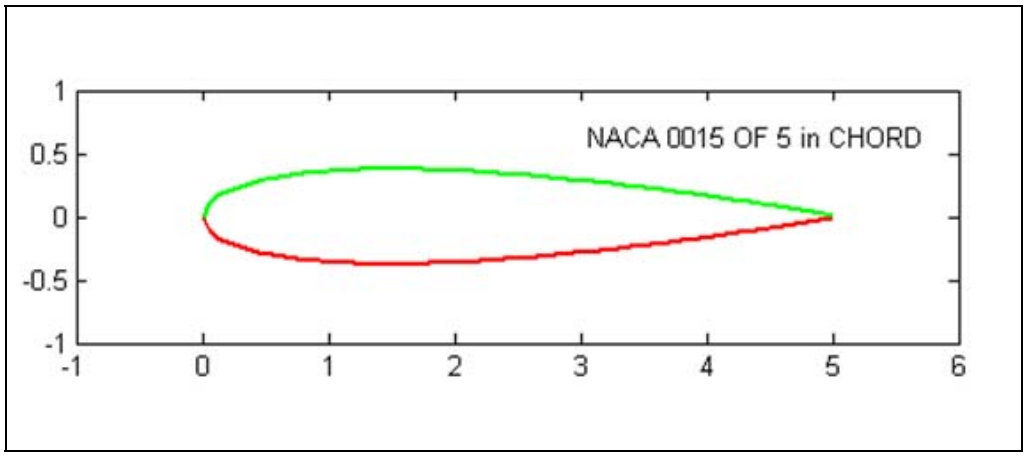

Figure 4.13 Generation of NACA 0015 with a chord length of 5 inches

Since the airfoil is symmetric and has uniform density, we can substitute as follows:

$$f(x) = y_t \tag{4.6}$$

$$g(x) = - y_t \tag{4.7}$$

And solve for A and X_{CG} when c = 5 inches as follows:

$$A = \int_0^c \left(y_t(x) - (-y_t(x))\right) dx \tag{4.8}$$

$$X_{cg} = \frac{1}{A} \int_0^c x\left(y_t(x) - (-y_t(x))\right) dx \tag{4.9}$$

Performing the integration and calculation process (detailed solution is in appendix B), we get the center of gravity of the original wing as:

X_{cg} = 2.1 in

Now we can use equation (4.1) and calculate the center of gravity of our wing model as follows:

$$X_{CG} = \frac{m_w d_w + 2(m_p d_p) + 2(m_{torsion\,spring} d_{ts}) + 2(m_b d_{fb}) + 2(m_b d_{ab}) + 2(m_{hex} d_{hex})}{m_w + 2(m_p) + 2(m_{torsion\,spring}) + 2(m_b) + 2(m_b) + 2(m_{hex})} \tag{4.10}$$

Substituting the values from tables 4.4 and 4.5, the center of gravity of the whole system (wing) from leading edge is calculated to be:

X_{CG} = 1.978 in

= 0.0502412 m

4.2.2 Mass moment of inertia about center of gravity:

Mass moment of inertia, usually denoted (*I*), is a measure of an object's resistance to change in rotation direction. Moment of inertia has the same relationship to angular acceleration as mass has to linear acceleration. Moment of inertia of a body depends on the distribution of mass in the body with respect to the axis of rotation.

It depends on the body's mass distribution and the axis chosen, with larger moments requiring more torque to change the body's rotation. It is an additive property such that the moment of inertia of a composite system is the sum of the moments of inertia of its component subsystems (all taken about the same axis).

One of its definitions is the second moment of mass with respect to distance from an axis *r*, integrating over the entire mass *Q*.

$$I = \int_Q r^2 \, dm \tag{4.11}$$

Where:

- dm = mass of an infinitesimally small part of the body.

Geometrically simple objects have moments of inertia that can be expressed mathematically, but it may not be straightforward to express symbolically the moment of inertia of more complex bodies.

In this section, the mass moment of inertia of every object is calculated with respect to the axis of the center of gravity of the wing calculated above (X_{CG} = 1.978 in). To perform this, we can apply the parallel axis theorem. For a single object, its mass moment of inertia taken about the axis of center of gravity of whole system can be given by:

$$I_{CG-i} = I_i + m_i\, d_i^2 \tag{4.12}$$

Where:

- $I_{CG\text{-}i}$ is the mass moment of inertia of the object taken about the axis of the center of gravity of whole system (wing).
- I_i is the mass moment of inertia of the object.
- d_i is the distance between the center of gravity of the object and the axis of rotation which is the center of gravity of the wing (X_{CG} = 1.978 in) in this case.

The total mass moment of inertia of all objects about the axis of the center of gravity can be given by:

$$I_{CG} = I_1 + m_1\, d_1^2 + I_2 + m_2\, d_2^2 + I_3 + m_3\, d_3^2 + ... + I_n + m_n\, d_n^2 = \sum_{i=1}^{n} \left(I_i + m_i\, d_i^2 \right) \tag{4.13}$$

The distances of different object from the center of gravity of whole system (wing) can be determined from figure 4.14.

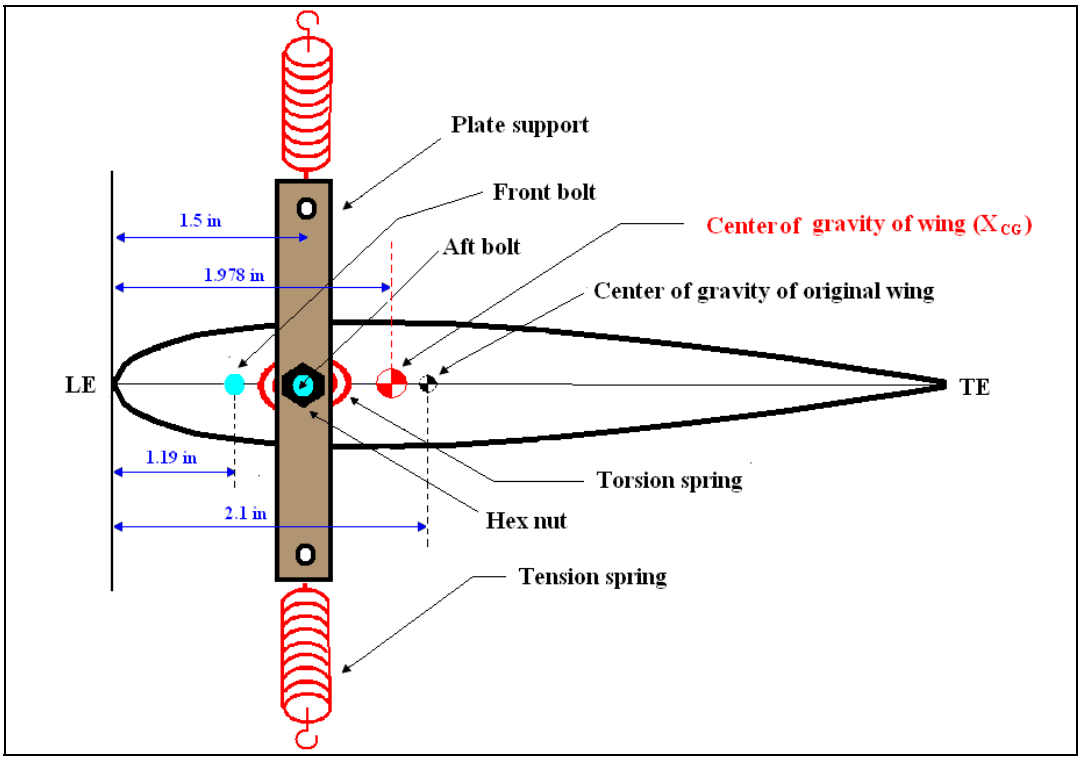

Figure 4.14 Center of gravity of the wing and distance of different components from LE for 1st experimental set-up (front view)

The mass moment of inertia includes all objects in table 4.4, in addition, the mass moment of inertia of the four attached tension springs is included in the calculation as well. The mass moment of inertia of tension springs must also be included in the calculation since they interact and resist the wing rotational motion (pitch mode). As shown in figure 4.15 and 4.16

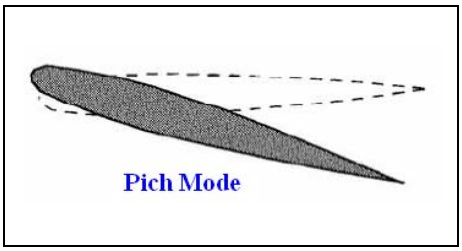

Figure 4.15 Pitch mode

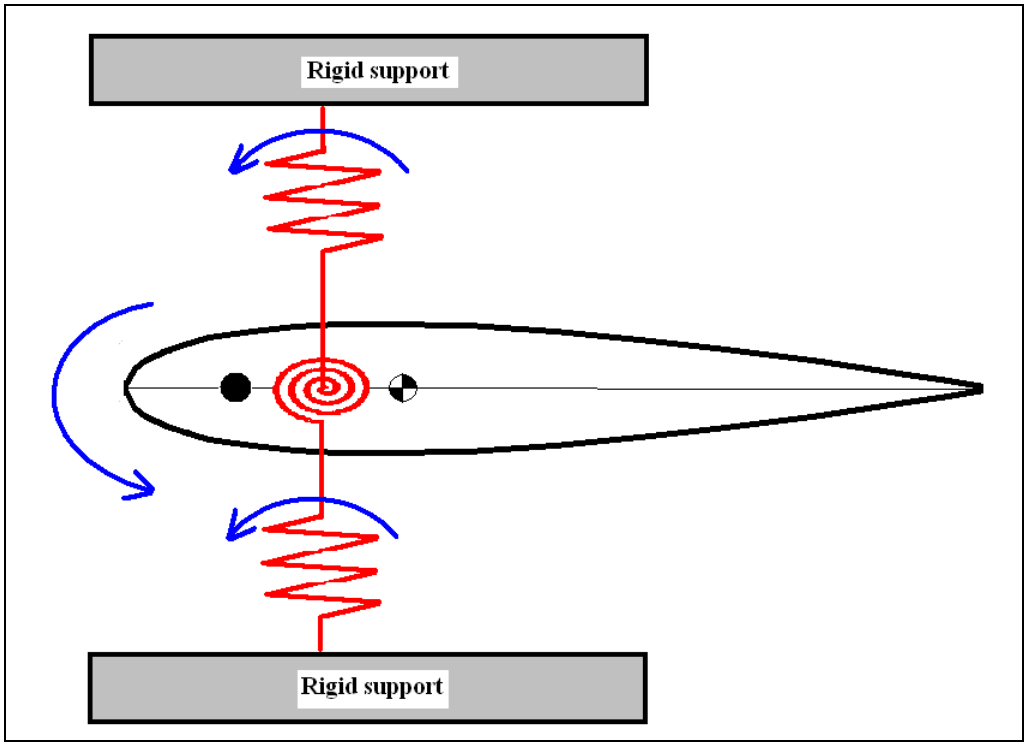

Figure 4.16 Tension springs resist rotational motion in pitch mode

4.2.2.1 Mass moment of inertia of tension spring:

Tension spring can be assumed as a hollow cylinder.

The mass moment of inertia of a hollow cylinder is given by:

$$I_{hollow\,cylinder} = \frac{m}{12}\left[3r_1^2 + 3r_2^2 + h^2\right] \tag{4.14}$$

Where:

- m is the mass of hollow cylinder
- r_1 is the inner radius
- r_2 is the outer radius
- h is the height of hollow cylinder

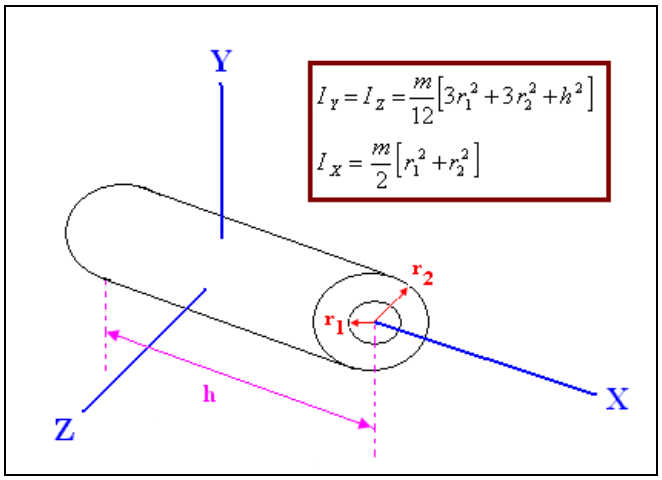

Figure 4.17 Mass moment of inertia of a hollow cylinder

In our case, the tension spring has a very small wire diameter which makes the outer radius is almost the same as the inner radius, from that, it can be assumed that ($r_1 = r_2$). The mass moment of inertia of tension spring can be given by:

$$I_{tension\ spring} = \frac{m}{12}\left[6r^2 + h^2\right] \tag{4.15}$$

The length of each tension spring is (4.5 in). Table 4.6 illustrates the calculation of all mass moment of inertia of tension springs used in the experiment.

Table 4.6 Mass moment of inertia of tension springs

Tension spring #	Mass (kg)	Outer diameter (m)	Mass moment of inertia (kg.m^2)
# 1	13.24 x 10^{-3}	11.13 x 10^{-3}	1.4619 x 10^{-5}
# 2	11.34 x 10^{-3}	9.53 x 10^{-3}	1.2475 x 10^{-5}
# 3	12.74 x 10^{-3}	9.53 x 10^{-3}	1.4015 x 10^{-5}
# 4	44.83 x 10^{-3}	19.05 x 10^{-3}	5.0840 x 10^{-5}
# 5	29.2 x 10^{-3}	12.7 x 10^{-3}	3.2379 x 10^{-5}
# 6	29.46 x 10^{-3}	12.7 x 10^{-3}	3.2667 x 10^{-5}

4.2.2.2 Mass moment of inertia of support plate:

The mass moment of inertia of a rectangular plate is given by:

$$I = \frac{m}{12}\left[a^2 + b^2\right] \tag{4.16}$$

Where:

- *m* is the mass of a solid plate
- *a, b* and *c* are dimensions of plate.

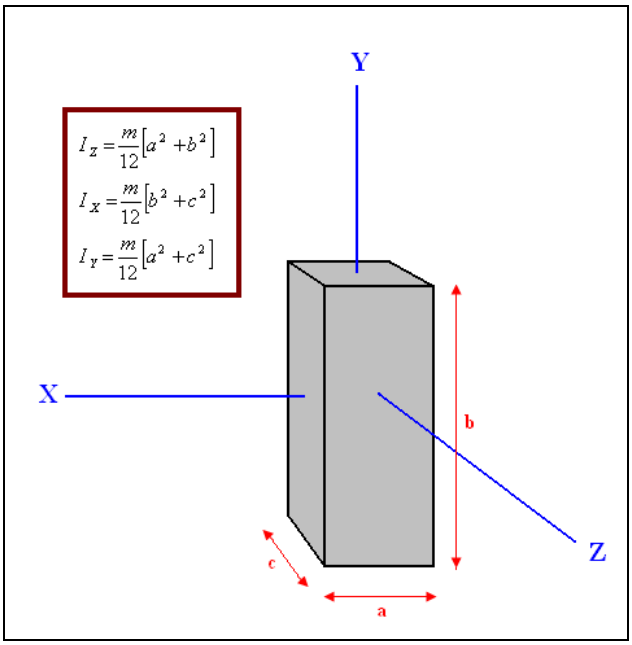

Figure 4.18 Mass moment of inertia of a plate

However, our support plate has three holes each of a diameter of 0.125 in as shown in figure 1.19.

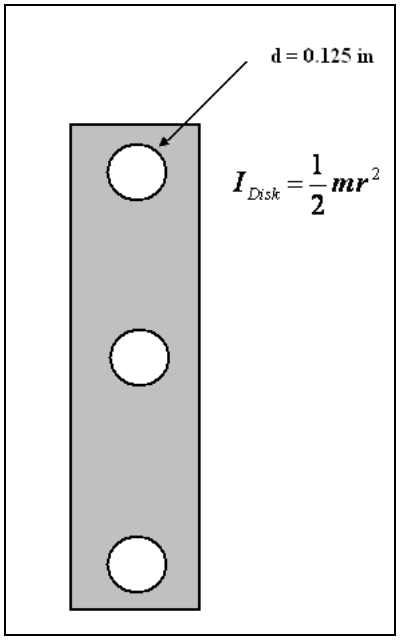

Figure 4.19 Support plate with three holes

To get the correct value of the mass moment of inertia of the support plate, we must consider the three holes and not to include them in the calculation. To perform this, we need to subtract the mass moment of inertia of three holes from the mass moment of inertia of the solid plate in figure 4.18. We can consider the holes as disks and calculate the mass moment of inertia for one hole by equation 4.17.

$$I_{Disk} = \frac{1}{2} m r^2 \tag{4.17}$$

Where:

- *m* is the mass of disk (hole in our case)
- *r* is the radius of disk.

The final equation form used to calculate the mass moment of inertia of the support plate is:

$$I_P = \frac{m_{solid-plate}}{12}\left[a^2 + b^2\right] - 3\left[\frac{1}{2} m_{1-hole}\, r_{hole}{}^2\right] \tag{4.18}$$

Where:

- $m_{solid\text{-}plate}$ is the mass of plate without holes
- $m_{1\text{-}hole}$ is the mass of one hole
- a, b are the length and height of the solid plate
- r_{hole} is the radius of one hole (0.0625 in = 1.5875 x 10^{-3} m)

The mass of the support plate (m_{plate}) was measured to be (0.6 x 10^{-3} kg) from table 4.4. However, $m_{solid\text{-}plate}$ and $m_{1\text{-}hole}$ need an extra work to be found.

$$m_{plate} = m_{solid-plate} - m_{3-holes} \tag{4.20}$$

Where:

- m_{plate} is the mass of the plate with the three holes (measured)
- $m_{solid\text{-}hole}$ is the mass of the solid plate (without holes)
- $m_{3\text{-}hole}$ is the mass of the three holes

Equation (4.20) is equivalent to equation 4.21:

$$\rho V_{plate} = \rho V_{solid-plate} - \rho V_{3-holes} \tag{4.21}$$

Where:

- V_{plate} is the volume of the support plate with the three holes
- $V_{solid\text{-}plate}$ is the volume of the solid plate (without holes)
- $V_{3\text{-}hole}$ is the volume of the three holes

- ρ is the material density

Since the density is constant, equation 4.21 becomes:

$$V_{plate} = V_{solid-plate} - V_{3-holes} \tag{4.22}$$

Referring to dimensions in figure 4.20, the volumes can be calculated as follows:

$$V_{solid-plate} = (c)(b)(a) \tag{4.23}$$

$$V_{3-holes} = 3\left[\left(\frac{\pi}{4}\right)(d)^2(c)\right] \tag{4.24}$$

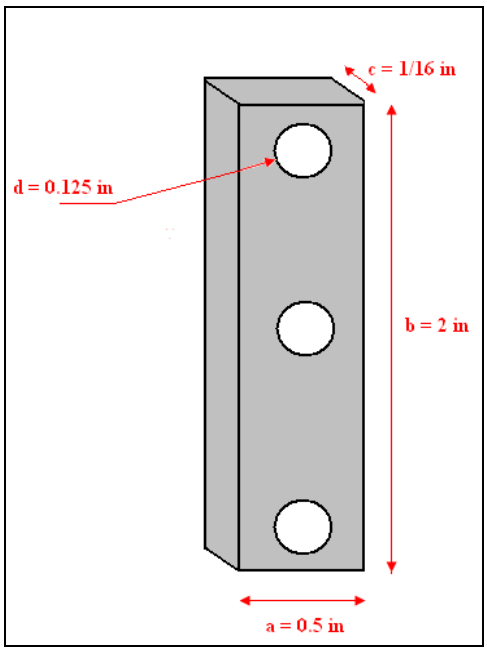

Figure 4.20 Support plate with dimensions

Substituting the values, we get:

$$V_{plate} = \left[\left(\frac{1}{16}in\right)(2in)(0.5in)\right] - 3\left[\left(\frac{\pi}{4}\right)(0.125in)^2\left(\frac{1}{16}in\right)\right]$$

V_{plate} = 60.199 x 10^{-3} in^3

= 9.865 x 10^{-7} m^3

Now, the density can be calculated as:

$$\rho = \frac{m_{plate}}{V_{plate}} \tag{4.25}$$

Substituting the values, we get:

$$\rho = \frac{0.6 \text{ x } 10^{-3}\ kg}{9.865 \text{ x } 10^{-7}\ m^3} = 608.2 \frac{kg}{m^3}$$

Now we can calculate all masses as follows:

$$m_{solid-plate} = \rho\ V_{solid-plate} \tag{4.26}$$

Substituting the values, we get:

$$m_{solid-plate} = \left(608.2 \frac{kg}{m^3}\right)\left[\left(\frac{1}{16} in\right)(2\,in)\,(0.5\,in)\,x\left(\frac{0.0254\,m}{in}\right)^3\right]$$

$m_{solid\text{-}plate}$ = 6.23 x 10^{-4} kg

$$m_{1-hole} = \rho V_{1-hole} \tag{4.27}$$

$$m_{3-holes} = \rho V_{3-holes} \tag{4.28}$$

Substituting the values, we get:

$$m_{1-hole} = \left(608.2 \frac{kg}{m^3}\right)\left[\left(\frac{\pi}{4}\right)(0.125\,in)^2\left(\frac{1}{16} in\right)\,x\left(\frac{0.0254\,m}{in}\right)^3\right]$$

$m_{1\text{-}hole}$ = 7.64 x 10^{-6} kg

$$m_{3-holes} = \left(608.2 \frac{kg}{m^3}\right)\,x3\left[\left(\frac{\pi}{4}\right)(0.125\,in)^2\left(\frac{1}{16} in\right)\,x\left(\frac{0.0254\,m}{in}\right)^3\right]$$

$m_{3\text{-}holes} = 2.29 \times 10^{-5}$ kg

Now we have all values to substitute into equation (4.18).

- $m_{solid\text{-}plate} = 6.23 \times 10^{-4}$ kg
- a = 0.5 in = 12.7×10^{-3} m
- b= 2 in = 50.8×10^{-3} m
- $m_{1\text{-}hole} = 7.64 \times 10^{-6}$ kg
- r_{hole} = 0.0625 in = 1.5875×10^{-3} m

Substituting the above values into equation (4.18), we get:

$$I_P = \frac{6.23 \times 10^{-4}}{12}\left[\left(12.7 \times 10^{-3}\right)^2 + \left(50.8 \times 10^{-3}\right)^2\right] - 3\left[\frac{1}{2}\left(7.64 \times 10^{-6}\right)\left(1.5875 \times 10^{-3}\right)^2\right]$$

$I_P = 1.4232 \times 10^{-7}$ kg.m^2

4.2.2.3 Mass moment of inertia of a bolt:

A bolt can be assumed as a solid cylinder.

The mass moment of inertia of a solid cylinder is given by:

$$I_{solid\ cylinder} = \frac{m}{2} r^2 \qquad (4.29)$$

Where:

- m is the mass of solid cylinder
- r is the radius
- h is the height of solid cylinder

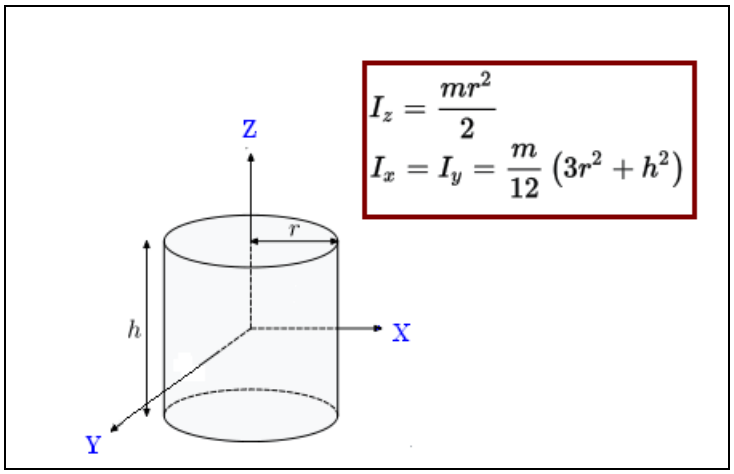

Figure 4.21 Mass moment of inertia of a solid cylinder

The internal thread of the bolt (female) is neglected and only the main external thread is considered in calculation.

The mass moment of inertia of the bolt can be given by:

$$I_{bolt} = \frac{m}{2} r^2 \tag{4.30}$$

Where:

- m is the mass of one bolt (0.4×10^{-3} kg)
- r is the radius of the bolt (0.0625 in = 1.5875×10^{-3} m)

Substituting the above values into equation (4.30), we get:

$I_{bolt} = 5.0403 \times 10^{-10}$ kg.m^2

4.2.2.4 Mass moment of inertia of a hex nut:

A hex nut can be assumed as a thick-walled cylindrical tube with open ends as shown in figure 2.22.

The mass moment of inertia of a thick-walled cylindrical tube with open ends is given by:

$$I = \frac{m}{2}\left[a^2 + b^2\right] \tag{4.31}$$

Where:

- m is the mass
- a is the inner radius
- b is the outer radius
- h is the height of solid cylinder

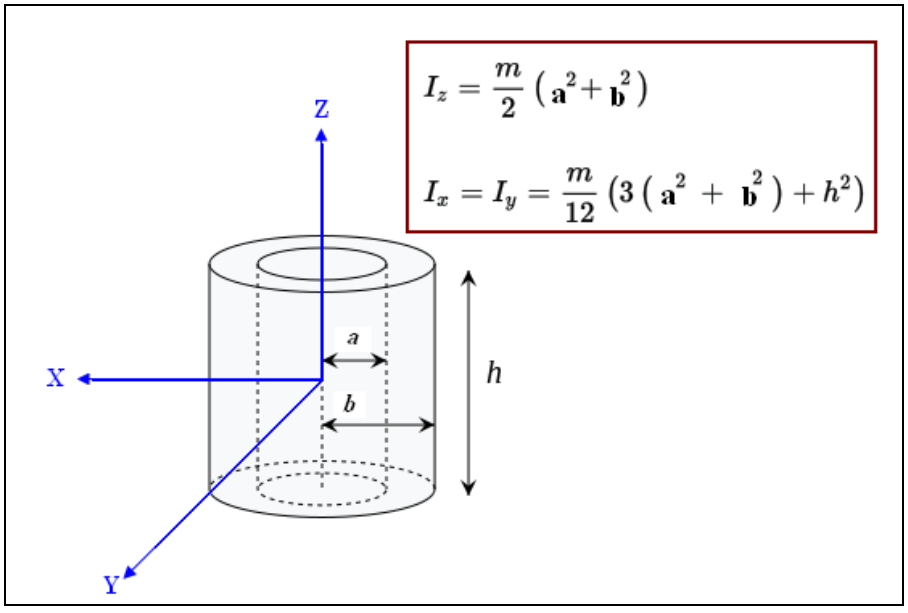

Figure 4.22 Mass moment of inertia of a thick-walled cylindrical tube

The mass moment of inertia of the hex nut can be calculated using equation (4.32):

$$I_{hex\,nut} = \frac{m}{2}\left[a^2 + b^2\right] \tag{4.32}$$

Where:

- m is the mass of the hex nut (0.16×10^{-3} kg)
- a is the inner radius of the hex nut (0.0625 in = 1.5875×10^{-3} m)
- b is the outer radius of the hex nut (0.125 in = 3.175×10^{-3} m)

Substituting the above values into equation (4.32), we get:

$I_{hex\,nut} = 1.008 \times 10^{-9}$ kg.m^2

4.2.2.5 Mass moment of inertia of a torsion spring:

A torsion spring can be considered as a thick-walled cylindrical tube with open ends as shown in figure 4.22.

The mass moment of inertia of the torsion spring can be calculated using equation (4.33):

$$I_{torsion\,spring} = \frac{m}{2}\left[a^2 + b^2\right] \tag{4.33}$$

Where:

- m is the mass of the torsion spring (0.57×10^{-3} kg)
- a is the inner radius of the torsion spring (0.221 in = 5.6134×10^{-3} m)
- b is the outer radius of the torsion spring (0.249 in = 6.3246×10^{-3} m)

Substituting the above values into equation (1.33), we get:

$I_{torsion\,spring} = 2.038 \times 10^{-8}$ kg.m^2

4.2.2.6 Mass moment of inertia of the original airfoil (NACA 0015 airfoil):

For irregular shapes, the mass moment of inertia can be evaluated by using equation (4.11). This could be performed by direct integration, however in some cases, the integration is very complicated and a numerical solution is used as an alternative. Applying equation (4.11) to the function of the NACA 0015 gives undefined answer, alternatively, the mass moment of inertia of NACA 0015 can be calculated by numerical solution.

The first step is to consider the center of gravity location of the wing (X_{cg} = 2.1 in = 0.05334 m) as the origin point. The second step is to split the airfoil into multiple rectangles e.g. (1000 rectangles). Third step is to apply equation (4.34) and perform the summation of all mass moment of inertia of all rectangles. Equation (1.33) is nothing but the parallel axis theorem.

$$I_{cg} = I_1 + m_1 d_1^2 + I_2 + m_2 d_2^2 + I_3 + m_3 d_3^2 + ... + I_n + m_n d_n^2 = \sum_{i=1}^{n} I_i + m_i d_i^2 \qquad (4.34)$$

Where:

- m_i is the mass of each rectangle
- d_i is the distance of each rectangle center of mass to the center of gravity of the airfoil.

m_i and d_i values depend on the instant location of (x,y) on the airfoil. The values of x and y are determined by the NACA 0015 equation (4.5). Shape and mass of each rectangle depend on the value of y, while the distance from the center of gravity of the airfoil depends on x. The width of each rectangle is fixed due the constant increment of x,

however the height changes due to the change in the value of y, which is based on the substituted value of x into equation (4.5).

Figure 4.23 illustrates the numerical solution method for the NACA 0015 airfoil.

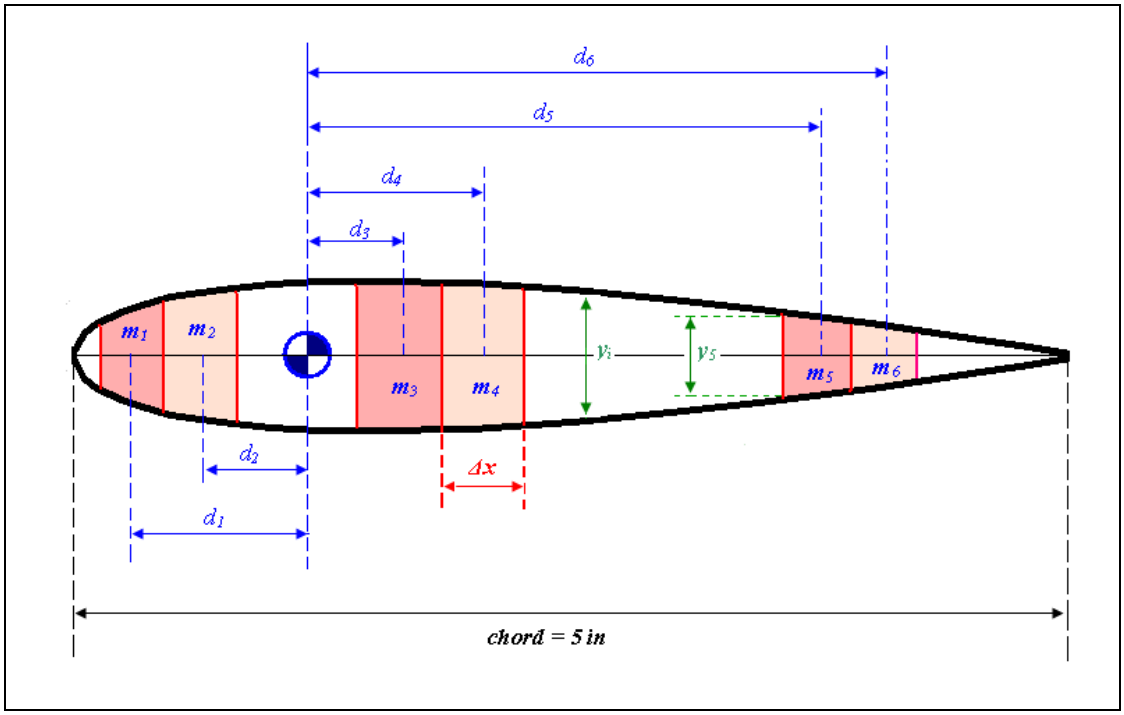

Figure 4.23 The numerical method to calculate mass moment of inertia of airfoil

The mass of each rectangle can be calculated by equation (1.34).

$$m_i = \rho L \Delta x_i \, y_i \tag{4.35}$$

Where:

- m_i is the mass of each rectangle
- ρ is the density of the airfoil material
- L is the airfoil span (12 in)

- $\Delta x_i = \dfrac{chord\ length\,(c)}{\#\ of\ segments}$

- y_i is the height of each rectangle and it is given by equation (4.36).

$$y_i = 2*5(15*c/100)\left[0.2969\sqrt{\frac{\Delta x_i}{c}} - 0.126\left(\frac{\Delta x_i}{c}\right) - 0.3516\left(\frac{\Delta x_i}{c}\right)^2 + 0.2843\left(\frac{\Delta x_i}{c}\right)^3 - 0.1015\left(\frac{\Delta x_i}{c}\right)^4\right] \tag{4.36}$$

The calculation is completed by a MATLAB code that was generated to solve the above problem. This code is in appendix C.

The mass moment of inertia of the original wing itself is:

$I_{airfoil}$ = 1.7122 x 10^{-5} kg.m^2

Now after finding all mass moment of inertia of individual parts of the wing, we can find the total mass moment of inertia about the center of gravity I_{CG} by applying the parallel axis theorem in equation (4.13). All distances from X_{CG} are illustrated in figure 4.14.

$$\begin{aligned} I_{CG} = {} & I_{airfoil} + m_{airfoil}\, d^2_{airfoil-CG} + 2\left[I_p + m_p\, d^2_{p-CG}\right] + \\ & + 2\left[I_{bolt} + m_{bolt}\, d^2_{forward\ bolt-CG}\right] + 2\left[I_{bolt} + m_{bolt}\, d^2_{aft\ bolt-CG}\right] + \\ & + 2\left[I_{hex\ nut} + m_{hex\ nut}\, d^2_{hex\ nut-CG}\right] + 2\left[I_{torsion\ spring} + m_{torsion\ spring}\, d^2_{torsion\ spring-CG}\right] + \\ & + 4\left[I_{tension\ spring} + m_{tension\ spring}\, d^2_{tension\ spring-CG}\right] \end{aligned} \tag{4.37}$$

All terms in equation 4.37 have been evaluated previously except the distance between the X_{CG} and the center of mass of the tension spring ($d_{tension\ \ spring\text{-}XG}$). Figure 4.24 illustrates how it is evaluated by applying the Pythagorean theorem.

$$d_{tension\ spring-CG} = \sqrt{3.125^2 + 0.478^2} = 3.161 \text{ in}$$

$$= 0.0803 \text{ m}$$

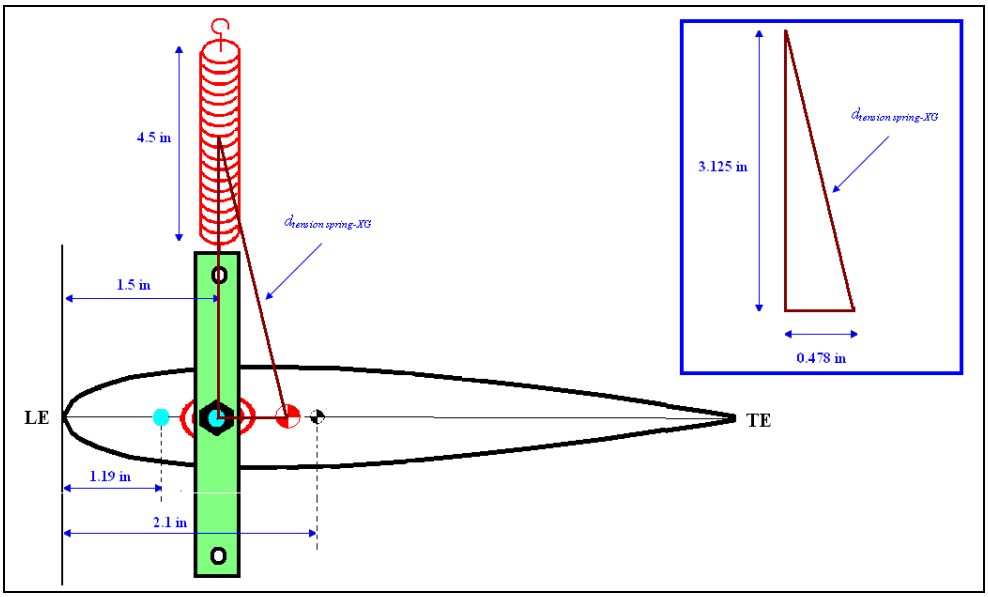

Figure 4.24 Distance between X_{CG} and center of mass of tension spring (1st experimental set-up)

Mass moments of inertia, masses and distances from X_{CG} for all objects are summarized in table 4.7 and 4.8.

Table 4.7 Mass moments of inertias, masses and distances from X_{CG} for different objects (1st experimental set-up)

Object	I (kg.m^2)	m (kg)	d (m)
NACA 0015 airfoil	1.7122×10^{-5}	18.81×10^{-3}	0.0031
Plate support	1.4232×10^{-7}	0.6×10^{-3}	0.0121
Forward bolt	5.0403×10^{-10}	0.4×10^{-3}	0.0200
Aft bolt	5.0403×10^{-10}	0.4×10^{-3}	0.0121
Hex nut	1.008×10^{-9}	0.16×10^{-3}	0.0121
Torsion spring	2.038×10^{-8}	0.57×10^{-3}	0.0121

Table 4.8 Mass moments of inertias, masses and distances from X_{CG} for various tension springs (1st experimental set-up)

Tension spring #	I (kg.m^2)	Mass (kg)	d (m)
# 1	1.4619 x 10^{-5}	13.24 x 10^{-3}	0.0803 m
# 2	1.2475 x 10^{-5}	11.34 x 10^{-3}	
# 3	1.4015 x 10^{-5}	12.74 x 10^{-3}	
# 4	5.0840 x 10^{-5}	44.83 x 10^{-3}	
# 5	3.2379 x 10^{-5}	29.2 x 10^{-3}	
# 6	3.2667 x 10^{-5}	29.46 x 10^{-3}	

Substituting values from tables 4.7 and 4.8 into equation (4.37), the total mass moments of inertia about the center of gravity for various tension spring types are tabulated in table 4.9.

Table 4.9 Mass moments of inertias about the center of gravity for various tension springs (1st experimental set-up)

Tension spring #	I_{CG} (kg.m^2)
# 1	4.2088 x 10^{-4}
# 2	3.6084 x 10^{-4}
# 3	4.0311 x 10^{-4}
# 4	0.0014
# 5	9.0109 x 10^{-4}
# 6	9.0895 x 10^{-4}

4.2.3 Mass moment of inertia about the elastic axis:

After all mass moments of inertia about the center of the gravity for various tension springs were evaluated in previous section, it is straightforward to find the mass moments of inertia about the elastic axis by applying the parallel axis theorem in equation (4.38).

$$I_{\alpha} = I_{CG} + m\,d^2 \tag{4.38}$$

Where:

- I_{α} is the mass moment of inertia about the elastic axis
- m is the total mass of the wing including all parts attached
- d is the distance between the center of gravity (X_{CG}) and the elastic axis (X_e) (figure 4.10)

$$d = X_{CG} - X_e \tag{4.39}$$

d = 1.978 in – 1.5 in = 0.478 in

d = 0.0121 m

We have two cases for the mass. One case is when $\left(\frac{1}{3}\right)$ of tension spring mass is included; and the other case is when it is not included. This would affect the value of I_{α}. The evaluation of I_{α} for both cases is presented in the next section

4.2.3.1 Mass moment of inertia about the elastic axis without inclusion of tension spring mass:

When the mass of the tension spring is neglected, then the mass of the wing remains the same. It includes all attached parts except the tension spring, such that (m = 0.0231 kg)**.**

Substituting into equation (4.38), we get the mass moments of inertia about the elastic axis for various tension springs in the case of not including the tension spring mass to the wing mass.

Table 4.10 Mass moments of inertias about elastic axis for various tension springs in case of not including the tension spring mass to the wing mass (1st experimental set-up)

Tension spring #	I_α (kg.m^2)
# 1	4.2428 x 10^{-4}
# 2	3.6424 x 10^{-4}
# 3	4.0651 x 10^{-4}
# 4	0.0014
# 5	9.0449 x 10^{-4}
# 6	9.1235 x 10^{-4}

4.2.3.2 Mass moment of inertia about the elastic axis with inclusion of one-third of tension sprig mass:

The mass moments of inertia about the elastic axis for various tension springs in the case of including $\left(\frac{1}{3}\right)$ of the tension spring mass to the wing mass are tabulated in table 4.11.

Table 4.11 Mass moments of inertias about elastic axis for various tension springs in case of including $\left(\frac{1}{3}\right)$ of the tension spring mass to the wing mass (1st experimental set-up)

Tension spring #	I_α (kg.m^2)
# 1	4.2688 x 10^{-4}
# 2	3.6647 x 10^{-4}
# 3	4.0902 x 10^{-4}
# 4	0.0014
# 5	9.1023 x 10^{-4}
# 6	9.1815 x 10^{-4}

By comparing the change in the values of the mass moments of inertia in both cases, we note that adding $\left(\frac{1}{3}\right)$ of the tension spring mass does not make a big change in the value of (I_α), the maximum difference between the two values does not exceed (0.18%) which can be neglected.

4.2.4 Radius of gyration about the elastic axis (r_α):

The radius of gyration about the elastic axis is introduced as a non-dimensional radius given by equation (4.40),

$$r_\alpha = \sqrt{\frac{I_\alpha}{m\,b^2}} \tag{4.40}$$

Where:

- I_α is the mass moment of inertia about the elastic axis
- m is the mass of the wing
- b is the half-chord length ($b = \frac{c}{2} = \frac{5\,in}{2} = 2.5\,in = 0.0635\,m$)

4.2.5 Mass ratio (μ):

μ is the mass ratio between the wing mass and the mass of the air around the wing. It is a dimensionless coefficient and given by equation (4.41).

$$\mu = \frac{m}{\pi\,\rho_{air}\,b^2\,L} \tag{4.41}$$

Where:

- m is the mass of the wing
- ρ_{air} is the air density
- L is the wing span (12 in = 0.3048 m)

4.2.6 (x_α):

x_α is the non-dimensional distance of wing center of gravity aft of the elastic axis in (semichords) and given by equation (4.42) and illustrated in figure 1.8.

x_α is positive if and only if the location of the elastic axis is in front of the center of gravity.

$$x_\alpha = \frac{X_{CG} - X_e}{b} = \frac{2d}{c} \tag{4.42}$$

4.2.7 (a_h):

a_h is the non-dimensional distance from center of chord to the elastic axis and given by equation (4.43) and illustrated in figure 4.10.

a_h is positive if and only if the location of the elastic axis is in front of the mid-chord.

$$a_h = \frac{b - X_e}{b} = 1 - \frac{2X_e}{c} \tag{4.43}$$

4.2.8 Uncoupled natural frequency in bending (ω_h):

ω_h is in radian per second and given by equation 4.44.

$$\omega_h = \sqrt{\frac{K_h}{m}} \tag{4.44}$$

Where:

- K_h is the tension spring constant in (N/m)
- m is the mass of the wing

4.2.9 Uncoupled natural frequency in torsion (ω_α):

ω_α is in radian per second and given by equation 4.45.

$$\omega_\alpha = \sqrt{\frac{K_\alpha}{I_\alpha}} \tag{4.45}$$

Where:

- K_α is the torsion spring constant in (N.m)

4.2.10 Ratio of uncoupled natural frequency ($\frac{\omega_h}{\omega_\alpha}$):

$\frac{\omega_h}{\omega_\alpha}$ is an important parameter in the calculation of Theodorsen coefficients. Referring to Theodorsen's paper [9], the flutter speed decreases as the frequency ratio increases until it reaches a value of one. When this ratio is grater than one, the flutter speed increase as $\frac{\omega_h}{\omega_\alpha}$ increases as shown in figure (4.25).

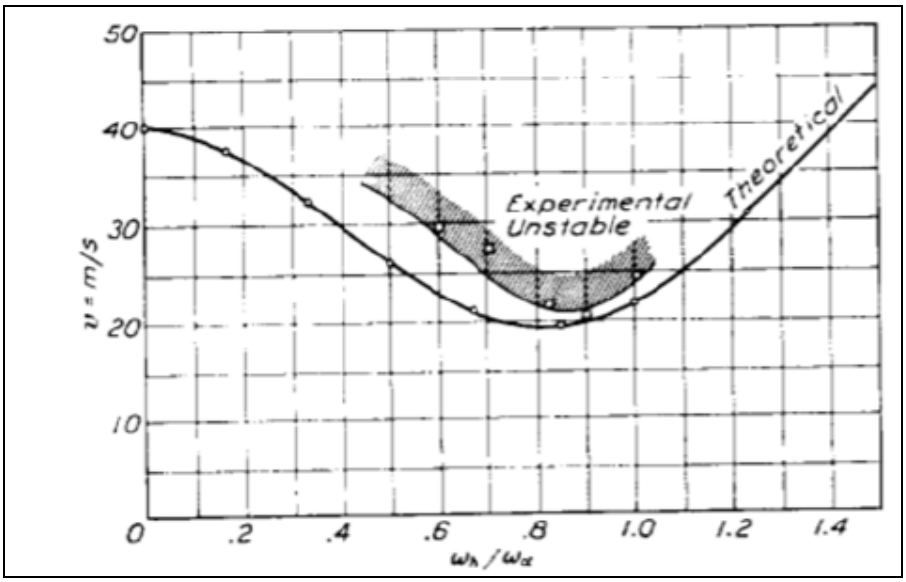

Figure 4.25 Theodorsen analysis of flutter speed against the frequency ratio (reproduced from ref. 5)

By using equations (4.44) and (4.45), the frequencies and their ratio can be evaluated for different tension springs.

The constant k_α for a single torsion spring is given to be 0.552 lbs-in = 0.0624 (N.m), there are two spring mounted in the wing. However, there are four tension springs attached to the wing. The values for every single tension spring constant are tabulated in table 4.2.

We solve one case for tension spring # 1 as an example case:

4.2.10.1 Case of not including the tension spring mass to the wing mass:

It should be remembered for this case that the mass of the wing does not change and it has the value of m = 0.0231 kg

$$\omega_h = \sqrt{\frac{4 * k_h}{m}} = \sqrt{\frac{4 * 17.52}{0.0231}} = 55.0895 \frac{\text{rad}}{\text{s}}$$

$$\omega_\alpha = \sqrt{\frac{2 * k_\alpha}{I_\alpha}} = \sqrt{\frac{2 * 0.0624}{4.2428 \text{ x } 10^{-4}}} = 17.1493 \frac{\text{rad}}{\text{s}}$$

$$\frac{\omega_h}{\omega_\alpha} = \frac{55.0895}{17.1493} = 3.2124$$

Performing calculations for all tension springs, we get:

Table 4.12 Frequency ratio for various tension springs in case of not including the tension spring mass to the wing mass

Tension spring #	k_h *(N/m)*	k_α *(N.m)*	$\omega_h \left(\frac{rad}{s}\right)$	$\omega_\alpha \left(\frac{rad}{s}\right)$	$\frac{\omega_h}{\omega_\alpha}$
# 1	17.52	0.0624	55.0895	17.1493	3.2124
# 2	28.03		69.6833	18.5086	3.7649
# 3	47.3		90.5212	17.5199	5.1668
# 4	213.73		192.4192	9.4293	20.4066
# 5	350.37		246.3676	11.7453	20.9758
# 6	402.93		264.1998	11.6946	22.5915

4.2.10.2 Case of including the $\left(\frac{1}{3}\right)$ of tension spring mass to the wing mass:

The mass of the wing changes for every single tension spring.

$$\omega_h = \sqrt{\frac{4 * k_h}{m}} = \sqrt{\frac{4 * 17.52}{0.0407}} = 41.4717 \frac{\text{rad}}{\text{s}}$$

$$\omega_\alpha = \sqrt{\frac{2 * k_\alpha}{I_\alpha}} = \sqrt{\frac{2 * 0.0624}{4.2688 \text{ x } 10^{-4}}} = 17.0969 \frac{\text{rad}}{\text{s}}$$

$$\frac{\omega_h}{\omega_\alpha} = \frac{41.4717}{17.09969} = 2.4257$$

Performing calculations for all tension springs, we get:

Table 4.13 Frequency ratio for various tension springs in case of including the $\left(\frac{1}{3}\right)$ tension spring mass to the wing mass

Tension spring #	k_h (N/m)	k_α (N.m)	m (kg)	$\omega_h \left(\frac{rad}{s}\right)$	$\omega_\alpha \left(\frac{rad}{s}\right)$	$\frac{\omega_h}{\omega_\alpha}$
# 1	17.52	0.0624	0.0407	41.4717	17.0969	2.4257
# 2	28.03		0.0382	54.1691	18.4522	2.9357
# 3	47.3		0.0401	68.7095	17.4662	3.9339
# 4	213.73		0.0829	101.5732	9.3998	10.8059
# 5	350.37		0.0620	150.3204	11.7083	12.8388
# 6	402.93		0.0624	160.7521	11.6577	13.7893

4.2.11 Results of Theodorsen Solution for Torsion-Tension spring Set-up

At this point, all parameters needed to find the Theodorsen coefficients are available and evaluated. Solving the determinant equation according to the sequence of steps in chapter 2 (section 2.4), we get the curves of $\sqrt{x}$ and the inverse of reduced frequency $\frac{1}{k}$ plotted for both cases (without and with the inclusion of the $\left(\frac{1}{3}\right)$ of tension spring mass) in the following figures.

4.2.11.1 Case of not including the tension spring mass to the wing mass:

4.2.11.1.1 Tension spring type #1

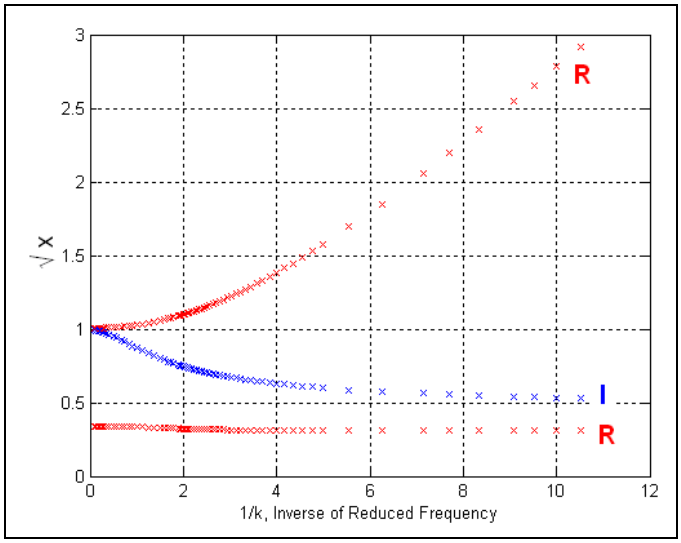

Figure 4.26 Solution of Flutter Determinant using Theodorsen Function for tension spring # 1 (1st setup) for no tension spring mass included

4.2.11.1.2 Tension spring type #2

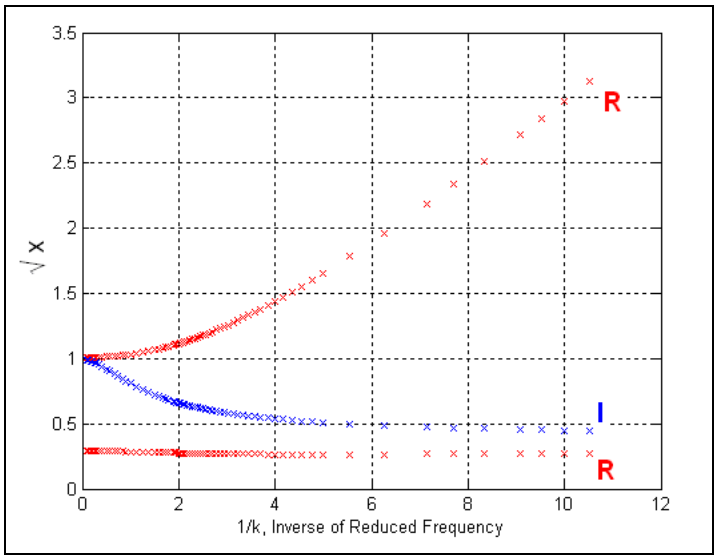

Figure 4.27 Solution of Flutter Determinant using Theodorsen Function for tension spring # 2 (1st setup) for no tension spring mass included

4.2.11.1.3 Tension spring type #3

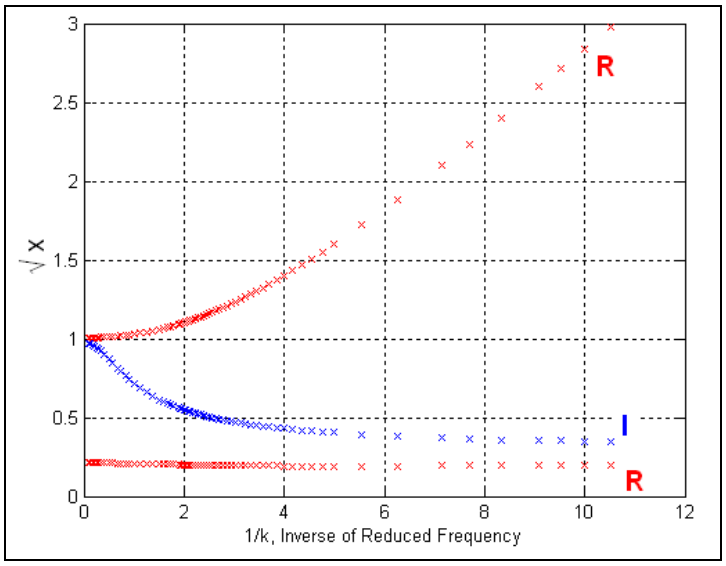

Figure 4.28 Solution of Flutter Determinant using Theodorsen Function for tension spring # 3 (1st setup) for no tension spring mass included

4.2.11.1.4 Tension spring type #4

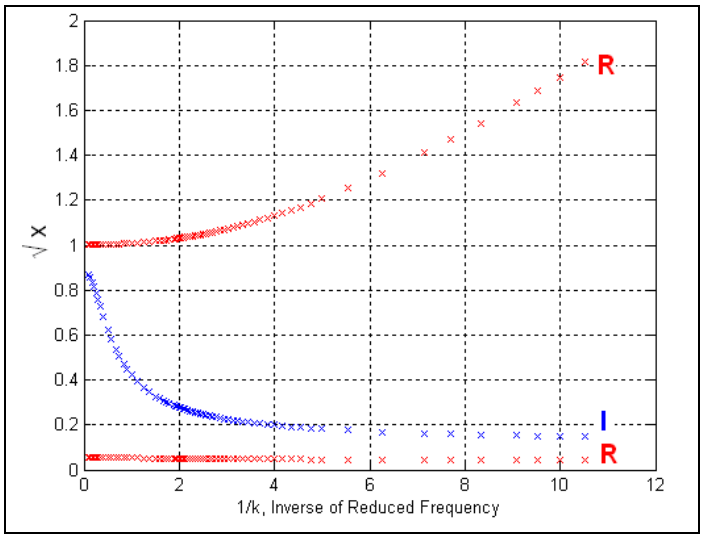

Figure 4.29 Solution of Flutter Determinant using Theodorsen Function for tension spring # 4 (1st setup) for no tension spring mass included

4.2.11.1.5 Tension spring type #5

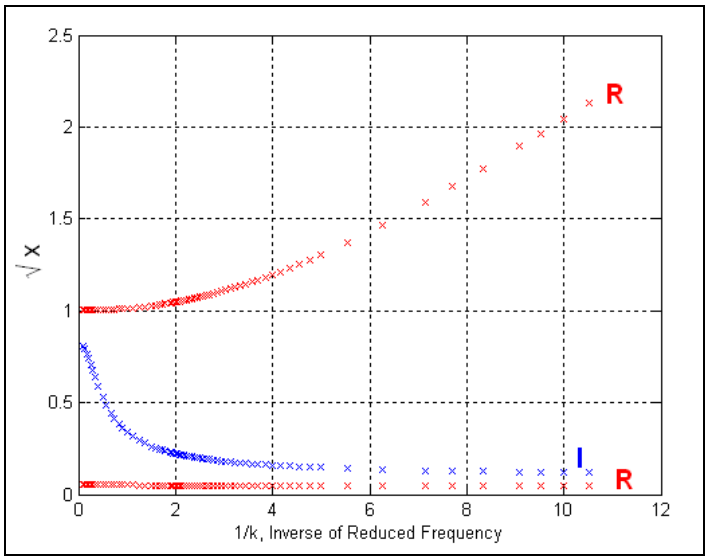

Figure 4.30 Solution of Flutter Determinant using Theodorsen Function for tension spring # 5 (1st setup) for no tension spring mass included

4.2.11.1.6 Tension spring type #6

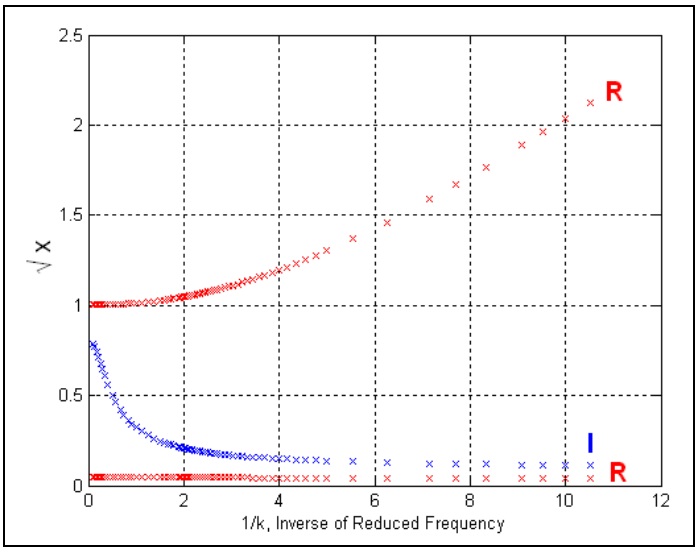

Figure 4.31 Solution of Flutter Determinant using Theodorsen Function for tension spring # 6 (1^{st} setup) for no tension spring mass included

Detailed discussion of the previous figures is provided in section 4.2.11.1.7.

4.2.11.1.7 Remarks on Theodorsen solution in the case of not including the tension spring mass to the wing mass and comparison with the experimental results of first set-up:

The obtained solutions for all tension spring types in figures 4.26, 4.27, 4.28, 4.29, 4.30 and 4.31 show no intersection between the real and imaginary curves of the flutter determinant which means that the Theodorsen solution indicates no flutter occurs in all cases. This result does not agree with the experimental solution where we have seen flutter occur for all different tension spring cases.

Table 4.14 shows comparison between the experiment and the Theodorsen solution in the case of not including the tension spring mass to the wing mass.

Table 4.14 Comparison of torsion-tension set-up experimental results with Theodorsen solution in the case of not including the tension spring mass to the wing mass

Tension spring #	# 1	# 2	# 3	# 4	# 5	# 6
Flutter speed (m/s) (Experimental)	10.2	11.5	13	17.2	16	20
Flutter speed (m/s) (Calculated) $U_F = \frac{1}{k}\frac{\omega_\alpha c}{2\sqrt{x}}$	No Flutter	No Flutter	No Flutter	No Flutter	No Flutter	No Flutter

This disagreement of the solution with the experiment might be due to the large value of frequency ratio (table4.12).

In the next section, $\left(\frac{1}{3}\right)$ of tension spring mass is included to the wing mass calculation for all different sets of tension springs as shown in the following figures.

4.2.11.2 Case of including $\left(\frac{1}{3}\right)$ of the tension spring mass to the wing mass:

4.2.11.2.1 Tension spring type #1

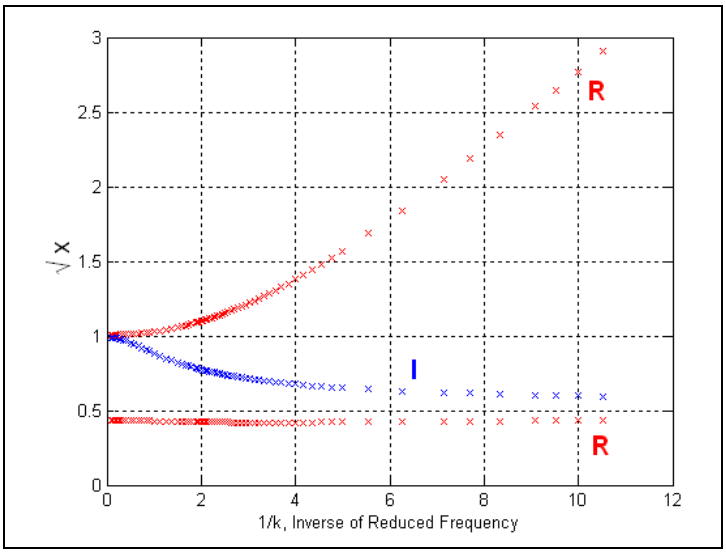

Figure 4.32 Solution of Flutter Determinant using Theodorsen Function for tension spring # 1 (1^{st} setup) for $\left(\frac{1}{3}\right)$ of tension spring mass included

4.2.11.2.2 Tension spring type #2

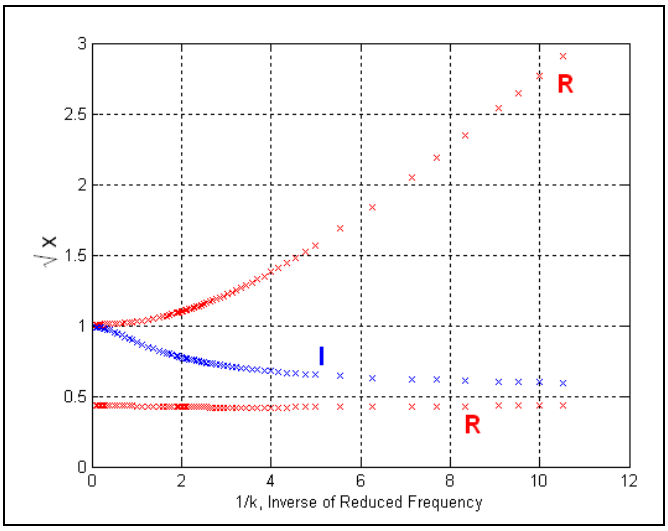

Figure 4.33 Solution of Flutter Determinant using Theodorsen Function for tension spring # 2 (1^{st} setup) for $\left(\frac{1}{3}\right)$ of tension spring mass included

4.2.11.2.3 Tension spring type #3

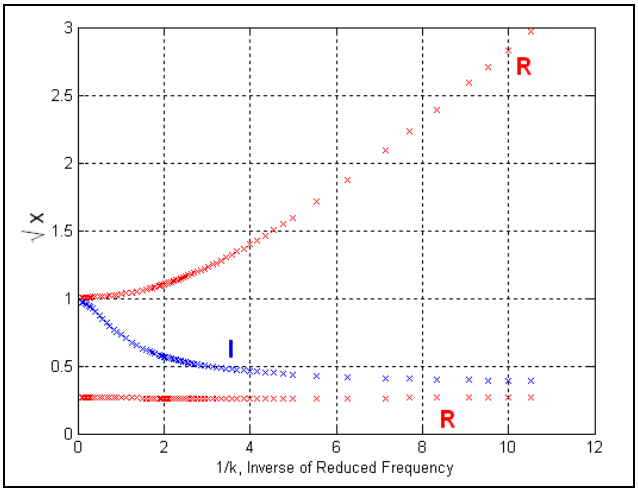

Figure 4.34 Solution of Flutter Determinant using Theodorsen Function for tension spring # 3 (1^{st} setup) for $\left(\frac{1}{3}\right)$ of tension spring mass included

4.2.11.2.4 Tension spring type #4

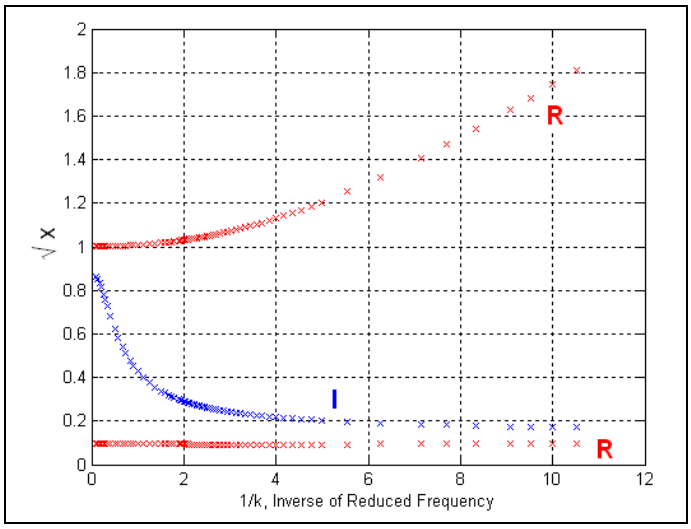

Figure 4.35 Solution of Flutter Determinant using Theodorsen Function for tension spring # 4 (1^{st} setup) for $\left(\frac{1}{3}\right)$ of tension spring mass included

4.2.11.2.5 Tension spring type #5

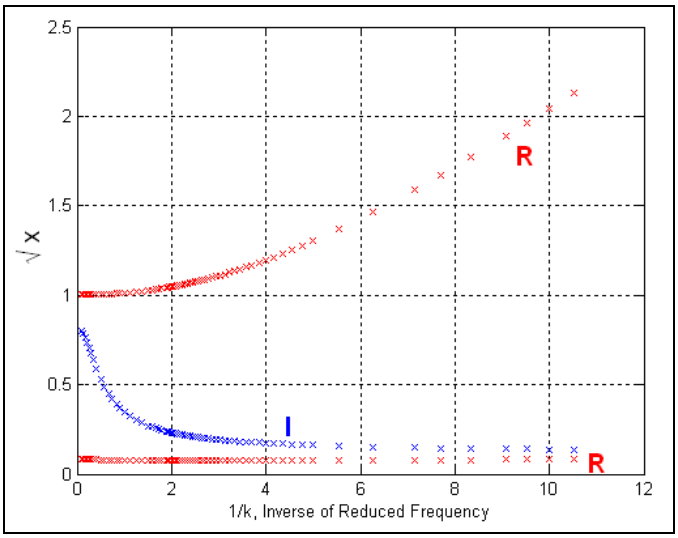

Figure 4.36 Solution of Flutter Determinant using Theodorsen Function for tension spring # 5 (1^{st} setup) for $\left(\frac{1}{3}\right)$ of tension spring mass included

4.2.11.2.6 Tension spring type #6

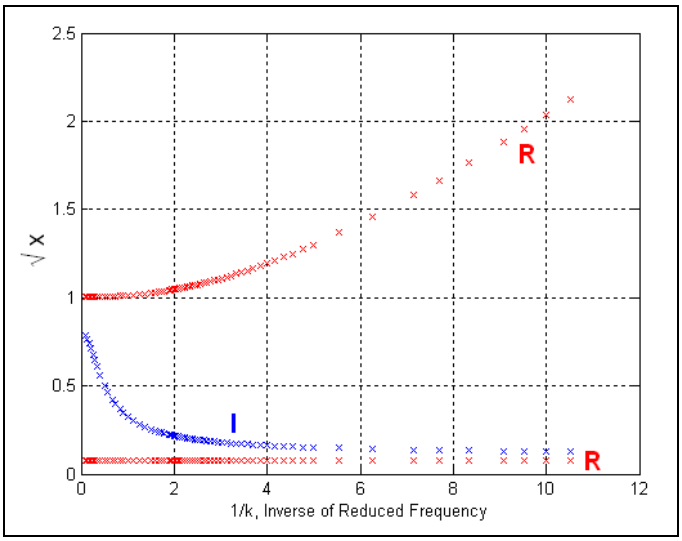

Figure 4.37 Solution of Flutter Determinant using Theodorsen Function for tension spring # 6 (1^{st} setup) for $\left(\frac{1}{3}\right)$ of tension spring mass included

Detailed discussion of the previous figures is provided in section 4.2.11.2.7.

4.2.11.2.7 Remarks on Theodorsen solution in the case of including one-third of the tension spring mass to the wing mass and comparison with the experimental results of first set-up:

The obtained solutions for all tension spring types in figures 4.32, 4.33, 4.35, 4.36, 4.37 and 4.38 are very similar to the solution in figures 4.26, 4.27, 4.28, 4.29, 4.30 and 4.31 respectively. Again, calculations indicate that no flutter occurs in all cases and there is agreement with the experimental results as shown in table 4.15.

Table 4.15 Comparison of torsion-tension set-up experimental results with Theodorsen solution in the case of including $\left(\frac{1}{3}\right)$ of the tension spring mass to the wing mass

Tension spring #	# 1	# 2	# 3	# 4	# 5	# 6
Flutter speed (m/s) (Experimental)	10.2	11.5	13	17.2	16	20
Flutter speed (m/s) (Calculated) $U_F = \frac{1}{k}\frac{\omega_\alpha c}{2\sqrt{x}}$	No Flutter	No Flutter	No Flutter	No Flutter	No Flutter	No Flutter

The inclusion of the mass of tension spring and the large value of the frequency ratio parameter were proposed in the previous section to be the reason for having no flutter in the calculated solutions.

The frequency ratio parameter was manipulated with different values and the solution was repeated several times, and it was concluded that the flutter did not occur because of the value of this parameter as was expected.

Figure 4.38 shows flutter occurs when the frequency ratio was fixed to a value of 0.4. The calculated flutter speed was 10.1 m/s.

$$U_F = \frac{1}{k}\frac{\omega_\alpha c}{2\sqrt{x}} = (1.63)\frac{(103.7\frac{rad}{s})(0.127\,m)}{2(1.065)} = 10.1\frac{m}{s}$$

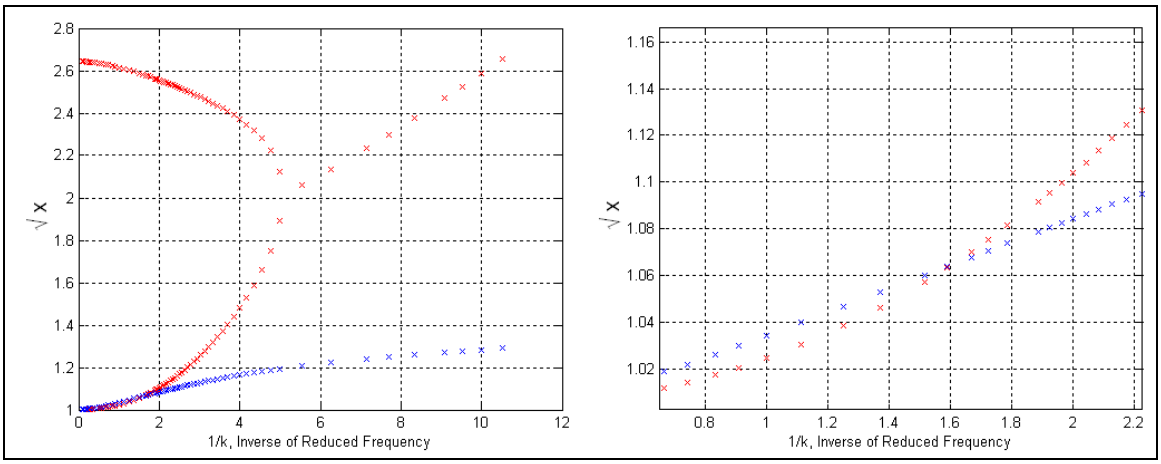

Figure 4.38 Solution of Flutter Determinant using Theodorsen Function for $\frac{\omega_h}{\omega_\alpha} = 0.4$

There was another observation that the curves are very similar in both cases. Looking at the values of frequency ratios in tables 4.12 and 4.13, it is observed that the value increases with almost the same increment for each spring, which is consistent with curves points similarity. This could indicate that the key problem in the solution was the large values of the frequency ratio.

The small torsion spring constant is accountable for the large values of the frequency ratio. It was hard to replace the torsion spring in this experimental set-up as it was mounted in the wing. There were associated problems with using torsion spring in the flutter wing model. It appears that the mathematical model does not in this case accurately model the true physics. In order for the ratio $\frac{\omega_h}{\omega_\alpha} = 0.4$, the torsion spring

constant would have to be considerably greater than the value provided by the supplier; this leads to a conclusion that the torsion spring was not linear. Flutter was observed experimentally but was not confirmed by calculation. For this reason and to avoid any complexities associated with the torsion spring, it was our primary goal to build and use a second experimental flutter model with no torsion springs.

CHAPTER 5

Second Experimental Set-up Results and Comparison with Theodorsen Solution

In this chapter, the experimental results for the second experimental set-up will be tabulated and compared with the calculated values from Theodorsen Function.

All experimental results belonging to the Red wing only are considered and discussed in this chapter. The experimental results for the other wings can be found in appendix A.

5.1 Tension-Tension spring Set-up (2nd Experimental Set-up)

As concluded from the previous chapter, the second experimental set-up with tension springs only was proposed to avoid complexities resulted from mounting the torsion spring to the flutter wing model. This resulted in a disagreement between the experimental results and the numerical solutions provided by the Theodorsen function method.

When only tension springs are used in the flutter model, a fixed spring constant ratio $\frac{K_h}{K_\alpha}$ will result, and $\frac{\omega_h}{\omega_\alpha}$ is then only influenced by the mass and the mass moment of inertia.

$$\frac{\omega_h}{\omega_\alpha} = \frac{\sqrt{\frac{K_h}{m}}}{\sqrt{\frac{K_\alpha}{I_\alpha}}} = \sqrt{\frac{K_h}{K_\alpha}} * \sqrt{\frac{I_\alpha}{m}} \tag{5.1}$$

The value of $\frac{K_h}{K_\alpha}$ is fixed and can be varied by trial and error to find the best value for $\frac{\omega_h}{\omega_\alpha}$ that matches calculations with the corresponding experimental results.

The change in the value of mass moment of inertia (I_α) is small for all cases, however the change in mass (m) is more dominant and could give a better explanation of mass influence on the frequency ratio, which makes the calculated results match the experimental results.

Therefore $\frac{\omega_h}{\omega_\alpha}$ is mainly a function of mass such that,

$$\frac{\omega_h}{\omega_\alpha} = f(m) \tag{5.2}$$

However, the frequency ratio is not the only effective parameter in the calculation. The value of natural frequency in torsion ω_α which depends on the value of spring constant is also involved in the equation that determines the flutter speed.

When the comparison of the calculated results with experiment is complete, it is easier to judge the influence of tension spring mass and spring constant on the flutter speed and derive an empirical formula that relates them to the flutter speed (or with each other if possible).

The second experimental flutter model under investigation is defined by independent two degrees of freedom, which are selected to be the vertical displacement (plunge), h, and the rotation (pitch), α. The plunge and pitch forces and moments are obtained by a set of eight tension springs as shown in figure 5.1.

Using similar tension springs would provide the rotation at the mid-point between the forward and aft tension springs; this rotation results in the effect of a torsion spring.

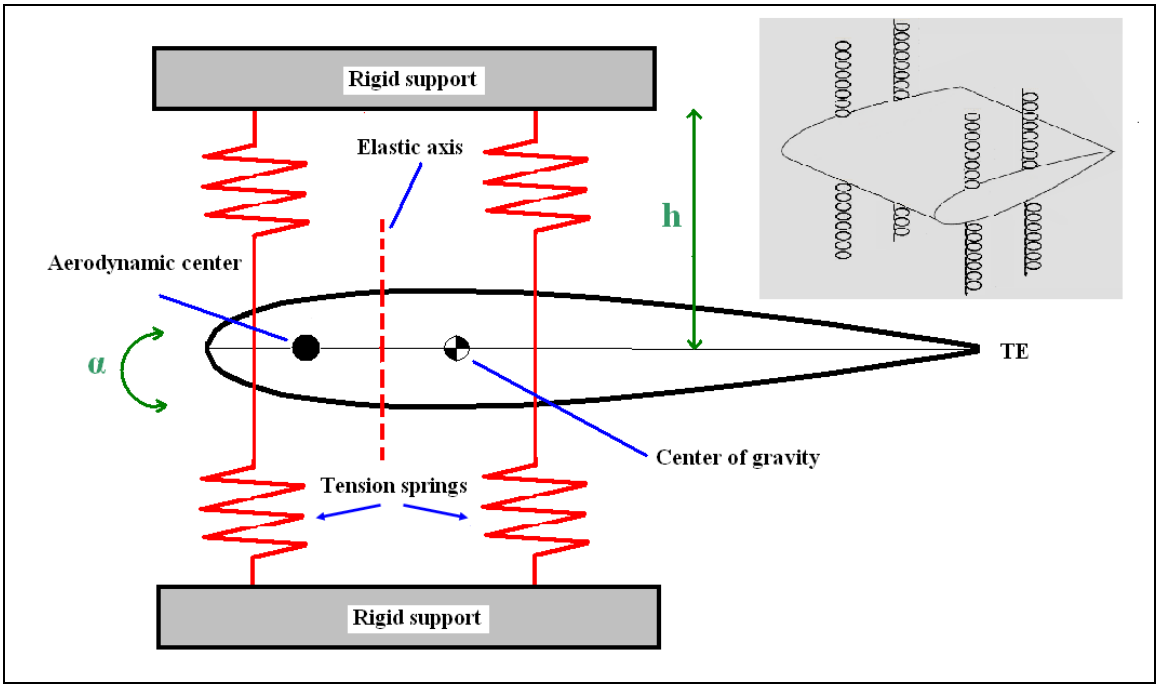

Figure 5.1 Second experimental set-up with eight tension springs

The wing technical data are given in table 5.1.

Table 5.1 Red wing technical data

Airfoil type	NACA 0015 (Red wing)
Weight of airfoil itself	11.51×10^{-3} (kg)
Weight of wing section	18.27×10^{-3} (kg)

Where the weight of wing section includes the weight of all components mounted into the airfoil as follows:

- Original wing (airfoil) = 11.51×10^{-3} kg
- Side Cap airfoil (plywood material) = $2 \times (2.1 \times 10^{-3}$ kg)
- Four plate supports (plywood material) = $4 \times (0.64 \times 10^{-3}$ kg)

Figure 5.2 Parts mounted in the Red wing

The Red wing while being tested in the wind tunnel as shown in figure 5.3.

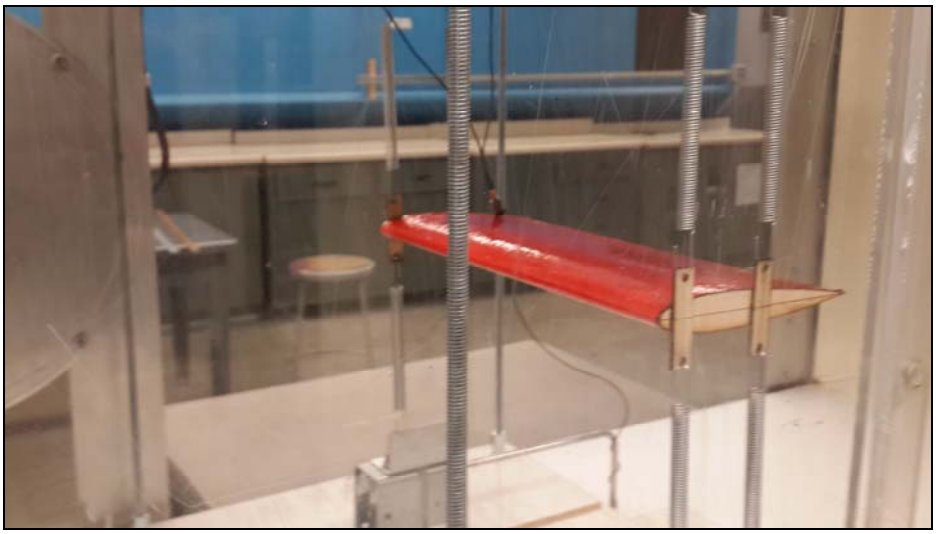

Figure 5.3 Testing the Red wing in the wind tunnel

The experiment was carried out for all six sets of tension spring used in the first experimental set-up. The technical data of all tension springs are given in table 4.2.

The experimental results for the second experimental set-up (tension-tension set-up) for the six sets of tension spring are tabulated in table 5.2.

The same set of apparatus for measuring the flutter speed and the frequency used in the first experimental set up was used again in the second experimental set-up. The flutter speed was measured and indicated automatically by the wind tunnel electronic board panel. However, the frequency was measured in two different ways, by using the electronic stroboscope and by the accelerometer.

The frequencies given in table 5.2 were all measured by using the accelerometer.

Table 5.2 Tension-tension set-up experimental results

Tension spring #	# 1	# 2	# 3	# 4	# 5	# 6
Flutter speed (m/s)	15.5	18.4	23	40.4	26	45
Flutter frequency (Hz)	24.47	31.34	38.7	17.94	25.46	28.97

The following flutter frequency figures were generated using the signal analyzer equipment, which indicates the accelerometer measurements. The maximum peak represents the value of the flutter frequency.

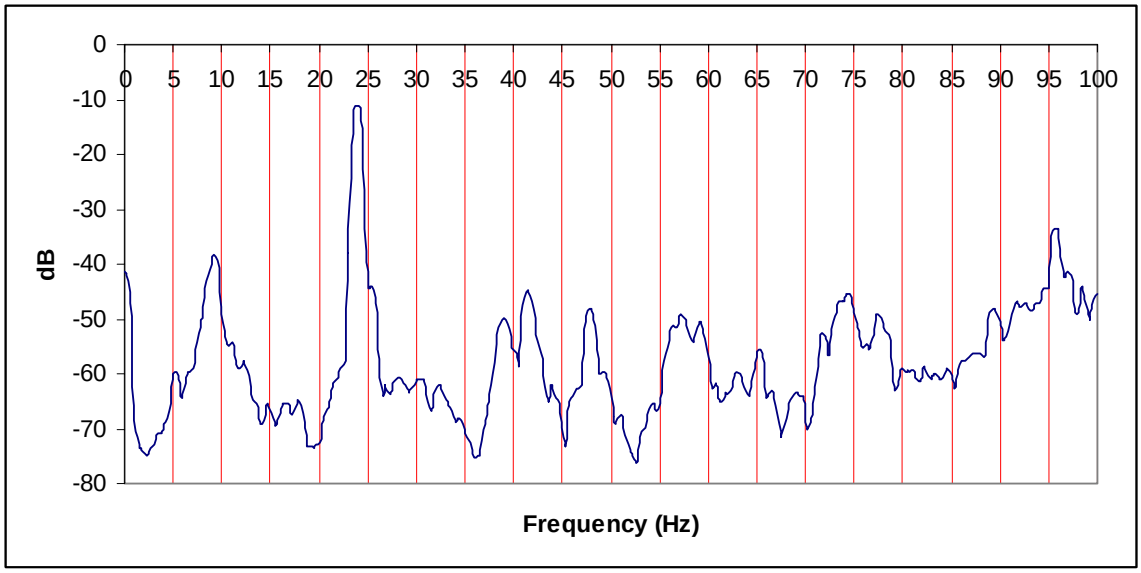

Figure 5.4 Frequency of the Red wing for tension spring # 1 (2nd experimental set-up)

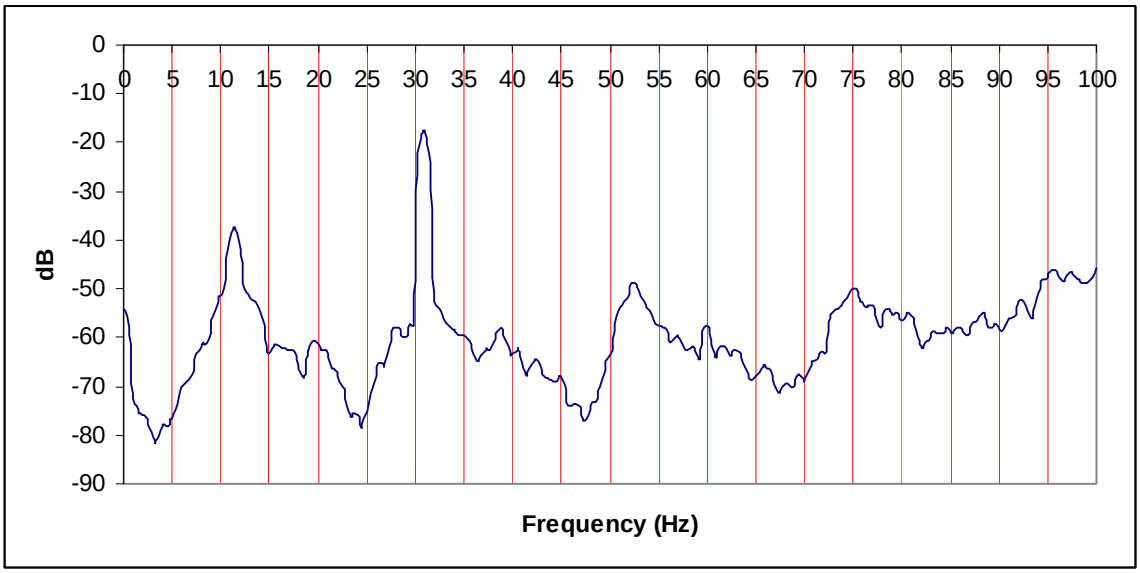

Figure 5.5 Frequency of the Red wing for tension spring # 2 (2nd experimental set-up)

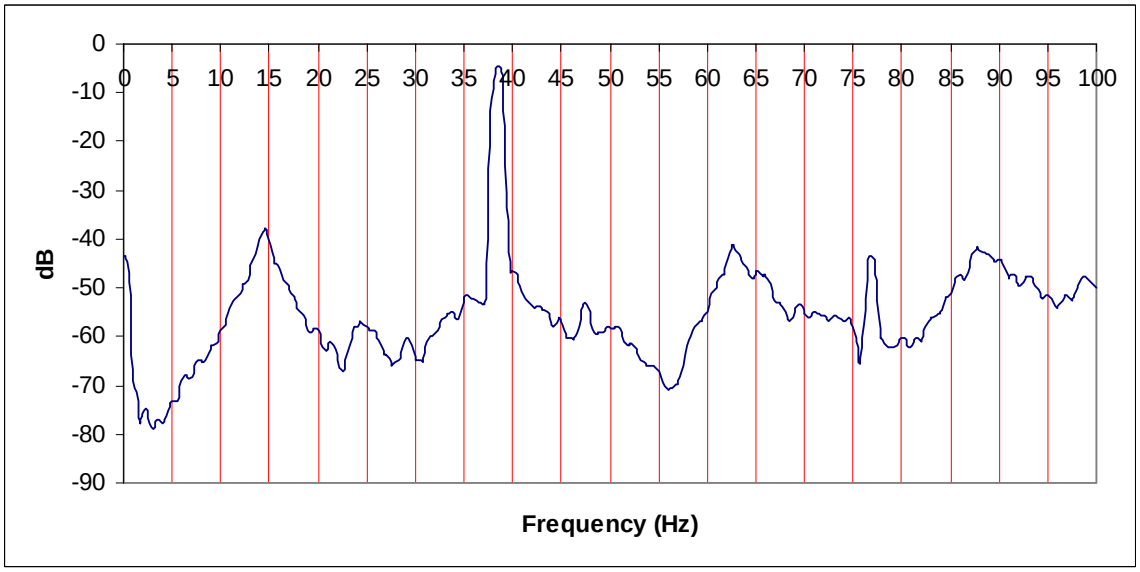

Figure 5.6 Frequency of the Red wing for tension spring # 3 (2nd experimental set-up)

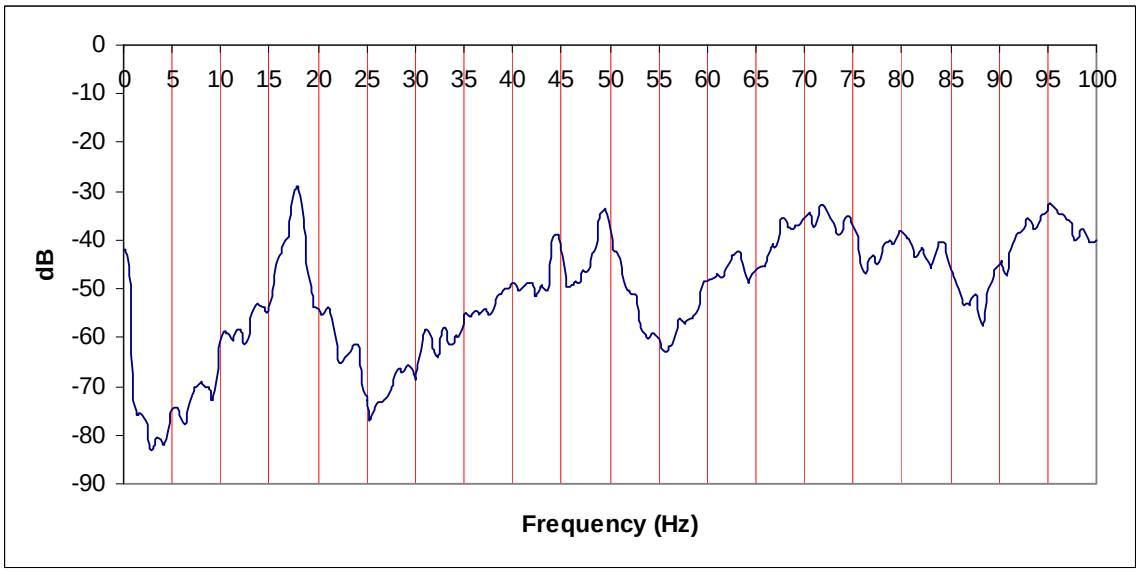

Figure 5.7 Frequency of the Red wing for tension spring # 4 (2nd experimental set-up)

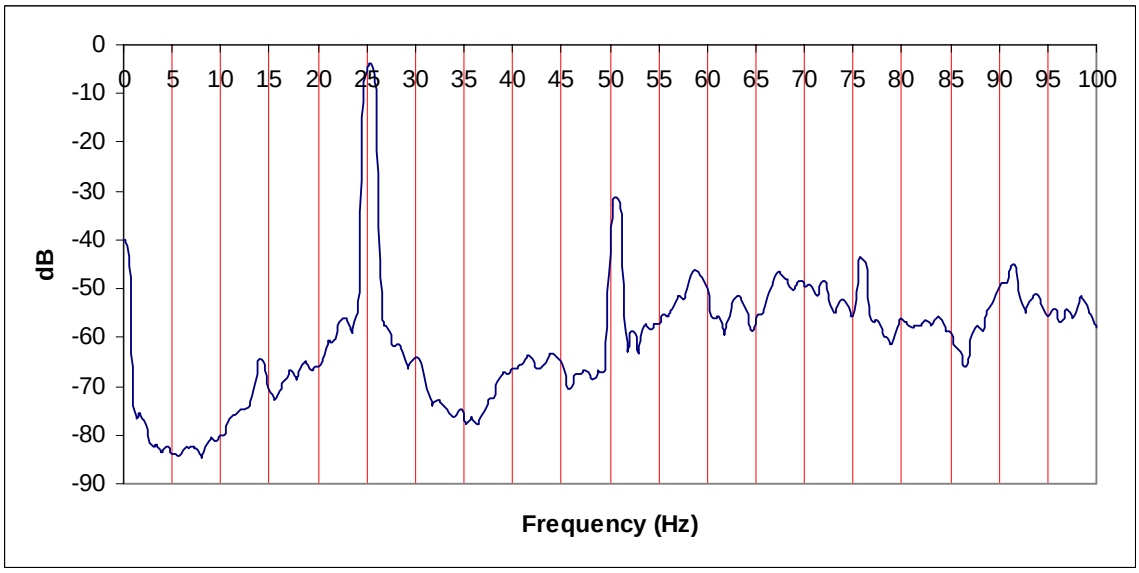

Figure 5.8 Frequency of the Red wing for tension spring # 5 (2nd experimental set-up)

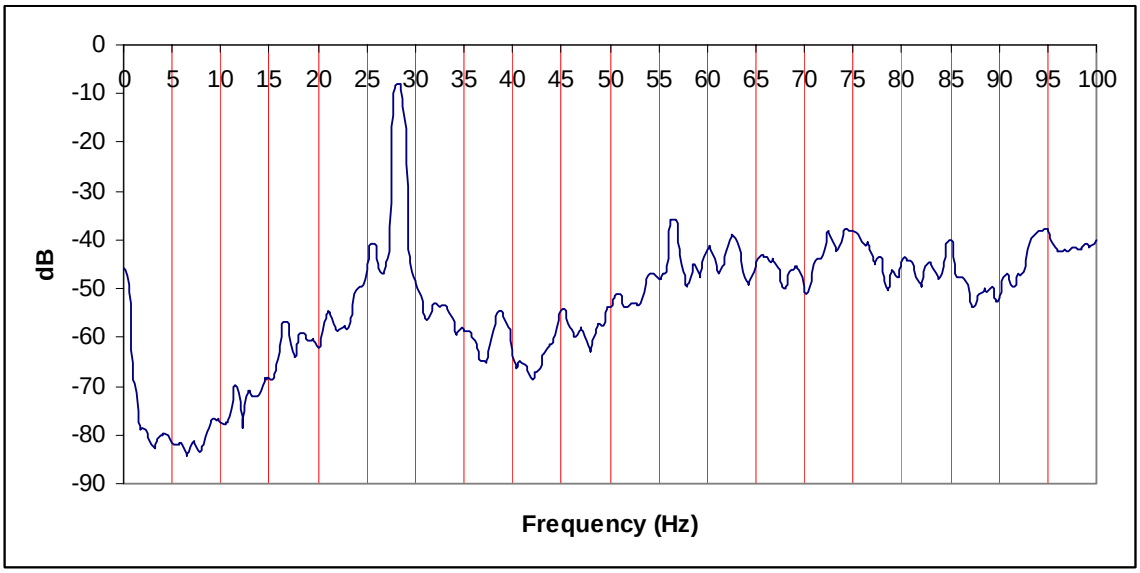

Figure 5.9 Frequency of the Red wing for tension spring # 6 (2nd experimental set-up)

5.1.1 Remarks on the results of Tension-Tension spring Set-up (2nd Experimental Set-up)

The experimental results in table 5.3 show that the flutter speed increased as the spring constant increased which is reasonable from theory. The main purpose is to investigate the impact of the mass of the tension springs on the flutter speed. The masses of spring #1, #2 and #3 are close to each other and as the spring constants of the three springs increase, it was expected to have an increase in the flutter speed.

Spring #4 has the largest mass among all other springs (44.83×10^{-3} kg) and spring constant of (213.73 N/m). If spring #4 is compared with spring #3 which has mass of (12.74×10^{-3}) and spring constant of (47.3 N/m), it would be expected to result in a higher value of flutter speed (40.4 m/s) due to the higher value of spring constant and the larger mass, and this is what was observed.

However, if comparison is made between spring #4 and spring #5 which has a higher spring constant (350.37 N/m) but a lower mass (29.2×10^{-3}) than #4, then we can get an explanation of the effect of spring mass on the flutter speed in both cases. The interesting observation is that the flutter speed is lower with spring #5 in spite of having a higher value of spring constant. This shows the importance of the spring mass and indicates that the spring mass is the responsible parameter for this result.

Similar observations were obtained from the first experimental set-up. This accumulation of knowledge leads to the conclusion that the spring mass plays an important role on airfoil flutter speed. In other words, increasing the spring mass causes an increase in flutter speed.

The flutter frequency in case of spring #4 is the lowest value of (17.94 Hz) among all other spring cases, which supports the above conclusion on the effect of spring mass according to the inverse relation between mass and frequency in equation (5.3).

$$\omega = \sqrt{\frac{K}{m}} \tag{5.3}$$

5.2 Theodorsen Solution for Tension-Tension spring Set-up (2nd Experimental set-up)

In a similar way as in the first experimental set-up, some terms must be evaluated before carrying out the Theodorsen solution. We need to first calculate related quantities like center of gravity (CG), the moment of inertia of all airfoil section about the center of gravity and about the elastic axis. The elastic axis is located at half the distance between the forward and aft springs as long as they have the same spring constant and shape. Figure 5.10 illustrates the nomenclatures of airfoil model parameters.

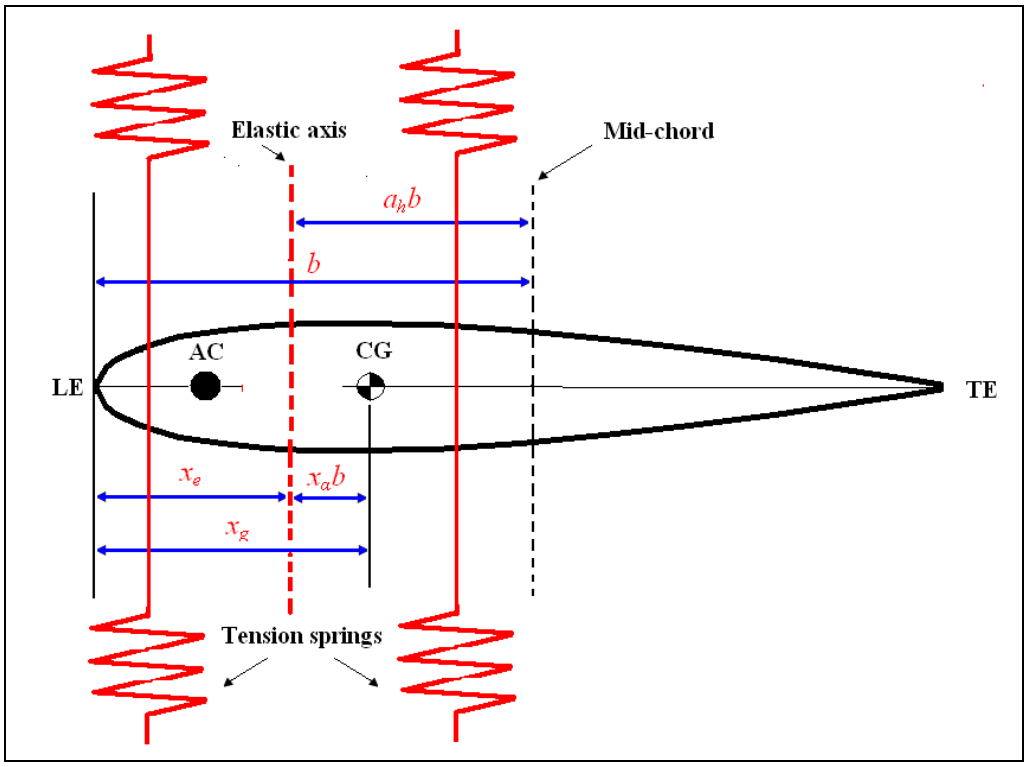

Figure 5.10 nomenclatures of airfoil model parameters of 2nd experimental set-up

5.2.1 Center of gravity:

The center of gravity is given by equation (4.1).

In the second experimental set-up, we have different components as shown in figure 5.11. The weights of different components and distances from leading edge (LE) are tabulated in table 5.3.

Table 5.3 Weights of airfoil components for 2nd experimental set-up

Object	Weight (kg)	Distance from LE (m)
Original wing (airfoil)	11.51×10^{-3} kg	(2.1 in) = 0.05334
Two side cap airfoils	$2 \times (2.1 \times 10^{-3}$ kg)	(2.1 in) = 0.05334
Two forward plate supports	$2 \times (0.64 \times 10^{-3}$ kg)	(0.5 in) = 0.0127
Two aft plate supports	$2 \times (0.64 \times 10^{-3}$ kg)	(2.5 in) = 0.0635

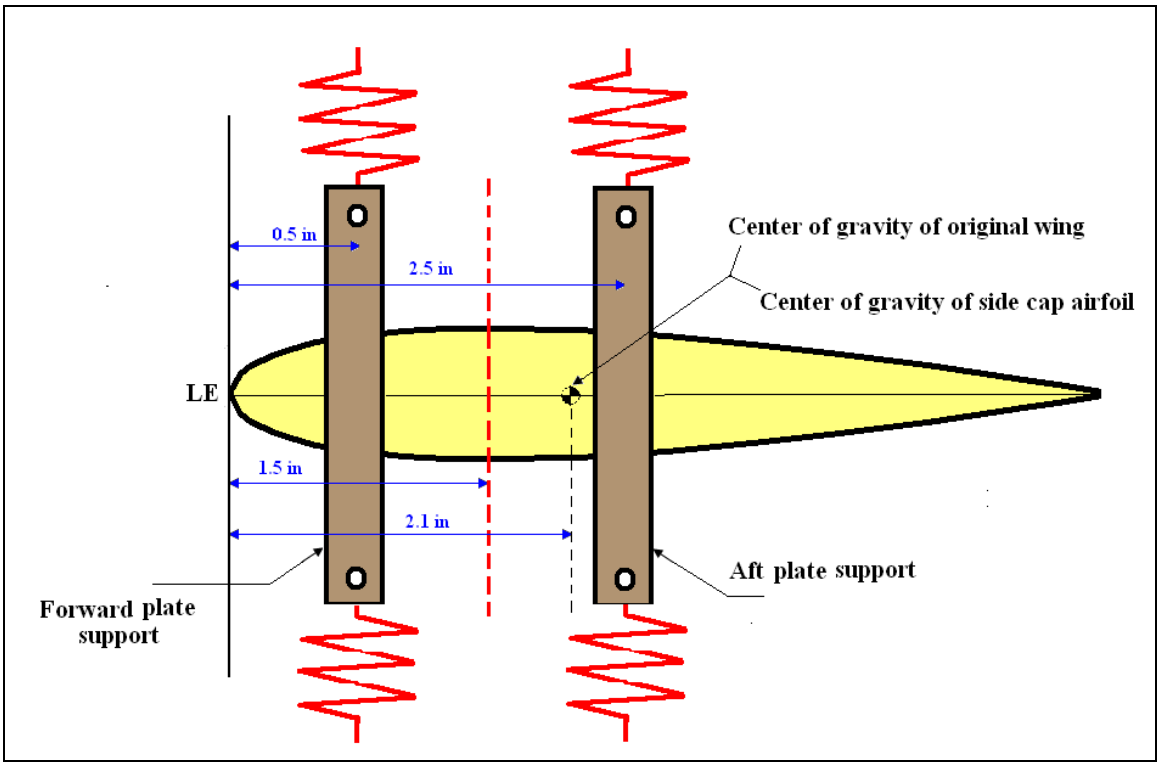

Figure 5.11 Front view of airfoil with different components for 2nd experimental set-up

The method for calculating of the center of the gravity of the original wing and the side cap airfoil was demonstrated in detail in chapter 4.

As long we have the same airfoil type (NACA 0015) with same chord length of (5 in), the center of gravity is the same as calculated for wing in the first experimental set-up.

$X_{cg} = 2.1$ in

$X_{cg\text{-}side\ cap} = 2.1$ in

Now we can use equation (4.1) and calculate the center of gravity of the Red wing model as follows:

$$X_{CG} = \frac{m_w d_w + 2(m_p d_{forward\ plate}) + 2(m_p d_{aft\ plate}) + 2(m_{side\ cap\ wing} d_{side\ cap\ wing})}{m_w + 4(m_p) + 2(m_{side\ cap\ wing})} \qquad (5.4)$$

Substituting the values from tables 5.3, the center of gravity of the whole system (wing) from leading edge is calculated to be:

X_{CG} = 2.0159 in

= 0.0512 m

5.2.2 Mass moment of inertia about center of gravity:

In this section, the mass moment of inertia of every wing component is calculated with respect to the axis of the center of gravity of the wing calculated above (X_{CG} = 2.0159 in). To perform this, we follow the same procedure used in chapter 4 applying equations (4.11), (4.12) and (4.13).

The distances of different components from the center of gravity of whole system (wing) can be determined from figure 5.12.

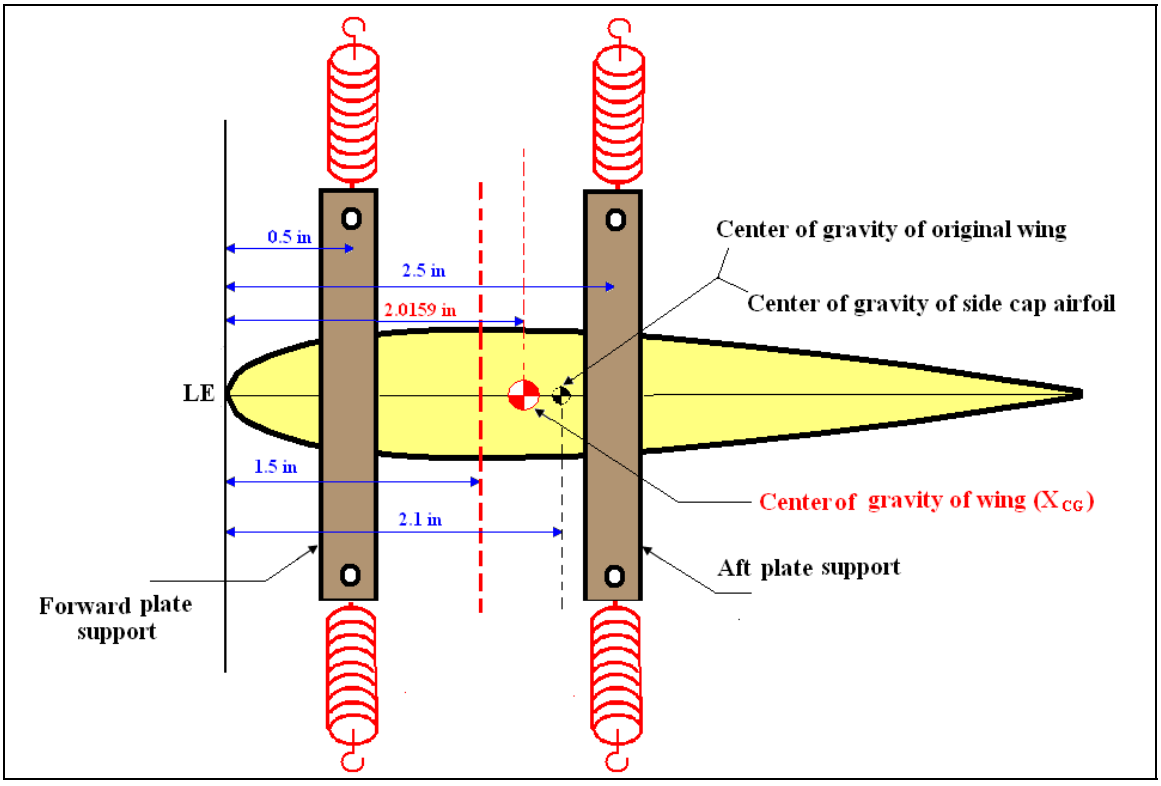

Figure 5.12 Center of gravity of the wing and distance of different components from LE for 2nd experimental set-up (front view)

5.2.2.1 Mass moment of inertia of a tension spring:

The mass moments of inertia of tension springs were calculated in section **4.2.2.1** in chapter 4 and are tabulated in table 5.4.

Table 5.4 Mass moment of inertia of tension springs

Tension spring #	Mass moment of inertia ($kg.m^2$)
# 1	1.4619×10^{-5}
# 2	1.2475×10^{-5}
# 3	1.4015×10^{-5}
# 4	5.0840×10^{-5}
# 5	3.2379×10^{-5}
# 6	3.2667×10^{-5}

5.2.2.2 Mass moment of inertia of support plate:

The method used to evaluate the mass moment of inertia of the support plate was discussed in section **4.2.2.2** in chapter 4. However, we have a small difference in the current support plate with only two holes and a higher value of mass of (0.64×10^{-3} kg). To calculate the mass moment of inertia of the support value for the current set-up, we follow the same sequence of steps in section **4.2.2.2** as follows:

In general, the mass moment of inertia of a rectangular plate is given by:

$$I = \frac{m}{12}\left[a^2 + b^2\right] \tag{5.5}$$

Where:

- m is the mass of a solid plate
- a, b and c are dimensions of plate.

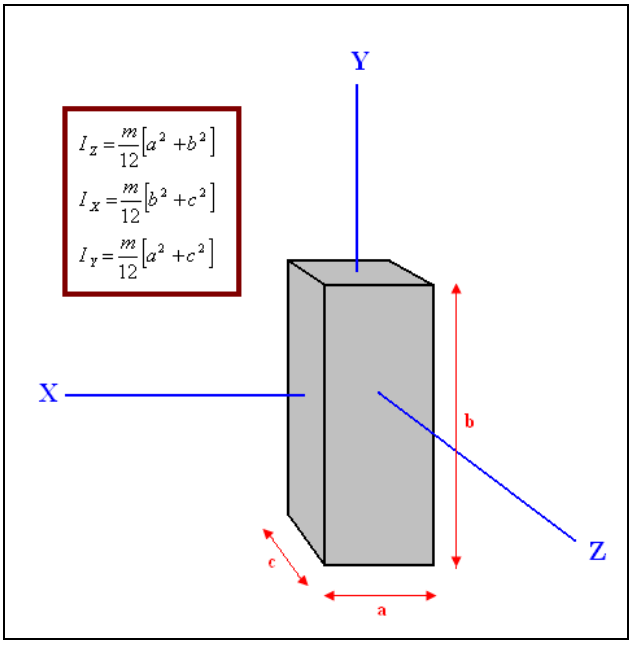

Figure 5.13 Mass moment of inertia of a solid plate

However, the current support plate has two holes each of a diameter of 0.125 in as shown in figure 5.14.

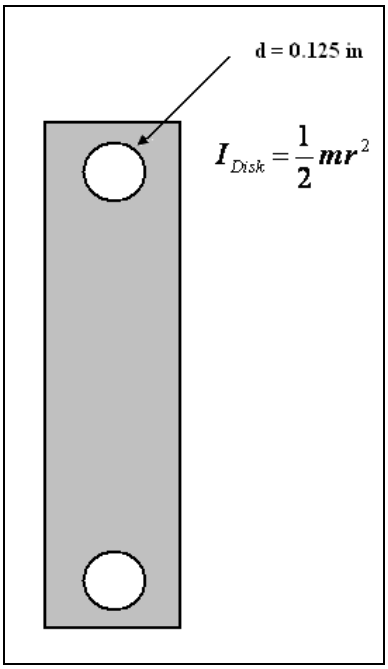

Figure 5.14 Support plate with two holes

To get the correct value of the mass moment of inertia of the support plate, we must consider the two holes and not to include them in the calculation. To perform this, we need to subtract the mass moment of inertia of these two holes from the mass moment of inertia of the solid plate in figure 5.13. We can consider the holes as disks and calculate the mass moment of inertia for one hole by equation 5.6.

$$I_{Disk} = \frac{1}{2} m r^2 \tag{5.6}$$

Where:

- m is the mass of disk (hole in our case)

- r is the radius of disk.

The final equation form used to calculate the mass moment of inertia of the support plate is:

$$I_P = \frac{m_{solid-plate}}{12}\left[a^2 + b^2\right] - 2\left[\frac{1}{2} m_{1-hole}\, r_{hole}{}^2\right] \tag{5.7}$$

Where:

- $m_{solid\text{-}plate}$ is the mass of plate without holes
- $m_{1\text{-}hole}$ is the mass of one hole
- a, b are the length and height of the solid plate
- r_{hole} is the radius of one hole (0.0625 in = 1.5875 x 10^{-3} m)

The mass of the support plate (m_{plate}) was measured to be (0.64 x 10^{-3} kg) from table 5.4. However, $m_{solid\text{-}plate}$ and $m_{1\text{-}hole}$ need an extra work to be found.

$$m_{plate} = m_{solid-plate} - m_{2-holes} \tag{5.8}$$

Where:

- m_{plate} is the mass of the plate with the two holes (measured)
- $m_{solid\text{-}hole}$ is the mass of the solid plate (without holes)
- $m_{2\text{-}hole}$ is the mass of the two holes

Equation (5.8) is equivalent to equation 5.9:

$$\rho V_{plate} = \rho V_{solid-plate} - \rho V_{2-holes} \tag{5.9}$$

Where:

- V_{plate} is the volume of the support plate with the two holes
- $V_{solid\text{-}hole}$ is the volume of the solid plate (without holes)

- $V_{2\text{-}hole}$ is the volume of the two holes
- ρ is the material density

Since the density is constant, equation 5.9 becomes:

$$V_{plate} = V_{solid-plate} - V_{2-holes} \tag{5.10}$$

Referring to dimensions in figure 5.15, the volumes can be calculated as follows:

$$V_{solid-plate} = (c)(b)(a) \tag{5.11}$$

$$V_{2-holes} = 2\left[\left(\frac{\pi}{4}\right)(d)^2(c)\right] \tag{5.12}$$

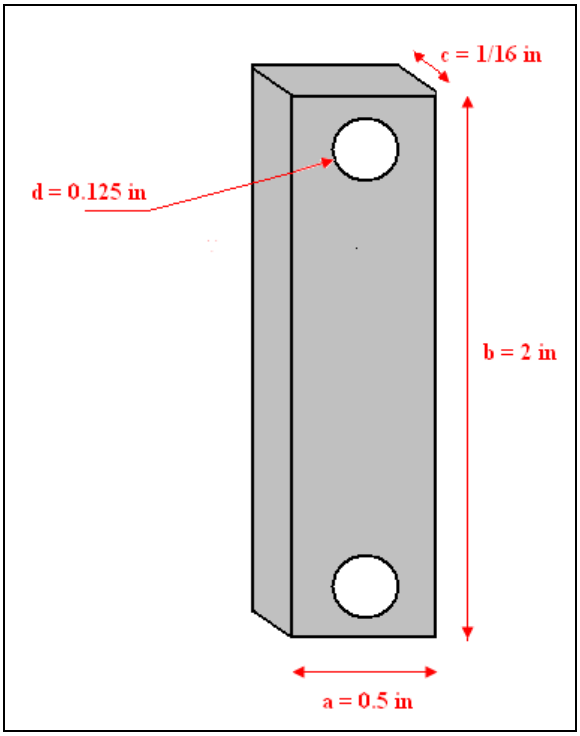

Figure 5.15 Support plate with dimensions

Substituting the values, we get:

$$V_{plate} = \left[\left(\frac{1}{16}in\right)(2\,in)\,(0.5\,in)\right] - 2\left[\left(\frac{\pi}{4}\right)(0.125\,in)^2\left(\frac{1}{16}in\right)\right]$$

$V_{plate} = 60.966 \text{ x } 10^{-3} \text{ in}^3$

$= 9.99 \text{ x } 10^{-7} \text{ m}^3$

Now, the density can be calculated as:

$$\rho = \frac{m_{plate}}{V_{plate}} \tag{5.13}$$

Substituting the values, we get:

$$\rho = \frac{0.64 \text{ x } 10^{-3}\ kg}{9.99 \text{ x } 10^{-7}\ m^3} = 640.64\,\frac{kg}{m^3}$$

Now we can calculate all masses as follows:

$$m_{solid-plate} = \rho\ V_{solid-plate} \tag{5.14}$$

Substituting the values, we get:

$$m_{solid-plate} = \left(640.64\,\frac{kg}{m^3}\right)\left[\left(\frac{1}{16}in\right)(2\,in)\,(0.5\,in)x\left(\frac{0.0254\,m}{in}\right)^3\right]$$

$m_{solid\text{-}plate} = 6.56 \text{ x } 10^{-4} \text{ kg}$

$$m_{1-hole} = \rho V_{1-hole} \tag{5.15}$$

$$m_{2-holes} = \rho V_{2-holes} \tag{5.16}$$

Substituting the values, we get:

$$m_{1-hole} = \left(640.64\,\frac{kg}{m^3}\right)\left[\left(\frac{\pi}{4}\right)(0.125\,in)^2\left(\frac{1}{16}in\right)\,x\left(\frac{0.0254\,m}{in}\right)^3\right]$$

$m_{1\text{-}hole} = 8.05 \times 10^{-6}$ kg

$$m_{2-holes} = \left(640.64 \frac{kg}{m^3}\right) x\, 2 \left[\left(\frac{\pi}{4}\right)(0.125\, in)^2 \left(\frac{1}{16} in\right) x \left(\frac{0.0254\, m}{in}\right)^3\right]$$

$m_{2\text{-}holes} = 1.61 \times 10^{-5}$ kg

Now we have all values to substitute into equation (5.7).

- $m_{solid\text{-}plate} = 6.56 \times 10^{-4}$ kg
- $a = 0.5$ in $= 12.7 \times 10^{-3}$ m
- $b = 2$ in $= 50.8 \times 10^{-3}$ m
- $m_{1\text{-}hole} = 8.05 \times 10^{-6}$ kg
- $r_{hole} = 0.0625$ in $= 1.5875 \times 10^{-3}$ m

Substituting the above values into equation (5.7), we get:

$$I_P = \frac{6.56 \times 10^{-4}}{12}\left[\left(12.7 \times 10^{-3}\right)^2 + \left(50.8 \times 10^{-3}\right)^2\right] - 2\left[\frac{1}{2}\left(8.05 \times 10^{-6}\right)\left(1.5875 \times 10^{-3}\right)^2\right]$$

$I_P = 1.4987 \times 10^{-7}$ kg.m^2

5.2.2.3 Mass moment of inertia of original wing (NACA 0015 airfoil):

The method used to evaluate the mass moment of inertia of an airfoil was discussed in detail in section 4.2.2.6 in chapter 4. As long it is the same airfoil type (NACA 0015) with same length of chord of (5 in) and same length of span of (12 in), we can follow exactly the same sequence of steps in section to evaluate the mass moment of inertia of the original wing. The mass of the current airfoil in the second set-up is different from the mass of the airfoil used in the first set-up.

The calculation is completed by a MATLAB code which was generated to solve the above problem. This code is in appendix D.

The mass moment of inertia of the original wing (airfoil) is:

$I_{airfoil} = 1.0525 \times 10^{-5}$ kg.m^2

5.2.2.4 Mass moment of inertia of side cap wing:

The side cap wing is of type (NACA 0015 airfoil) with same length of chord of (5 in). It has the length of span of (1/16 in), and it has a mass value of (2.1×10^{-3} kg). The mass moment of inertia of the side cap wing can be evaluated using the method used above, considering only the different values of mass and span.

The mass moment of inertia of the side cap wing was evaluated using SOLIDWORKS to be:

$I_{side\ cap\ wing} = 1.9174 \times 10^{-6}$ kg.m^2

Now after finding all mass moments of inertia of individual components of the wing, we can find the total mass moment of inertia about the center of gravity I_{CG} by applying the parallel axis theorem in equation (4.13). All distances from X_{CG} are illustrated in figure 5.12.

$$\begin{aligned} I_{CG} = I_{airfoil} + m_{airfoil}\, d^2_{airfoil-CG} + 2\left[I_{side\,cap\,wing} + m_{side\,cap\,wing}\, d^2_{side\,cap\,wing-CG}\right] + \\ + 2\left[I_p + m_p\, d^2_{fordward\ plate-CG}\right] + 2\left[I_p + m_p\, d^2_{aft\ plate-CG}\right] + \\ + 4\left[I_{tension\,spring} + m_{tension\,spring}\, d^2_{forward\ spring-CG}\right] \\ + 4\left[I_{tension\,spring} + m_{tension\,spring}\, d^2_{aft\ spring-CG}\right] \end{aligned} \tag{5.17}$$

All terms in equation 5.17 have been evaluated previously except the distances between the X_{CG} and the center of mass of the tension springs hanged to the forward and aft support plates ($d_{forward\ spring\text{-}XG}$), ($d_{aft\ spring\text{-}XG}$). Figure 5.16 illustrates how both are evaluated by applying the Pythagorean theorem.

$$d_{forward\,spring-CG} = \sqrt{(X_{CG} - 0.5)^2 + 3.125^2} = 3.473 \text{ in}$$

$$= 0.0882 \text{ m}$$

$$d_{aft\,spring-CG} = \sqrt{3.125^2 + (2.5 - X_{CG})^2} = 3.162 \text{ in}$$

$$= 0.0803 \text{ m}$$

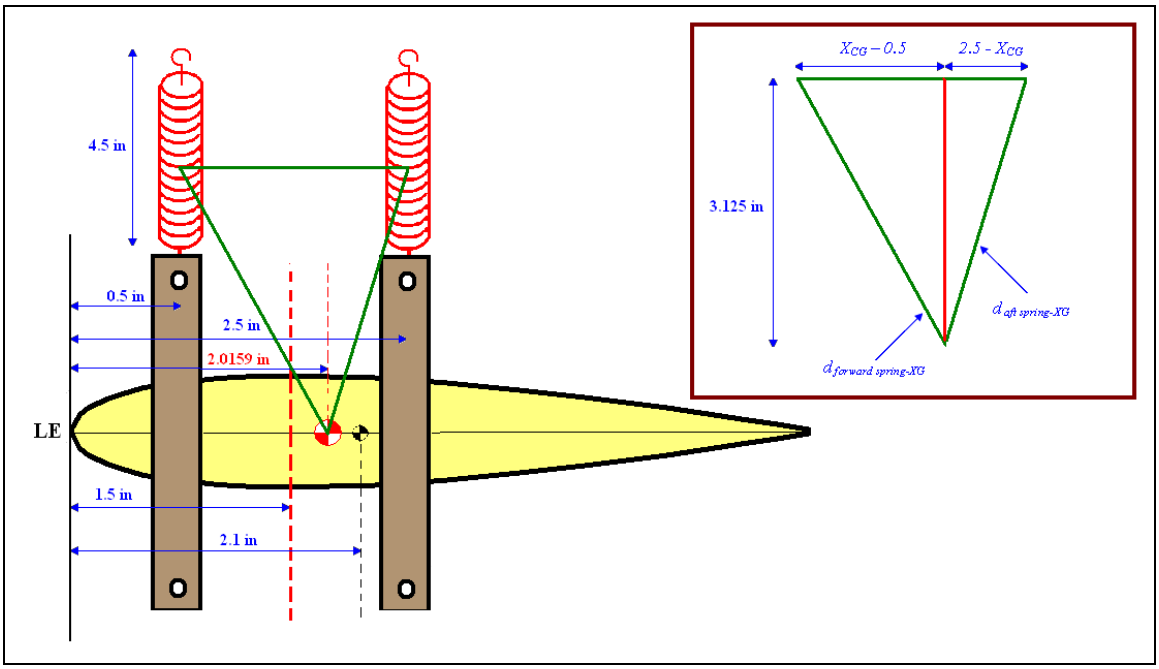

Figure 5.16 Distance between X_{CG} and center of mass of tension spring (2nd experimental set-up)

Mass moments of inertia, masses and distances from X_{CG} for all components are summarized in table 5.5 and 5.6.

Table 5.5 Mass moments of inertias, masses and distances from X_{CG} for different components (2nd experimental set-up)

Object	I (kg.m^2)	m (kg)	d (m)
Original wing (airfoil)	1.0525×10^{-5}	11.51×10^{-3}	0.0021
Side cap wing	1.9174×10^{-6}	2.1×10^{-3}	0.0021
Forward plate support	1.4987×10^{-7}	0.64×10^{-3}	0.0385
Aft plate support	1.4987×10^{-7}	0.64×10^{-3}	0.0123

Table 5.6 Mass moments of inertias, masses and distances from X_{CG} for various tension springs (2^{nd} experimental set-up)

Tension spring #	I (kg.m^2)	Mass (kg)	d (m)
# 1	1.4619×10^{-5}	13.24×10^{-3}	Forward spring = 0.0882
# 2	1.2475×10^{-5}	11.34×10^{-3}	
# 3	1.4015×10^{-5}	12.74×10^{-3}	
# 4	5.0840×10^{-5}	44.83×10^{-3}	Aft spring = 0.0803
# 5	3.2379×10^{-5}	29.2×10^{-3}	
# 6	3.2667×10^{-5}	29.46×10^{-3}	

Substituting values from tables 5.5 and 5.6 into equation (5.17), the total mass moments of inertia about the center of gravity for various tension spring types are tabulated in table 5.7.

Table 5.7 Mass moments of inertia about the center of gravity for various tension springs (2^{nd} experimental set-up)

Tension spring #	I_{CG} (kg.m^2)
# 1	8.8791×10^{-4}
# 2	7.6257×10^{-4}
# 3	8.5460×10^{-4}
# 4	0.0030
# 5	0.0019
# 6	0.0020

5.2.3 Mass moment of inertia about the elastic axis:

After all mass moments of inertia about the center of the gravity for various tension springs were evaluated, it is straightforward to find the mass moments of inertia about the elastic axis by applying the parallel axis theorem as follows:

$$I_{\alpha} = I_{CG} + m\,d^2 \tag{5.18}$$

Where:

- I_{α} is the mass moment of inertia about the elastic axis
- m is the total mass of the wing including all parts attached
- d is the distance between the center of gravity (X_{CG}) and the elastic axis (X_e) (figure 5.10)

$$d = X_{CG} - X_e \tag{5.19}$$

= 2.0159 in – 1.5 in = 0.5159 in

= 0.0131 m

We have two cases for the mass. One case is when $\left(\frac{1}{3}\right)$ of tension spring mass included; and the other case is when it is not included. This would affect the value of I_{α}. The evaluation of I_{α} for both cases is presented in the next section

5.2.3.1 Mass moment of inertia about the elastic axis with inclusion of $\left(\frac{1}{3}\right)$ tension spring mass:

The mass moments of inertia about the elastic axis for various tension springs in the case of including one-third of the tension spring mass to the wing mass are tabulated in table 5.8.

Table 5.8 Mass moments of inertias about elastic axis for various tension springs in case of including $\left(\frac{1}{3}\right)$ of the tension spring mass to the wing mass (2^{nd} experimental set-up)

Tension spring #	I_α (kg.m^2)
# 1	8.9711 x 10^{-4}
# 2	7.7090 x 10^{-4}
# 3	8.6357 x 10^{-4}
# 4	0.0030
# 5	0.0019
# 6	0.0020

5.2.3.2 Mass moment of inertia about the elastic axis without inclusion of tension sprig mass:

When the mass of the tension springs is neglected, then the mass of the wing remains the same. It includes all attached parts except the tension spring, such that (m = 0.0183 kg)**.**

Substituting into equation (5.18), we get the mass moments of inertia about the elastic axis for various tension springs in the case of not including the tension spring mass to the wing mass.

Table 5.9 Mass moments of inertias about elastic axis for various tension springs in case of not including the tension spring mass to the wing mass (2nd experimental set-up)

Tension spring #	I_α (kg.m^2)
# 1	8.9105 x 10^{-4}
# 2	7.6571 x 10^{-4}
# 3	8.5774 x 10^{-4}
# 4	0.0030
# 5	0.0019
# 6	0.0020

By comparing the change in the values of the mass moments of inertia in both cases, we note that adding one-third of the tension spring mass does not make a big change in the value of (I_α), the maximum difference between the two values does not exceed (0.18%) which can be neglected.

5.2.4 Radius of gyration about the elastic axis (r_α):

The radius of gyration about the elastic axis is introduced as a non-dimensional radius. It was discussed in chapter 4 and given by equation (4.40) as follows:

$$r_\alpha = \sqrt{\frac{I_\alpha}{m\,b^2}}$$

5.2.5 Mass ratio (μ):

μ is the mass ratio between the wing mass and the mass of the air around the wing. It was discussed in chapter 4 and given by equation (4.41) as follows:

$$\mu = \frac{m}{\pi\,\rho_{air}\,b^2\,L}$$

5.2.6 (x_α):

x_α is the non-dimensional distance of wing center of gravity aft of the elastic axis in (semichords). It was discussed in chapter 4 and given by equation (4.42) as follows:

$$x_\alpha = \frac{X_{CG} - X_e}{b} = \frac{2\,d}{c}$$

5.2.7 (a_h):

a_h is the non-dimensional distance from center of chord to the elastic axis. It was discussed in chapter 4 and given by equation (4.43) as follows:

$$a_h = \frac{b - X_e}{b} = 1 - \frac{2\,X_e}{c}$$

5.2.8 Uncoupled natural frequency in bending (ω_h):

ω_h is in radian per second and given by equation 4.44.

$$\omega_h = \sqrt{\frac{K_h}{m}}$$

5.2.9 Uncoupled natural frequency in torsion (ω_α):

ω_α is in radian per second and given by equation 4.45.

$$\omega_\alpha = \sqrt{\frac{K_\alpha}{I_\alpha}}$$

5.2.10 Ratio of uncoupled natural frequency ($\frac{\omega_h}{\omega_\alpha}$):

$\frac{\omega_h}{\omega_\alpha}$ is an important parameter in the calculation of Theodorsen coefficients. As discussed earlier in this chapter, the advantage of implementing the second experimental set-up with tension springs is to avoid complexities resulted from mounting torsion spring to the flutter wing model.

Considering equation (5.1), it will have a fixed spring constant ratio $\frac{K_h}{K_\alpha}$, and then $\frac{\omega_h}{\omega_\alpha}$ is only influenced by the mass and the mass moment of inertia. It will be easier to estimate the correct value for frequency ratio.

$$\frac{\omega_h}{\omega_\alpha} = \frac{\sqrt{\frac{K_h}{m}}}{\sqrt{\frac{K_\alpha}{I_\alpha}}} = \sqrt{\frac{K_h}{K_\alpha}} * \sqrt{\frac{I_\alpha}{m}}$$

As stated earlier, the change in the value of mass moment of inertia (I_α) is very small for all cases in both experimental set-ups, however the change in mass (m) is more dominant. Therefore $\frac{\omega_h}{\omega_\alpha}$ can be considered as function of mass only as shown in equation (5.2).

The experimental results are quite reliable as they were repeated several times providing a good level of confidence.

We can use the experimental results of the first case (tension type #1) to determine the value of $\frac{K_h}{K_\alpha}$ to be used later in different cases.

The flutter speed and frequency of the first case (tension type #1) for the second experimental set-up are:

$U_{F(experimental)}$ = 15.5 m/s, and

By rearranging equation (5.1), we get:

$$\frac{K_h}{K_\alpha} = \left(\frac{\omega_h}{\omega_\alpha}\right)^2 \left(\frac{m}{I_\alpha}\right) \tag{5.20}$$

With the known values for m and I_α of the first case (tension type #1), we get:

m = 0.0536 kg (including one-third of spring mass)

$I_\alpha = 8.9711 \times 10^{-4}$ kg.m^2

Substitute the values into equation (5.20):

$$\left(\frac{K_h}{K_\alpha}\right)_{Fixed} = 59.75\left(\frac{\omega_h}{\omega_\alpha}\right)^2$$

By trial and error, the best value of frequency ratio to match the experimental value of flutter speed was:

$$\frac{\omega_h}{\omega_\alpha} = 0.42$$

For this value, we have:

$1/k = 2.1$ (inverse of reduced frequency)

$\omega_\alpha = 121.8$ rad/s

$\sqrt{x} = 1.057$

$$U_F = \frac{1}{k}\frac{\omega_\alpha c}{2\sqrt{x}} = (2.1)\frac{(121.8\frac{rad}{s})(0.127\,m)}{2(1.057)} = 15.4\frac{m}{s}$$

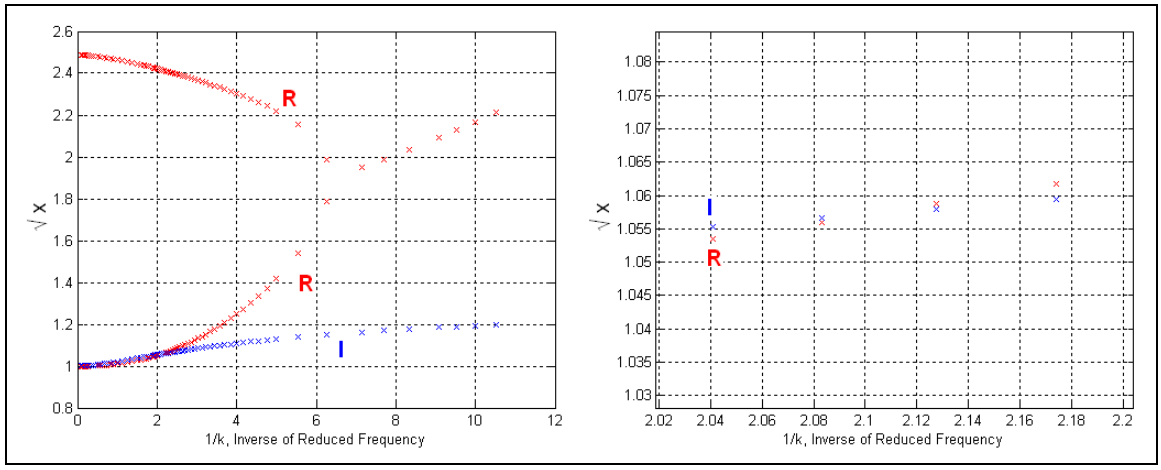

Figure 5.17 Solution of Flutter Determinant using Theodorsen Function ($\frac{\omega_h}{\omega_\alpha} = 0.42$) for tension spring # 1 (2nd setup) for one-third of tension spring mass included

Considering the value of 0.42 for the frequency ratio, we have the spring constant ratio to be:

$$\left(\frac{K_h}{K_\alpha}\right)_{Fixed} = 59.75(0.42)^2$$

$$\left(\frac{K_h}{K_\alpha}\right)_{Fixed} = 10.54$$

$$K_\alpha = \frac{K_h}{10.54} \tag{5.21}$$

K_h is a given value and it changes according to the spring type. K_α can be calculated and it depends on the value of K_h.

Now the frequency ratio of the second experimental set-up can be evaluated as follows:

$$\omega_h = \sqrt{\frac{8\,k_h}{m}} \tag{5.22}$$

The factor 8 involved into equation (5.22) is because of the eight springs used in the experiment.

Substituting back into equation (5.1), we get:

$$\frac{\omega_h}{\omega_\alpha} = \sqrt{\frac{K_h}{K_\alpha}} * \sqrt{\frac{I_\alpha}{m}} = \sqrt{10.54}\sqrt{\frac{I_\alpha}{m}} \tag{5.23}$$

5.2.11 Results and Discussion of Theodorsen Solution for Tension-Tension spring Set-up (2nd experimental set-up)

At this point, all parameters needed to find the Theodorsen coefficients are available and evaluated. Solving the determinant equation according to the sequence of steps in chapter 2, we get the curves of $\sqrt{x}$ and the inverse of reduced frequency $\frac{1}{k}$. The Theodorsen's solution is used here as a tool to investigate the behavior of spring mass for all different sets of tension spring. The solution is carried out for two cases, the first case is for the inclusion of the $\left(\frac{1}{3}\right)$ mass of tension spring and the second case is for mass fraction that provides the best matching with the experimental result. From this solution, we can have an idea about the portion of spring mass that should be included.

5.2.11.1 Case of including the one-third of tension spring mass to the wing mass:

5.2.11.1.1 Tension spring type #1

As discussed in previous section, the calculated result for this case was based on the experimental value of the flutter speed (15.5 m/s). As explained, that step was taken to determine the fixed value for $\frac{K_h}{K_\alpha}$ and then using it in the other calculation cases.

Therefore, we expect matching with the experimental result.

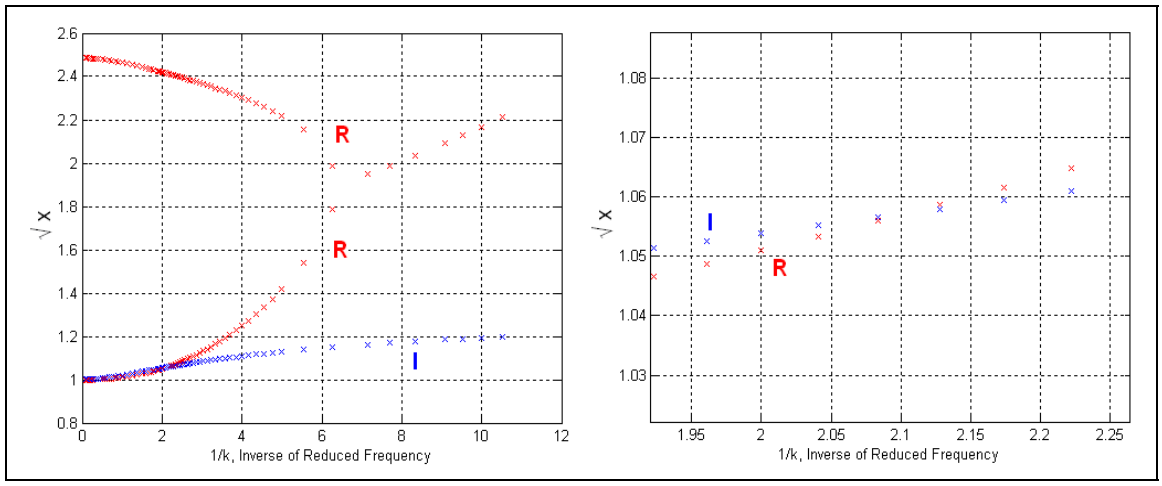

Figure 5.18 Solution of Flutter Determinant using Theodorsen Function for tension spring # 1 (2nd setup) for $\left(\frac{1}{3}\right)$ of tension spring mass included

For this case, we have:

$1/k = 2.1$ (inverse of reduced frequency), $\frac{\omega_h}{\omega_\alpha} = 0.42$, $\omega_\alpha = 121.8$ rad/s, $\sqrt{x} = 1.057$

$$U_F = \frac{1}{k}\frac{\omega_\alpha c}{2\sqrt{x}} = (2.1)\frac{(121.8\frac{rad}{s})(0.127\,m)}{2(1.057)} = 15.4\frac{m}{s}$$

5.2.11.1.2 Tension spring type #2

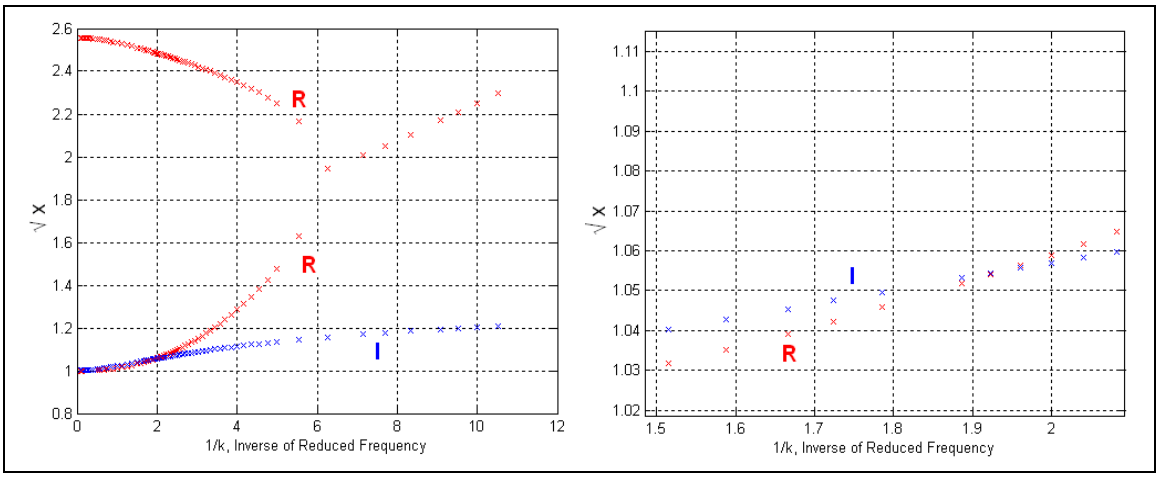

Figure 5.19 Solution of Flutter Determinant using Theodorsen Function for tension spring # 2 (2nd setup) for $\left(\frac{1}{3}\right)$ of tension spring mass included

For this case, we have:

$1/k = 1.94$, $\frac{\omega_h}{\omega_\alpha} = 0.41$, $\omega_\alpha = 165.79$ rad/s, $\sqrt{x} = 1.055$

$$U_F = \frac{1}{k}\frac{\omega_\alpha c}{2\sqrt{x}} = (1.94)\frac{(165.79\frac{rad}{s})(0.127\,m)}{2(1.055)} = 19.36\frac{m}{s}$$

To get a closer value for the calculated flutter speed with the experimental flutter speed (18.4 m/s), the solution was repeated decreasing the mass of the spring (from $\frac{1}{3}$ spring mass to $\frac{1}{3.2}$ spring mass).

Performing this, we get:

$$1/k = 1.84\ ,\ \frac{\omega_h}{\omega_\alpha} = 0.41,\ \omega_\alpha = 165.83 \text{ rad/s},\ \sqrt{x} = 1.05$$

$$U_F = \frac{1}{k}\frac{\omega_\alpha c}{2\sqrt{x}} = (1.84)\frac{(165.83\frac{rad}{s})(0.127\,m)}{2(1.05)} = 18.45\frac{m}{s}$$

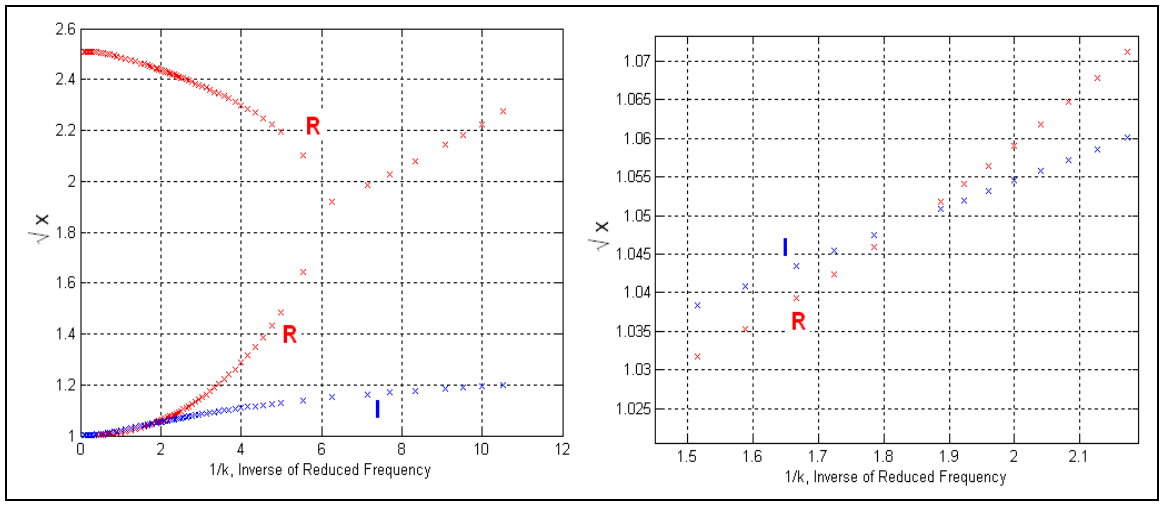

Figure 5.20 Solution of Flutter Determinant using Theodorsen Function for tension spring # 2 (2nd setup) for $\left(\frac{1}{3.2}\right)$ of tension spring mass included

5.2.11.1.3 Tension spring type #3

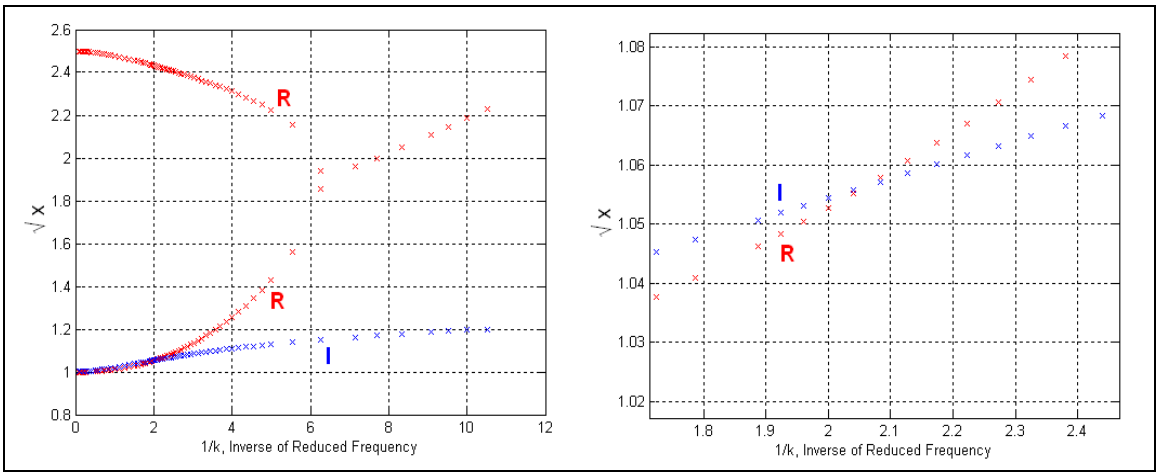

Figure 5.21 Solution of Flutter Determinant using Theodorsen Function for tension spring # 3 (2nd setup) for $\left(\frac{1}{3}\right)$ of tension spring mass included

For this case, we have:

$$1/k = 2.06\ ,\ \frac{\omega_h}{\omega_\alpha} = 0.418,\ \omega_\alpha = 203.48 \text{ rad/s},\ \sqrt{x} = 1.057$$

$$U_F = \frac{1}{k}\frac{\omega_\alpha\, c}{2\sqrt{x}} = (2.06)\frac{(203.48\frac{rad}{s})(0.127\,m)}{2(1.057)} = 25.18\frac{m}{s}$$

To get a closer value for the calculated flutter speed with the experimental flutter speed (23 m/s), the solution was repeated decreasing the mass of the spring (from $\frac{1}{3}$ spring mass to $\frac{1}{3.5}$ spring mass).

Performing this, we get:

$$1/k = 1.85,\ \frac{\omega_h}{\omega_\alpha} = 0.439,\ \omega_\alpha = 203.6 \text{ rad/s},\ \sqrt{x} = 1.045$$

$$U_F = \frac{1}{k}\frac{\omega_\alpha c}{2\sqrt{x}} = (1.85)\frac{(203.6\frac{rad}{s})(0.127\,m)}{2(1.045)} = 22.9\frac{m}{s}$$

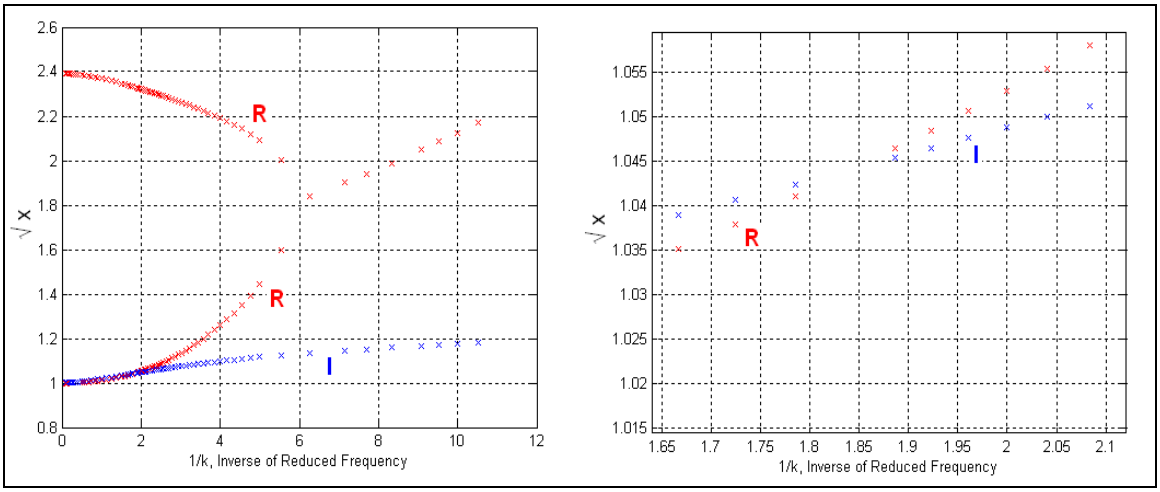

Figure 5.22 Solution of Flutter Determinant using Theodorsen Function for tension spring # 3 (2nd setup) for $\left(\frac{1}{3.5}\right)$ of tension spring mass included

5.2.11.1.4 Tension spring type #4

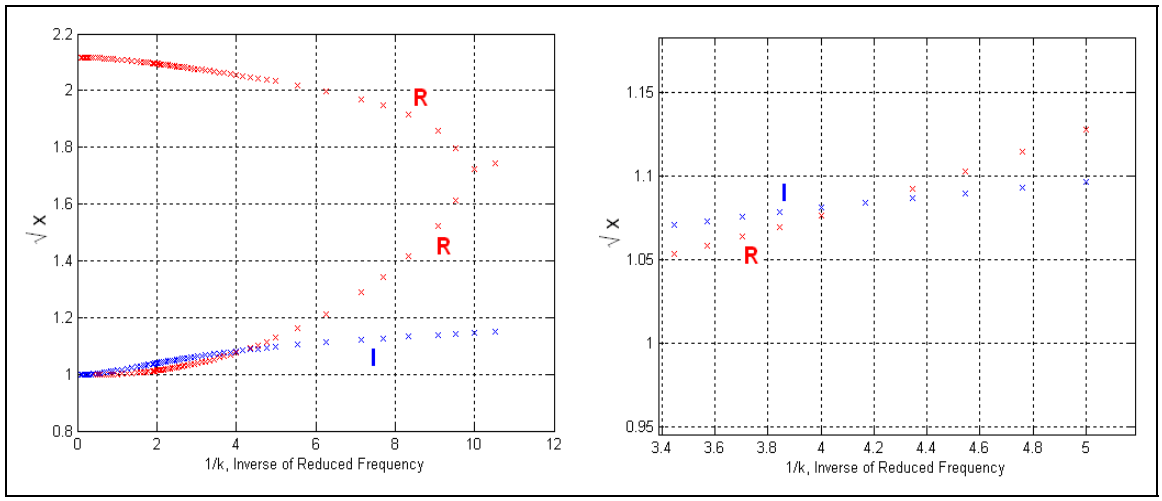

Figure 5.23 Solution of Flutter Determinant using Theodorsen Function for tension spring # 4 (2nd setup) for $\left(\frac{1}{3}\right)$ of tension spring mass included

For this case, we have:

$$1/k = 4.2,\ \frac{\omega_h}{\omega_\alpha} = 0.48,\ \omega_\alpha = 231.6 \text{ rad/s},\ \sqrt{x} = 1.085$$

$$U_F = \frac{1}{k}\frac{\omega_\alpha c}{2\sqrt{x}} = (4.2)\frac{(231.6\frac{rad}{s})(0.127\,m)}{2(1.085)} = 56.9\frac{m}{s}$$

To get a closer value for the calculated flutter speed with the experimental flutter speed (40.4 m/s), the solution was repeated decreasing the mass of the spring (from $\frac{1}{3}$ spring mass to $\frac{1}{5}$ spring mass).

Performing this, we get:

$$1/k = 2.75,\ \frac{\omega_h}{\omega_\alpha} = 0.59,\ \omega_\alpha = 231.04 \text{ rad/s},\ \sqrt{x} = 1.033$$

$$U_F = \frac{1}{k}\frac{\omega_\alpha c}{2\sqrt{x}} = (2.75)\frac{(231.94\frac{rad}{s})(0.127\,m)}{2(1.033)} = 39.2\frac{m}{s}$$

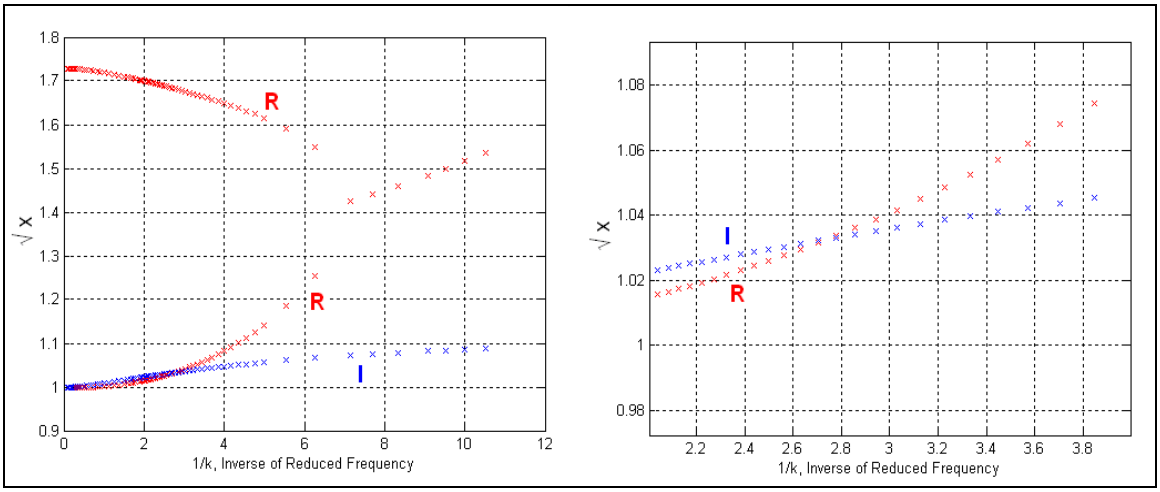

Figure 5.24 Solution of Flutter Determinant using Theodorsen Function for tension spring # 4 (2nd setup) for $\left(\frac{1}{5}\right)$ of tension spring mass included

5.2.11.1.5 Tension spring type #5

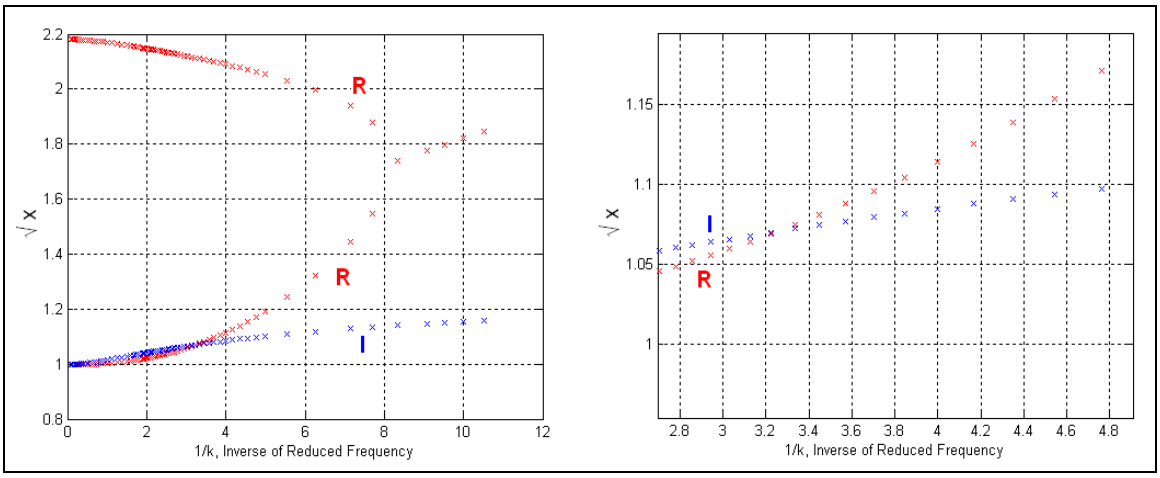

Figure 5.25 Solution of Flutter Determinant using Theodorsen Function for tension spring # 5 (2nd setup) for $\left(\frac{1}{3}\right)$ of tension spring mass included

For this case, we have:

$$1/k = 3.25,\ \frac{\omega_h}{\omega_\alpha} = 0.47,\ \omega_\alpha = 363.15 \text{ rad/s},\ \sqrt{x} = 1.07$$

$$U_F = \frac{1}{k}\frac{\omega_\alpha c}{2\sqrt{x}} = (3.25)\frac{(363.15\frac{rad}{s})(0.127\,m)}{2(1.07)} = 70\frac{m}{s}$$

To get a closer value for the calculated flutter speed with the experimental flutter speed (26 m/s), the solution was repeated decreasing the mass of the spring (from $\frac{1}{3}$ spring mass to $\frac{1}{10}$ spring mass).

Performing this, we get:

$$1/k = 1.13,\ \frac{\omega_h}{\omega_\alpha} = 0.71,\ \omega_\alpha = 364 \text{ rad/s},\ \sqrt{x} = 1.006$$

$$U_F = \frac{1}{k}\frac{\omega_\alpha c}{2\sqrt{x}} = (1.13)\frac{(364\frac{rad}{s})(0.127\,m)}{2(1.006)} = 26\frac{m}{s}$$

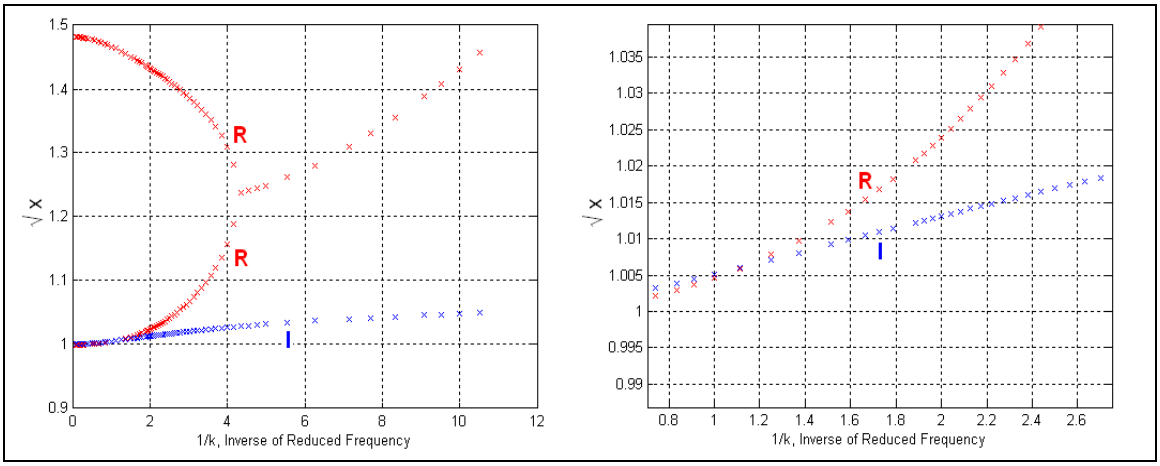

Figure 5.26 Solution of Flutter Determinant using Theodorsen Function for tension spring # 5 (2nd setup) for $\left(\frac{1}{10}\right)$ of tension spring mass included

5.2.11.1.6 Tension spring type #6

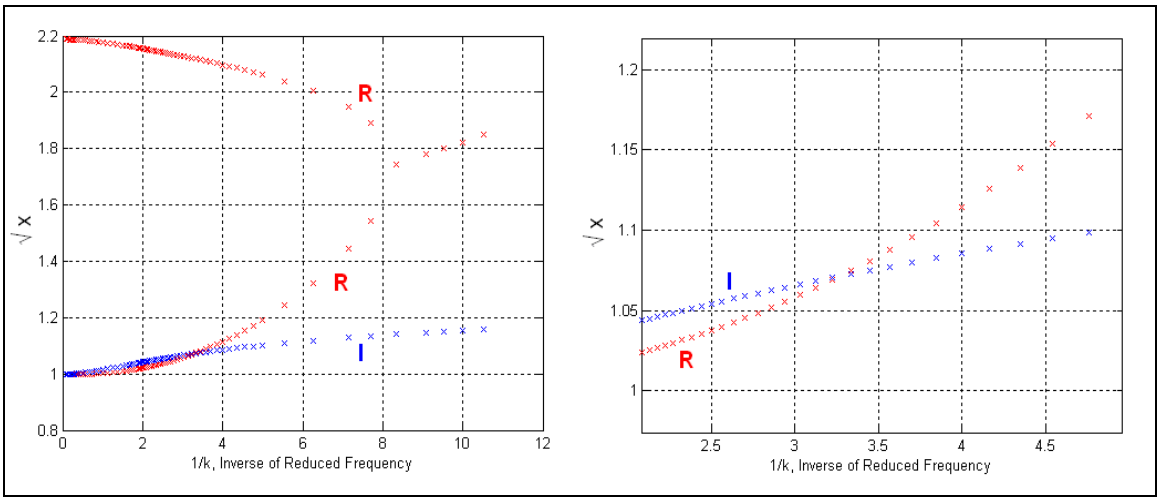

Figure 5.27 Solution of Flutter Determinant using Theodorsen Function for tension spring # 6 (2nd setup) for $\left(\frac{1}{3}\right)$ of tension spring mass included

For this case, we have:

$$1/k = 3.25,\ \frac{\omega_h}{\omega_\alpha} = 0.468,\ \omega_\alpha = 389.4 \text{ rad/s},\ \sqrt{x} = 1.072$$

$$U_F = \frac{1}{k}\frac{\omega_\alpha c}{2\sqrt{x}} = (3.25)\frac{(389.4\frac{rad}{s})(0.127\,m)}{2(1.072)} = 74.96\frac{m}{s}$$

To get a closer value for the calculated flutter speed with the experimental flutter speed (45 m/s), the solution was repeated decreasing the mass of the spring (from $\frac{1}{3}$ spring mass to $\frac{1}{6}$ spring mass).

Performing this, we get:

$$1/k = 1.85,\ \frac{\omega_h}{\omega_\alpha} = 0.61,\ \omega_\alpha = 390.07 \text{ rad/s},\ \sqrt{x} = 1.019$$

$$U_F = \frac{1}{k}\frac{\omega_\alpha c}{2\sqrt{x}} = (1.85)\frac{(390.07\frac{rad}{s})(0.127\,m)}{2(1.019)} = 45\frac{m}{s}$$

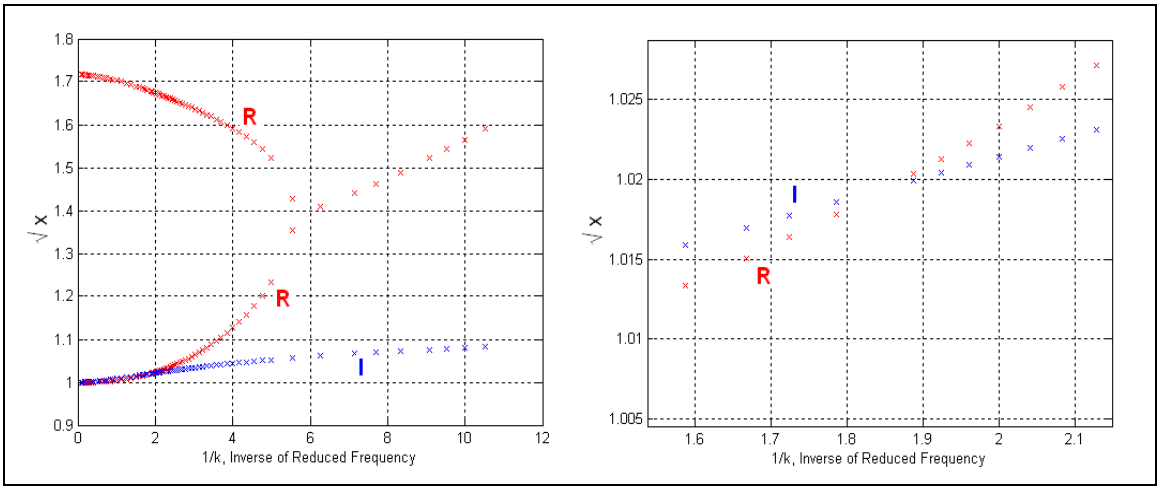

Figure 5.28 Solution of Flutter Determinant using Theodorsen Function for tension spring # 6 (2nd setup) for $\left(\frac{1}{6}\right)$ of tension spring mass included

Detailed discussion of the previous figures is provided in section 5.2.11.3

5.2.11.2 Case of not including the one-third of tension spring mass to the wing mass:

As the Theodorsen's solution was carried out for no spring mass added to the wing mass, the following was observed:

For the tension type spring #4, the calculated flutter speed was around 64.4 m/s, which is far from the experimental value (40.2 m/s). To get a better value from the solution we need to decrease the mass, which means cutting some part of the wing itself to achieve that targeted value. This of course is not possible for this situation.

Based on this, it was concluded that excluding the mass of the spring was not an appropriate and it would lead to incorrect results.

5.2.11.3 Discussion and conclusion of Theodorsen Solution for Tension-Tension spring Set-up (2nd experimental set-up)

As stated previously in this chapter that both factors of spring mass and constant have direct and indirect effect on the calculation of the frequency ratio $\frac{\omega_h}{\omega_\alpha}$ which is involved in most all coefficients of Theordorsen flutter determinant, and torsion frequency ω_α which is involved in the flutter speed equation. The only part that could be replaced in the experiment is the spring type, which has different spring mass and constant.

The focus in this work is to investigate the effectiveness of the spring mass on the flutter speed. Therefore, varying the value of the spring mass in the Theodorsen solution would be the key to understanding that.

In the experimental results, it was clearly observed that the mass of the spring affects the value of flutter speed as discussed in section 5.1.1. However, the question that arises and should be clarified is how much portion of spring mass should be included. Is the $\left(\frac{1}{3}\right)$ factor proposed correct?

To answer this, the value of mass spring in Theodorsen solution was changed in each case until a match with experimental value of flutter speed was achieved. In other words, the Theodorsen solution is being used as the tool to determine the amount of included spring mass used in the calculation.

By looking to the generated figures above, there is a good matching between the calculated values of flutter speed with the experimental results in the case of tension spring #2. The error difference is only 5.2%. However, the purpose is to find out how

much spring mass should be included for best matching with the experimental result, and therefore, by trial and error, it was found that for best matching, only $\left(\frac{1}{3.2}\right)$ of spring mass should be included.

For the case of tension spring #3, the calculated value was 25.18 m/s while the experimental value was 23 m/s. the matching is still good and the error difference is only 9.4%. For best matching, the spring mass should have been decreased to $\left(\frac{1}{3.5}\right)$.

For the case of tension spring #4, the calculated value was 56.9 m/s, while the experimental value was 40.2 m/s. no matching in this case and the error difference is large of 41.5%. For best matching, the spring mass was decreased to be $\left(\frac{1}{5}\right)$.

In the case of tension spring #5, the calculated value was 70 m/s, while the experimental value was 26 m/s. the error difference is huge of 169.2%. For best matching, only $\left(\frac{1}{10}\right)$ of the spring mass was included.

Similarly, In the case of tension spring #6, the calculated value was 74.96 m/s while the experimental value was 45 m/s. the error difference is large of 66.6%. For best matching, the spring mass was decreased to be $\left(\frac{1}{6}\right)$.

From above, we see the different values of mass fractions to be included for each case. Actually the fraction of mass does not provide clear image since the mass of each spring is different form the other. However, it is noted that there is some relationship between

the included portion of spring mass and the spring constant. Table 5.10 illustrates the value of mass and corresponding value of constant for best matching in all cases.

Table 5.10 Mass fractions included for best matching

Case	Spring constant K_h (N/m)	Mass fraction (kg)	Mass value (kg)
Tension # 1	8 x (17.52)	$\left(\frac{1}{3}\right)$ x 8 x (13.24 x 10^{-3})	0.0353
Tension # 2	8 x (28.03)	$\left(\frac{1}{3.2}\right)$ x 8 x (11.34 x 10^{-3})	0.0284
Tension # 3	8 x (47.3)	$\left(\frac{1}{3.5}\right)$ x 8 x (12.74 x 10^{-3})	0.0291
Tension # 4	8 x (213.73)	$\left(\frac{1}{5}\right)$ x 8 x (44.83 x 10^{-3})	0.0717
Tension # 5	8 x (350.37)	$\left(\frac{1}{10}\right)$ x 8 x (29.2 x 10^{-3})	0.0234
Tension # 6	8 x (402.93)	$\left(\frac{1}{6}\right)$ x 8 x (29.46 x 10^{-3})	0.0393

By looking at table 5.10, there is a remarkable observation that with the increase in the spring constant, there is a decreased mass fraction included. This indicates the coupling effect of both parameters on the solution.

To explain the correlation, we consider the firs three cases in which the mass of spring is almost the same and the spring constants are quite small, the included mass fraction is about $\left(\frac{1}{3}\right)$. However, in cases #4, #5 and #6 in which the spring mass is large but the spring constants are large as well, the mass fraction included is smaller and it could reach $\left(\frac{1}{10}\right)$.

The remarkable conclusion from this observation is that when a spring with a small constant is used, the mass of the spring is more dominant as in cases #1, #2 and #3. However, when the spring constant is large, it becomes more dominant over the spring mass as in cases #4, #5 and #6.

It is obviously useful to generate a relation that shows the link between both parameters and their correlated effect on the wing flutter speed. This is only possible either when using springs with exactly same spring constant and different masses or using spring with same mass and different spring constants. Moreover, springs should have the same length and shape. Unfortunately, finding springs with certain properties in the market is very difficult if it not impossible.

CHAPTER 6

Summary:

6.1 Conclusions

In this study, a model to determine experimentally the flutter speed of a two-dimensional airfoil with two degrees of freedom was designed, built and installed in the University of Minnesota wind tunnel.

Two experimental set-ups were used. In the first experimental set-up, a set of torsion and tension springs similar to the typical wing flutter model in the literature was used. In the second experimental set-up, the wing model used only tension springs.

In both experimental set-ups, six sets of different tension springs were used. All springs had the same length but different spring constants, diameters and masses. The purpose of this study was to experimentally investigate the effect of the tension spring mass on the wing flutter speed.

The experimental results were compared with the calculated values of flutter speeds using a mathematical model, which was based on the Theodorsen's function approach.

The key conclusions based on the experimental results and the solutions using Theodorsen's function are summarized as the main observations as follows:

The first observation is that the second experimental set-up was preferred over the first experimental set-up for two reasons. The first reason was associated with the torsion spring in terms of difficulty of manufacture and design in the first set-up. The second

reason was the advantage of having a fixed value for the spring constant ratio $\frac{K_h}{K_\alpha}$ in the second set-up.

The second and remarkable observation was that the spring mass has a significant effect on the flutter speed and a certain portion of spring mass must be added to the total mass of the wing when the mathematical calculation is performed in order to make theory and experiment agree . The value of $\left(\frac{1}{3}\right)$ spring mass as the hypothesis proposed in Chapter 1 provided a good agreement between the experimental and calculated results at low values of spring constant. It was observed that at higher values of spring constant, the portion of the added spring mass is reduced. This may indicate that if the spring is very stiff, the entire spring may not deflect linearly. In fact, the portion of the spring near the wall may not deflect at all. Thus the fraction of added spring mass may be less than $\frac{1}{3}$. For example if the velocity profile of the spring were cubic, such that $v(x)=v_0\frac{x^3}{L^3}$, then the added mass would be $\frac{1}{7}$ the mass of the spring. Since the spring constants are large for the cases in which the added mass deviates substantially from $\frac{1}{3}$, this could account for the fact that the added mass is reduced.

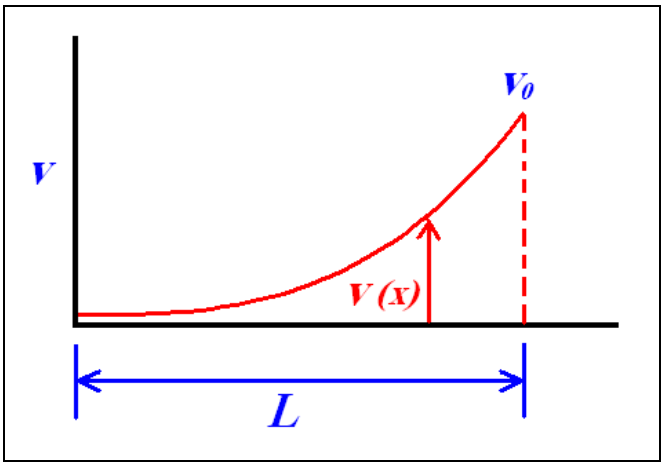

Figure 6.1 Cubic velocity profile of the spring

This correlation between the spring stiffness and added mass of spring is important and it would have been very useful to generate a relation that demonstrates their effect on flutter speed; unfortunately, this was not possible due to the lack of springs with the same mass and shape but different stiffness or springs with the same stiffness and shape but different mass. The conclusion that can be drawn from this point is that the effect of spring mass may be small and can be neglected when testing large, heavy models in large wind tunnels; however, for cheap and suitable testing in small wind tunnels with small, light models, the inclusion of the spring mass is important.

The experiments were conducted for different airfoils with different masses, similar results were obtained, which indicates quite reliable level of confidence of the above conclusions.

6.2 Recommendations for Future Work

The main goal of future work is to repeat the experiment with springs which have the same size and mass but different stiffness, or with the same size and stiffness but different mass. This may enable us to figure out the correlated effect of spring mass and stiffness on flutter speed, and what exactly the amount of spring mass should be included. Repeating the experiment with different locations of both center of gravity and elastic axis may provide a better understanding of the problem and to determine whether this affects the contribution of the spring mass or not.

The last recommendation is to compare the experimental results to different mathematical models of flutter.

REFERENCES

[1] Dewey H. Hodges and G. Alvin Pierce, "Introduction to Structural Dynamics and Aeroelasticity", Cambridge University Press, first edition, 2002.

[2] Philip Curtis Wheeler, "An Explication of Airfoil Section Bending-Torsion Flutter", Master of Science, Department of Civil and Environmental Engineering, University of Maryland, 2004

[3] Riccy Kurniawan, "Numerical Study of Flutter of a Two-Dimensional Aeroelastic System", Proceedings of the World Congress on Engineering, 2013 Vol III, WCE 2013, July 3 - 5, 2013, London, U.K.

[4] **Collar, A.R.**, "The First Fifty Years of Aeroelasticity,"*Aerospace*, vol. 5, no. 2, (Royal Aeronautical Society), February 1978, pp. 12–20.

[5] Jan R. Wright, Jonathan E. Cooper, "Introduction to Aircraft Aeroelasticity and Loads", John Wiley & Sons, Inc., second edition, 2015, pp. 181

[6] Lancaster, F.W., "Torsional Vibrations of the Tail of an Aeroplane," Reports and Memoranda, no. 276, July 1916, *in* "AIAA Selected Reprint Series, Volume V, Aerodynamic Flutter," I. E. Garrick, ed., March 1969, pp. 12–15.

[7] M. W. Kehoe. "A historical overview of flight flutter testing," NASA Technical Memorandum 4720, 1995.

[8] Von Schlippe, B., "The Question of Spontaneous Wing Oscillations (Determination of Critical Velocity Through Flight-Oscillation Tests)," NACA TM-806, October 1936.

[9] Theodore Theodorsen, "General Theory of Aerodynamic Instability and the Mechanism of Flutter", NACA TR-496, Washington, DC, 1935.

[10] Voigt H., "Wind-Tunnel Investigations on Flexural-Torsional Wing Flutter ", NACA TM-877, Washington, DC, 1938.

[11] Theodorsen T. and Garrick I. E, "A Theoretical and Experimental Investigation of the Flutter Problem", NACA TR-685, Sep. 1940

[12] Fung, **Y. C.** "An Introduction to the Theory of Aeroelasticity", John Wiley & Sons, Inc., New York, 1955.

[13] Brett M. Brooking, "Flutter Analysis of a Two-Dimensional Airfoil Containing Structural Hysteresis Nonlinearities", Master of Engineering, Ottawa-Carleton Institute

for Mechanical and Aerospace Engineering, Carleton University, Ottawa, Ontario, Canada, 1998.

[14] Schwartz, M.D., and Wrisley, D.L., "Final Report on the Investigation of Flight Flutter Testing Techniques for the Bureau of Aeronautics, U. S. Navy," Aeroelastic and Structures Research Laboratory, Massachusetts Institute of Technology, December 1950.

[15] Kachadourian, G., Goldman, R.L., and Roha, D.M., "Flight Flutter Testing of the P6M," *in* "Proceedings of the 1958 Flight Flutter Testing Symposium," NASA SP-385, 1958, pp. 91–96.

[16] Kehoe, M.W., "Aircraft Flight Flutter Testing at the NASA Ames-Dryden Flight Research Facility," NASA TM-100417, May 1988.

[17] Mahaffey, P.T., "Flight Flutter Testing the B-58 Airplane," *in* "Proceedings of the 1958 Flight Flutter Testing Symposium," NASA SP-385, 1958, pp. 121–125.

[18] Stringham, R.H., Jr., and Lenk, E.J., "Flight Flutter Testing Using Pulse Techniques," *in* "Proceedings of the 1958 Flight Flutter Testing Symposium," NASA SP-385, 1958, pp. 69–72.

[19] Meany, J.J., "The Evolution of Flutter Excitation at McDonnell Aircraft," *in* "14th Annual Symposium Proceedings," Society of Flight Test Engineers, August 1983, pp. 4.6-1–4.6-11.

[20] Laure, P., Millet, M., and Piazzoli, G., "Pyrotechnic Bonkers for Structural Tests in Flight," ONERA TP no. 1389 E, 1974.

[21] Dublin, M., and Peller, R., "Flight Flutter Testing of Supersonic Interceptors," *in* "Proceedings of the 1958 Flight Flutter Testing Symposium," NASA SP-385, 1958, pp. 111–120.

[22] Bartley, J., "Flight Flutter Testing of Multi-Jet Aircraft," *in* "Proceedings of the 1958 Flight Flutter Testing Symposium," NASA SP-385, 1958, pp. 103–110.

[23] Huttsell, L. J., Noll, T. E., and Holsapple, D. E., " Wind tunnel Investigation of Supersonic Wing-tail Flutter," *in* "Proceedings of the 1976 Flutter Testing Symposium," NASA SP-415, 1976, pp. 193–212.

[24] Fazle Ali, "Theoretical and Experimental Analysis of Flutter", Master of Aerospace Engineering, University of Minnesota, 1979.

[25] Jennifer Heeg, "An analytical and experimental study to investigate flutter suppression via piezoelectric actuation", Master of Science, School of Engineering and Applied Science, George Washington University, 1991

[26] Jieun Song, Seung Jin Song and Taehyoun Kim, "Experimental Determination of Unsteady Aerodynamic Coefficients and Flutter Behavior of a Rigid Wing", 51st AIAA/ASME/ASCE/AHS/ASC Structures, Structural Dynamics, and Materials Conference, 12 - 15 April 2010, Orlando, Florida

[27] W. Garrard, Aerospace Engineering and Mechanics Department, University of Minnesota, private communication, January 2017.

[28] Bispllighoff, Raymond L., Ashley, Holt, Halfman, and Robert L, "Aeroelasticity" Addison-Wesley Publishing Company, 1955

[29] Moran, Jack., "An Introduction to Theoretical and Computational Aerodynamics" Dover Publications, Inc., page 7, Mineola, New York 1984

[30] G. Dimitriadis, "Lecture Series of Aeroelasticity and Experimental Aerodynamics (AERO0032-1)-lecture 6", University of Liège, Belgium, 2014.

[31] Garrick I, E., " Propulsion of a Flapping and Oscillating Airfoil ", NACA TM-567, 1936

[32] Zimmerman, N. H., Weissenburger, J.T., "Prediction of Flutter Onset Speed Based on Flight Testing at Subcritical Speeds," Journal o f Aircraft, Vol**.** 1, No. 4, 1964

[34] Brignac, W.J., Ness, H.B., Smith, L.M., "The Random Decrement Technique Applied to the YF-16 Flight Flutter Tests," AIAA Paper No. 75-776, presented at the AIAA/ASME/SAE 16th Structures, Structural Dynamics, and Materials Conference, Denver, Colorado, May 1975

[35] Houbolt, J.C., "Subcritical Flutter Testing and System Identification", NASA CR-132480, August 1974

[36] Nash, D.E., Katz, H., and Moody, W.C., "F-15 Flight Flutter Testing: Aircraft Systems and Test Operations," AIAA 1975 Aircraft Systems and Technology Meeting, August 1975

[37] Baird, E. F., and Clark, W. B., "Recent Developments in Flight Flutter Testing in the United States," Presented at 34th Meeting of the AGARD Structures and Materials Panel, April 1972, AGARD Report 596

[38] Peloubet, R. P., Jr., "YF-16 Active-Control-System/ Structural Dynamics Interaction Instability," Presented at 16th AIAA/ASME/SAE Structures, Structures Dynamics and Materials Conference, May 1975

[39] Miao, Wen-Liu, Huber and Helmut B., "Rotor Aeroelastic Stability Coupled With Helicopter Body Motion," NASA SP-352, 1974 pp, 137-146.

[40] Redd, L. T., Gilman, J., Jr., Cooley, D. E. and Sevart, F. D., "Wind-Tunnel Investigation of a B-52 Model Flutter Suppression System," Journal of Aircraft, vol. 11, no. 11, pp. 659-663, Nov. 1974

[41] I. Gursul, R. Gordnier, and M. Visbal, "Unsteady aerodynamics of nonslender delta wings", Progress in Aerospace Sciences, Vol. 41, 2005, pp. 515-557.

[42] D. Tang, J.K. Henry, and E.H. Dowell, "Limit Cycle Oscillations of Delta Wing Models in Low Subsonic Flow," AIAA J., Vol. 37, No. 11, 1999, pp. 1355-1362.

[43] P.J. Attar, E.H. Dowell, and D.M. Tang, "A Theoretical and Experimental Investigation of the Effects of a Steady Angle of Attack on the Nonlinear Flutter of a Delta Wing Plate Model," J. of Fluids and Structures, Vol. 17, 2003, pp. 243-259.

[44] Ueda, T., "Aeroelastic Analysis Considering Structural Uncertainty," Aviation, Vol. 9, No. 1, 2005, pp. 3–7

[45] Ostenfeld-Rosenthal, P., Madsen, H. O., and Larsen, A., "Probabilistic Flutter Criteria for Long Span Bridges," Journal of Wind Engineering and Industrial Aerodynamics, Vol. 42, Nos. 1–3, 1992, pp. 1265–1276.

[46] Kuttenkeuler, J., and Ringertz, U. T., "Aeroelastic Design Optimization with Experimental Verification," Journal of Aircraft, Vol. 35, No. 3, 1998,pp. 505–507.

[47] Yurkovich, R., "Status of Unsteady Aerodynamic Prediction for Flutter of High-Performance Aircraft," Journal of Aircraft, Vol. 40, No. 5, 2003, pp. 832-842.

[48] Chen, X., Zha, G., and Yang, M., "Numerical Simulation of 3-D Wing Flutter with Fully Coupled Fluid-Structural Interaction," Computers & Fluids, Vol. 36, 2007, pp. 856-867.

[49] Liu, F., Cai, J., Zhu, Y., Tsai, H.M., Wong, A.S.F., "Calculation of Wing Flutter by a Coupled CFD-CSD Method," AIAA Journal of Aircraft, Vol. 38, No. 2, 2001, pp. 334-342.

[50] Cella, U., and Biancolini, M., "Aeroelastic Aanalysis of Aircraft Wind-Tunnel Model Coupling Structural and Fluid Dynamic Codes," Journal of Aircraft, Vol. 49, No. 2, 2012, pp. 407-414.

[51] Bohbot, J., Darracq, D., "Time Domain Analysis of Two D.O.F. Airfoil Flutter using an Euler/Turbulent Navier–Stokes Implicit Solver," International Forum on Aeroelasticity and Structural Dynamics, Madrid, Spain, June 5–7, 2001.

[52] Rival, D. and C. Tropea, "Characteristics of Pitching and Plunging Airfoils under Dynamic-Stall Conditions," Journal of Aircraft, 2010. 47(1): p. 80-86.

[54] De Marqui Junior, C., et al., "Design of an Experimental Flutter Mount System," Journal of the Brazilian Society of Mechanical Sciences and Engineering, 2007, 29(3): p. 246-252.

[55] Robinson, B. A., Batina, J. T., and Yang, H. T. Y., "Aeroelastic Analysis of Wings Using the Euler Equations with a Deforming Mesh," Journal of Aircraft, Vol. 28, No. 11, 1991, pp. 778-788.

[56] Edwards, J. W., Bennett, R. M., Whitlow, W., Jr., and Seidel, D. A., "Time-Marching Transonic Flutter Solutions Including Angle-of-Attack Effects," AIAA Paper 82-3685, May 1982.

[57] Mohr, R. W, Batina, J. T., and Yang, H. T. Y., "Mach Number Effects on Transonic Aeroelastic Forces and Flutter Characteristics," Journal of Aircraft, Vol. 26, No. 11, 1989, pp. 1038-1046.

[58] Horikawa, H. and Dowell, E. H., "An Elementary Explanation of the Flutter Mechanism with Active Feedback Controls," Journal of Aircraft, Vol. 16, No. 4, April 1979, pp. 225 -232.

[59] Kinsey, T., and Dumas, G., "Parametric study of an oscillating airfoil in a power-extraction regime," AIAA Journal, Vol. 46, No.6, 2008, pp.1318-1330.

[60] Xiao, Q. and Liao, W., "Numerical study of asymmetric effect on a pitching foil," International Journal of Modern Physics, Vol. 20, 2009, pp. 1663-1680.

APPENDIX

APPENDIX A

Experimental Results of other wings (2nd Experimental Set-up)

➔ The EPP 1.3 Black Wing

It is made of foam (EPP 1.3), it has a mass of 9.82 x 10^{-3} kg, a chord length of 5 inches and a span of 12 inches.

Table A.1 The experimental results of the EPP 1.3 Black Wing

Tension spring #	# 1	# 2	# 3	# 4	# 5	# 6
Flutter speed (m/s)	14.6	18.2	22.9	40.1	25.5	44.6

➔ The EPP 1.9 Black Wing

It is made of foam (EEP 1.9), it has a mass of 17.74 x 10^{-3} kg, a chord length of 5 inches and a span of 12 inches.

Table A.2 The experimental results of the EPP 1.9 Black Wing

Tension spring #	# 1	# 2	# 3	# 4	# 5	# 6
Flutter speed (m/s)	16	18.9	23.9	40.9	26.8	46

➔ The EPS 2 Purple Wing

It is made of foam (EPS 2), it has a mass of 16.69 x 10^{-3} kg, a chord length of 5 inches and a span of 12 inches.

Table A.3 The experimental results of the EPS 2 Purple Wing

Tension spring #	# 1	# 2	# 3	# 4	# 5	# 6
Flutter speed (m/s)	15.9	18.7	23.6	40.5	26.5	45.8

➔ The XPS 2.3 Grey Wing

It is made of foam (EPS 2), it has a mass of 18.96 x 10^{-3} kg, a chord length of 5 inches and a span of 12 inches.

Table A.4 The experimental results of the XPS 2.3 Grey Wing

Tension spring #	# 1	# 2	# 3	# 4	# 5	# 6
Flutter speed (m/s)	16.3	19.1	24.2	41.3	27.2	46.4

APPENDIX B

Calculation of center of gravity of main airfoil and side cap airfoil

The center of gravity X_{cg} can be evaluated using equation (4.2).

$$X_{cg} = \frac{1}{A}\int_a^b x\left(f(x) - g(x)\right)dx$$

f(x) = y(t), *y(t)* is the upper function of airfoil NACA 0015

g(x) = - y(t), *y(t)* is the lower function of airfoil NACA 0015

$$y_t = 5t\left[0.2969\sqrt{\frac{x}{c}} - 0.126\left(\frac{x}{c}\right) - 0.3516\left(\frac{x}{c}\right)^2 + 0.2843\left(\frac{x}{c}\right)^3 - 0.1015\left(\frac{x}{c}\right)^4\right]$$

$$A = \int_a^b \left(f(x) - g(x)\right)dx$$

*a=0, b=c, t=15*c/100*

$$A = \int_0^c \left(y(t) - (-y(t))\right)dx = \int_0^c 2\,y(t)\,dx$$

$$A = -\frac{0.03045\,x^5}{c^3} + \frac{0.106613\,x^4}{c^2} - \frac{0.1758\,x^3}{c} + 0.2969\,c\,x\sqrt{\frac{x}{c}} - 0.0945\,x^2$$

And

$$X_{cg} = \frac{1}{A}\int_0^c x\left(y(t) - (-y(t))\right)dx = \frac{1}{A}\int_0^c x\,2\,y(t)\,dx$$

$$X_{cg} = \frac{1}{A}\,\frac{0.17814\,c^4\,x^2\sqrt{\frac{x}{c}} - 0.063\,c^3\,x^3 - 0.13185\,c^2\,x^4 + 0.08529\,c\,x^5 - 0.025375\,x^6}{c^3}$$

The value of c = 5 in,

A = 2.56906 in^2

$$X_{cg} = \frac{1}{A}(5.40062)$$

X_{cg} = 2.1 in = 0.05334

APPENDIX C

Calculation of mass moment of inertia about the center of gravity I_{cg} of the main airfoil for the first experimental set up

The method is explained in section 4.2.2.6. The following MATLAB code was written to evaluate the I_{cg}:

```
% NUMERICAL CALCULATION OF MASS MOMENT OF INERTIA OF THE MAIN AIRFOIL (FIRST EXP. SET-UP)
clear all
clc
c=5*0.0254; % chord length in m (5 inch)
m_w=18.81E-3 ;  % mass of MAIN AIRFOIL (BLUE WING) in kg
VOLUME=30.863379*(0.0254)^3 % the volume is calculated from the SOLIDWORKS (m^3);
rho=m_w/VOLUME;  % the diensity of airofil
L=12*0.0254; % span of airfoil in m (12 inch)
t=0.15*c % the maximum thickness of airfoil

n=1000 % number of segments
length=5*0.0254 % LENGTH OF THE OBJECT (AIRFOIL CHORD) in m
delta_x=length/n % length of each rectangular segment in m
x=delta_x:delta_x:length;
% the height of each rectangular segment in m is:
y=2*(5.*t.*(0.2969.*sqrt(x./c)-0.1260.*(x./c)-0.3516.*(x./c).^2+0.2843.*(x./c).^3-0.1015.*(x./c).^4));
m=rho*L.*delta_x.*y;            % mass of each rectangular segment in kg/m^3
r=abs(2.1*0.0254-(1.*x));        % distance from main CG to cg of each rectangular segment in m
I_cg=m./12.*(delta_x.^2+y.^2);  % moment of inertia of each rectangular segment in (kg.m^2)
I_CG=I_cg+m.*r.^2;        % moment of inertia of each segment about the CG in (kg.m^2)
fprintf ('     x=a       y=b        m          r       I_cg       I_CG')
[x' y'  m'  r'  I_cg'   I_CG']

I_CG_TOTAL=sum(I_CG)    % THE MASS MOMENT OF INERTIA OF AIRFOIL ABOUT THE CENTER OF GRAVITY in (kg.m^2)

```

APPENDIX D

Calculation of mass moment of inertia about the center of gravity I_{cg} of the main airfoil for the second experimental set up

The method is explained in section 5.2.2.3 and it is similar to the calculation in appendix C but with different airfoil mass in this case. The following MATLAB code was written to evaluate the I_{cg}:

```
% NUMERICAL CALCULATION OF MASS MOMENT OF INERTIA OF THE MAIN AIRFOIL (SECOND EXP. SET-UP)
clear all
clc
c=5*0.0254; % chord length in m (5 inch)
m_w=11.51E-3 ;  % mass of MAIN AIRFOIL (RED WING) in kg
VOLUME=30.863379*(0.0254)^3 % the volume is calculated from the SOLIDWORKS (m^3);
rho=m_w/VOLUME;  % the diensity of airofil
L=12*0.0254; % span of airfoil in m (12 inch)
t=0.15*c % the maximum thickness of airfoil

n=1000 % number of segments
length=5*0.0254 % LENGTH OF THE OBJECT (AIRFOIL CHORD) in m
delta_x=length/n % length of each rectangular segment in m
x=delta_x:delta_x:length;
% the height of each rectangular segment in m is:
y=2*(5.*t.*(0.2969.*sqrt(x./c)-0.1260.*(x./c)-0.3516.*(x./c).^2+0.2843.*(x./c).^3-0.1015.*(x./c).^4));
m=rho*L.*delta_x.*y;            % mass of each rectangular segment in kg/m^3
r=abs(2.1*0.0254-(1.*x));        % distance from main CG to cg of each rectangular segment in m
I_cg=m./12.*(delta_x.^2+y.^2);  % moment of inertia of each rectangular segment in (kg.m^2)
I_CG=I_cg+m.*r.^2;        % moment of inertia of each segment about the CG in (kg.m^2)
fprintf ('     x=a       y=b        m          r       I_cg       I_CG')
[x' y'  m'  r'  I_cg'   I_CG']

I_CG_TOTAL=sum(I_CG)    % THE MASS MOMENT OF INERTIA OF AIRFOIL ABOUT THE CENTER OF GRAVITY in (kg.m^2)
```

APPENDIX E

Sample Calculation of Flutter speed and Related Terms

Given data:

Mass of main airfoil = 11.51×10^{-3} kg

Mass of side cap airfoil = 2.1×10^{-3} kg

Mass of support plate = 0.64×10^{-3} kg

Mass of tension spring type # 1 = 13.24×10^{-3} kg

Spring constant k_h = 17.52 N/m

Airfoil span = 12 in = 0.3048 m

Airfoil chord = 5 in = 0.127 m

Air density = 1.23 kg/m^3

Calculation:

➔ The total mass of the Red wing including $\frac{1}{3}$ of each spring mass is:

$M = 11.51 \times 10^{-3} + 2*(2.1 \times 10^{-3}) + 4*(0.64 \times 10^{-3}) + 8*(1/3)*(13.24 \times 10^{-3})$

$= 0.0536$

➔ The center of gravity X_{CG}:

Using equation (4.1) and the data in table 5.4

X_{CG} = 0.0512 m, (from leading edge)

➔ The location of the elastic axis X_e:

X_e lays at mid-distance between the forward and the aft tension springs such that:

X_e = 1.5 in = 0.0381 m, (from leading edge)

➔ Distance between the elastic axis and the center of gravity d is:

$d = X_{CG} - X_e = 0.0131$ m

➔ Moment of inertia about the center of gravity I_{CG}:

Using equation (5.17) and data in tables 5.6 and 5.7, we get

$I_{CG} = 8.8791 \times 10^{-4}$ kg.m^2

➔ Moment of inertia about the elastic axis I_α:

$I_\alpha = I_{CG} + M\, d^2$

$I_\alpha = 8.9711 \times 10^{-4}$ kg.m^2

➔ The total tension spring constant of 8 tension springs K_h:

$K_h = 8 * k_h$

$K_h = 140.15$ N/m

➔ The total torsion spring constant K_α:

$$K_\alpha = \frac{K_h}{10.54}$$

$K_\alpha = 13.3$ N.m

➔ The uncoupled natural frequency in bending (ω_h):

$$\omega_h = \sqrt{\frac{K_h}{M}}$$

$\omega_h = 51.15$ rad/s

➔ The uncoupled natural frequency in torsion (ω_α):

$$\omega_\alpha = \sqrt{\frac{K_\alpha}{I_\alpha}}$$

ω_α = 121.8 rad/s

➔ The non-dimensional radius of gyration about the elastic axis (r_α):

$$r_\alpha = \sqrt{\frac{I_\alpha}{M\,b^2}}$$

r_α = 2.0378

➔ The mass ratio (μ):

$$\mu = \frac{m}{\pi\,\rho_{air}\,b^2\,L}$$

μ = 11.2813

➔ The non-dimensional distance of wing center of gravity aft of the elastic axis in semichords (x_α):

$$x_\alpha = \frac{X_{CG} - X_e}{b} = \frac{2\,d}{c}$$

x_α = 0.2064

➔ The non-dimensional distance from center of chord to the elastic axis (a_h):

$$a_h = \frac{b - X_e}{b} = 1 - \frac{2\,X_e}{c}$$

$a_h = 0.4$

➔ The coefficients:

For the inverse of reduced frequency *1/k* = 1.25

The corresponding value of the real part of Theodorsen function *F* and the imaginary part *G* from table 2.1 are:

$F = 0.5541$

$G = -0.1165$

$k = 0.8$

$$A_R = -(\mu + 1) - \frac{2G}{k} = -11.99$$

$$A_I = \frac{2F}{k} = 1.3853$$

$$B_R = -(\mu x_\alpha - a_h) + \frac{2F}{k^2} - \left(\frac{1}{2} - a_h\right)\frac{2G}{k} = -0.1678$$

$$B_I = \frac{1}{k}\left[1 + \frac{2G}{k} + \left(\frac{1}{2} - a_h\right)2F\right] = 1.0245$$

$$D_R = -(\mu x_\alpha - a_h) + \left(\frac{1}{2} + a_h\right)\frac{2G}{k} = -2.1906$$

$$D_I = -\left(\frac{1}{2} + a_h\right)\frac{2F}{k} = -1.2467$$

$$E_R = -\left(\mu r_\alpha^2 + a_h^2 + \frac{1}{8}\right) + \left(\frac{1}{4} - a_h^2\right)\frac{2G}{k} - \left(\frac{1}{2} + a_h\right)\frac{2F}{k^2} = -48.7167$$

$$E_I = \frac{1}{k}\left[\left(\frac{1}{2} - a_h\right) - \left(\frac{1}{2} + a_h\right)\frac{2G}{k} - \left(\frac{1}{4} - a_h^2\right)2F\right] = 0.3280$$

For no damping ($g_h = 0$, and $g_\alpha = 0$), we get:

$$\Delta_R = (1 - g_h g_\alpha)\mu^2 r_\alpha^2 \frac{\omega_h^2}{\omega_\alpha^2} x^2 + \left[\mu \frac{\omega_h^2}{\omega_\alpha^2}(E_R - g_h E_I) + \mu r_\alpha^2 (A_R - g_\alpha A_I) \right] x + A_R E_R - B_R D_R - A_I E_I + B_I D_I$$

$\Delta_R = 93.2724\, x^2 - 658.6924\, x + 582.0154$

$$\Delta_I = (g_h + g_\alpha)\mu^2 r_\alpha^2 \frac{\omega_h^2}{\omega_\alpha^2} x^2 + \left[\mu \frac{\omega_h^2}{\omega_\alpha^2}(g_h E_R + E_I) + \mu r_\alpha^2 (A_I + g_\alpha A_R) \right] x + A_I E_R - B_R D_I + A_R E_I - B_I D_R$$

$\Delta_I = 65.5479\, x - 69.3823$

Setting $\Delta_R = 0$, we get:

$\sqrt{x} = 2.45, 1.017$ for real values

and

$\Delta_I = 0$, we get:

$\sqrt{x} = 1.029$ for imaginary value

Plotting $\frac{1}{k}$ VS $\sqrt{x}$ for all values i.e. (1.25,2.45), (1.25,1.017) and (1.25,1.029) for the value of $1/k = 1.25$.

Repeating the above process for series of values for the inverse of the reduced frequency $1/k$, we get:

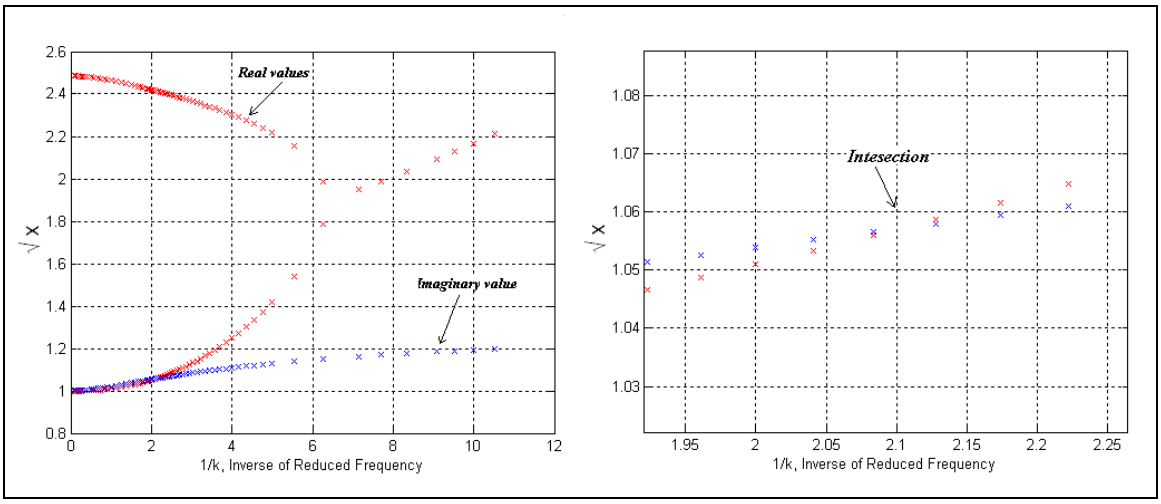

Figure E.1 Solution of Flutter Determinant using Theodorsen Function for tension spring # 1

From figure E.1, we get:

$1/k = 2.1$ (inverse of reduced frequency), $\sqrt{x} = 1.057$

$$U_F = \frac{1}{k}\frac{\omega_\alpha c}{2\sqrt{x}} = (2.1)\frac{(121.8\frac{rad}{s})(0.127\,m)}{2(1.057)} = 15.4\frac{m}{s}$$

APPENDIX F

Theodorsen's Function

Main reference: G. Dimitriadis, "Lecture Series of Aeroelasticity and Experimental Aerodynamics (AERO0032-1)-lecture 6", University of Liège, Belgium, 2014

Note: A lot of stuff is taken from this source and all figures are reproduced from it.

In Theodorsen's approach, three major assumptions are assumed.

- The flow is always attached, i.e. the motion's amplitude is small
- The wing is a flat plate
- The wake is flat

The third assumption is not problematic as the motion is already assumed to be small (first assumption), then the flat wake assumption has a little influence on the results.

The flow is potential and the model is based on elementary solution of the Laplace solution.

$$\nabla^2 \phi = 0 \tag{F.1}$$

Where ϕ is the velocity potential. Such solution are:

- The free stream

$$\phi = U\cos(\alpha)x + U\sin(\alpha)y \tag{F.2}$$

- The source and sink

$$\phi = \frac{\sigma}{2\pi}\ln(r) = \frac{\sigma}{2\pi}\ln\sqrt{(x-x_0)^2 - (y-y_0)^2} \tag{F.3}$$

- The vortex

$$\phi = -\frac{\Gamma}{2\pi}\theta = -\frac{\Gamma}{2\pi}\tan^{-1}\left(\frac{y-y_0}{x-x_0}\right) \tag{F.4}$$

- The doublet

$$\phi = \frac{\mu}{2\pi}\frac{\cos\theta}{r} = \frac{\mu}{2\pi}\frac{x}{x^2+y^2} \tag{F.5}$$

The wing is modeled as a circle to be mapped onto a flat plate through conformal mapping as shown in figure F.1.

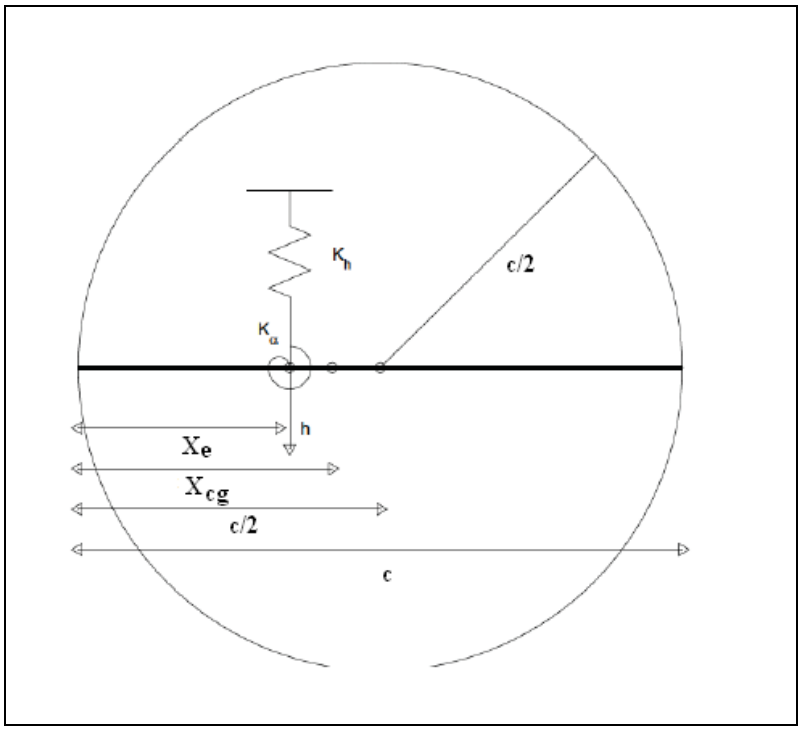

Figure F.1 Modeling the wing as a circle

The wing has a chord length of c, (Xe) is the location of elastic axis and (Xcg) is the location of the center of the gravity.

The following singularities were considered by Theodorsen

- A free stream speed of U and zero angle of attack.
- A pattern of sources of double strength ($+2\sigma$) on the top surface of the flat plate, balanced by sinks of double strength (-2σ) on the bottom surface.
- A pattern of vortices ($+\Delta\Gamma$) on the flat plate, balanced by opposite ($-\Delta\Gamma$) in the wake.

The complete flow field is shown in figure F.2

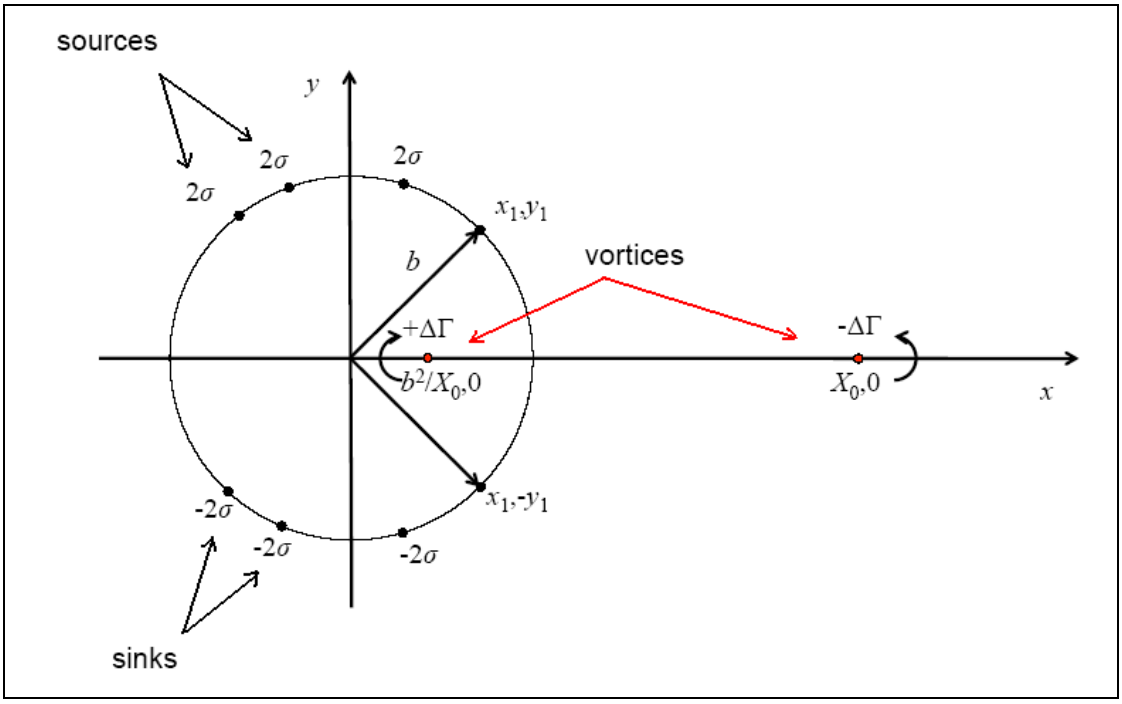

Figure F.2 Flow field (circle)

Where (b) represent the wing half-chord.

The Joukowski's conformal transformation is used to map the wing (circle shape) to flat plate as shown in figure F.3. Points inside the circle are transformed outside the flat plate; therefore, the vortices inside the circle are mapped on the wake.

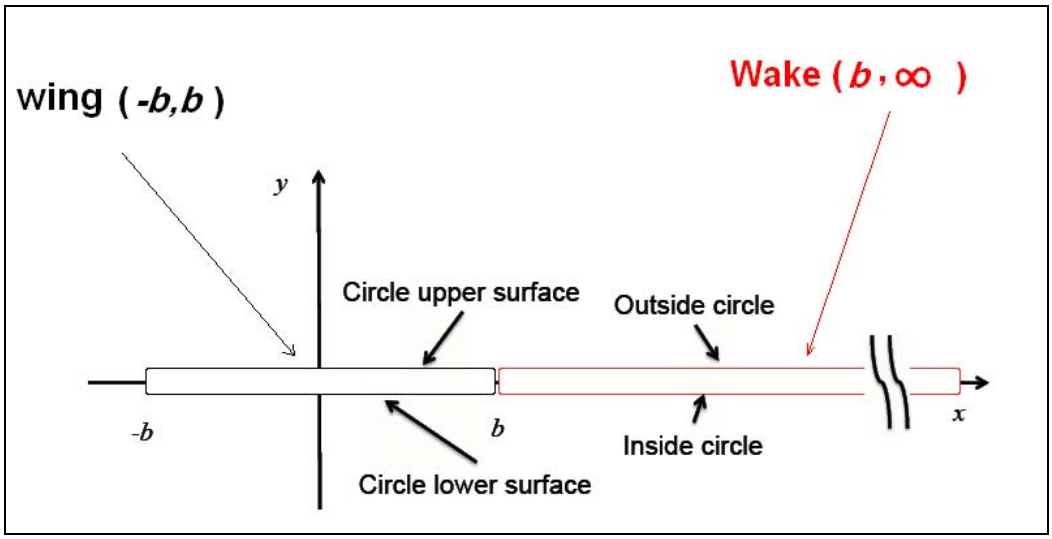

Figure F.3 Complete flow field after transformation

There are two boundary conditions, the impermeability condition at which the flow can not across the solid boundary; and the Kutta condition at which the flow must separate at the trailing edge. The impermeability condition is fulfilled by the source and sink distribution, while the Kutta condition is fulfilled by the vortex distribution. Kelvins' theorem is automatically fulfilled because for every vortex $+\Delta\Gamma$ there is a counter-vortex $-\Delta\Gamma$, Therefore, the total change in vorticity is always zero.

For a moving wing, the velocity induced by the source distribution normal to the wing's surface must be equal to the velocity due to the wing's motion and the free stream, i.e.

$$\frac{\partial \phi}{\partial n} = -w \tag{F.6}$$

Where n is a unit vector normal to the surface and w is the external upwash.

The source strength across a solid boundary is given by:

$$-\frac{\partial \phi}{\partial n} = \sigma \tag{F.7}$$

If the potential of the internal flow is assumed to be constant, then:

$$\sigma = w \tag{F.8}$$

For two-degree of freedom of wing, the total upwash due to its pitch and plunge motions is given by:

$$w = -\left[U\alpha + \dot{h} + \left(b(\bar{x}_1 + 1) - x_e\right)\dot{\alpha} \right] \tag{F.9}$$

Where x_e is the location of the elastic axis.

$$\bar{x} = \frac{x}{b} \tag{F.10}$$

Where x is measured from the half-chord.

The potential induced by a source at a point (x_1,y_1) is given by:

$$d\phi(x_1, y_1) = \frac{\sigma}{2\pi} \ln \sqrt{(x - x_1)^2 + (y - y_1)^2} = \frac{\sigma}{4\pi} \ln\left[(x - x_1)^2 + (y - y_1)^2\right] \tag{F.11}$$

The potential induced by a source at a point (x_1,y_1) and sink at a point $(x_1,-y_1)$ of double strength for both source and sink is given by:

$$d\phi(x_1, \pm y_1) = \frac{\sigma}{2\pi} \ln\left[\frac{(x - x_1)^2 + (y - y_1)^2}{(x - x_1)^2 + (y + y_1)^2} \right] \tag{F.12}$$

Using the non-dimensional coordinates in equation (F.10), $\bar{x} = \frac{x}{b}$, $\bar{y} = \sqrt{1 - \bar{x}^2}$, we get:

$$d\phi(\bar{x}_1, \pm \bar{y}_1) = \frac{\sigma}{2\pi} \ln\left[\frac{(\bar{x} - \bar{x}_1)^2 + (\bar{y} - \bar{y}_1)^2}{(\bar{x} - \bar{x}_1)^2 + (\bar{y} + \bar{y}_1)^2} \right] \tag{F.13}$$

The total potential is then give by:

$$\phi(\bar{x},\bar{y}) = \frac{b}{2\pi}\int_{-1}^{1}\sigma \ln\left[\frac{(\bar{x}-\bar{x}_1)^2+(\bar{y}-\bar{y}_1)^2}{(\bar{x}-\bar{x}_1)^2+(\bar{y}+\bar{y}_1)^2}\right]d\bar{x}_1 \tag{F.14}$$

Substituting from equation (F.8) for the value of the upwash, we get:

$$\phi(\bar{x},\bar{y}) = \frac{b}{2\pi}\int_{-1}^{1}\left[U\alpha + \dot{h} + \left(b(\bar{x}_1+1)-x_e\right)\dot{\alpha}\right]\ln\left[\frac{(\bar{x}-\bar{x}_1)^2+(\bar{y}-\bar{y}_1)^2}{(\bar{x}-\bar{x}_1)^2+(\bar{y}+\bar{y}_1)^2}\right]d\bar{x}_1 \tag{F.15}$$

Performing the integration, the potentials on the upper and lower surface are given by:

$$\phi(\bar{x},\bar{y}) = b\left(U\alpha + \dot{h} - x_e\dot{\alpha}\right)\sqrt{1-\bar{x}^2} + \frac{b^2\dot{\alpha}}{2}(\bar{x}+2)\sqrt{1-\bar{x}^2} \tag{F.16}$$

$$\phi(\bar{x},\bar{y})_{lower} = -\phi(\bar{x},\bar{y}) \tag{F.17}$$

The static pressure on the surface can be given the unsteady Bernoulli equation (F.18).

$$p = -\rho\left(\frac{q^2}{2}+\frac{\partial\phi}{\partial t}\right) + Const. \tag{F.18}$$

Where ρ is the air density and q is local air velocity.

Since the wing lies on the x-axis, the local velocity is tangential to the wing surface.

$$q = U\cos\alpha + u = U\cos\alpha + \frac{\partial\phi}{\partial x} \approx U + \frac{\partial\phi}{\partial x} \tag{F.19}$$

The pressures on the upper and lower surface are:

$$p_{upper} = -\rho\left[\frac{1}{2}\left(U+\frac{\partial\phi}{\partial x}\right)^2 + \frac{\partial\phi}{\partial t}\right] + Const. \tag{F.20}$$

$$p_{lower} = -\rho\left[\frac{1}{2}\left(U - \frac{\partial\phi}{\partial x}\right)^2 - \frac{\partial\phi}{\partial t}\right] + Const. \tag{F.21}$$

The pressure difference is then:

$$\Delta p = p_{upper} - p_{lower} = -2\rho\left(U\frac{\partial\phi}{\partial x} + \frac{\partial\phi}{\partial t}\right) = -2\rho\left(\frac{U}{b}\frac{\partial\phi}{\partial\bar{x}} + \frac{\partial\phi}{\partial t}\right) \tag{F.22}$$

The non-circulatory lift and moment about the elastic axis are given by equations (F.23) and (F.24) respectively.

$$L_{nc} = \int_0^c \Delta p\, dx = b\int_{-1}^{1} \Delta p\, d\bar{x} \tag{F.23}$$

$$M_{nc} = \int_0^c \Delta p\left(x - x_e\right)dx = b\int_{-1}^{1} \Delta p\left[b\left(\bar{x}+1\right) - x_e\right]d\bar{x} \tag{F.24}$$

Substituting for the pressure difference from equation (F.22), we get:

$$L_{nc} = -2b\rho\int_{-1}^{1}\left(\frac{U}{b}\frac{\partial\phi}{\partial\bar{x}} + \frac{\partial\phi}{\partial t}\right)d\bar{x} = -2b\rho\,\phi\Big|_{-1}^{+1} - 2b\rho\int_{-1}^{1}\frac{\partial\phi}{\partial t}d\bar{x} = -2b\rho\int_{-1}^{1}\frac{\partial\phi}{\partial t}d\bar{x} \tag{F.25}$$

Where $\phi(1) = \phi(-1)$=0.

Carrying out the integration, we obtain:

$$L_{nc} = b^2\rho\pi\left[\ddot{h} - \left(x_e - \frac{c}{2}\right)\ddot{\alpha} + U\dot{\alpha}\right] \tag{F.26}$$

$$\begin{aligned} M_{nc} &= -2\rho bU\int_{-1}^{1}\bar{x}\frac{\partial\phi}{\partial\bar{x}}d\bar{x} - 2\rho b\int_{-1}^{1}\frac{\partial\phi}{\partial t}\left(\bar{x}b + b - x_e\right)d\bar{x} \\ &= 2\rho bU\int_{-1}^{1}\phi\, d\bar{x} - 2\rho b\int_{-1}^{1}\frac{\partial\phi}{\partial t}\left(\bar{x}b + b - x_e\right)d\bar{x} \end{aligned} \tag{F.27}$$

Carrying out the integration, we obtain:

$$M_{nc} = \rho\pi b^2\left(x_e - \frac{c}{2}\right)\left(\ddot{h} - \left(x_e - \frac{c}{2}\right)\ddot{\alpha}\right) - \frac{\rho\pi b^4}{8}\ddot{\alpha} + \rho\pi b^2 U\dot{h} + \rho\pi b^2 U^2\alpha \qquad \text{(F28)}$$

We need to find the circulatory lift and moment due to the wake. This is achieved by satisfying the Kutta condition using the vortex distribution.

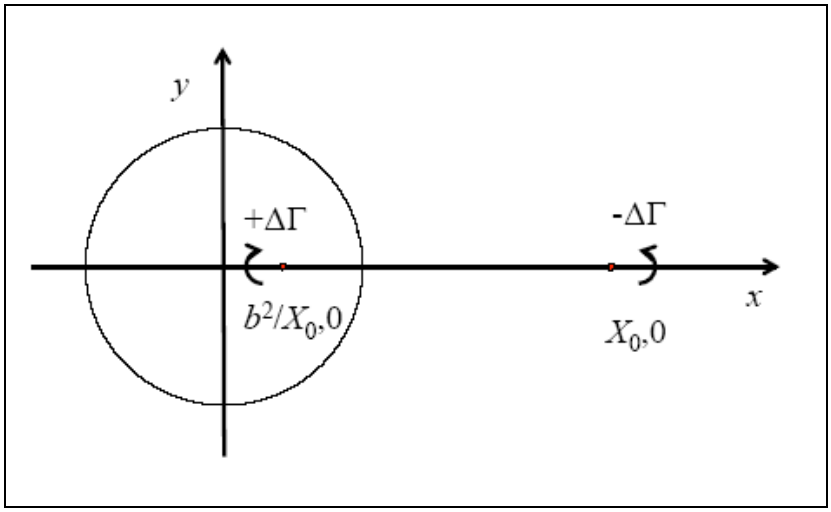

Figure F.4 Distribution of vortices

The induced potential by the vortices at (X_0.0) and (b^2/X_0,0) is given by:

$$\phi_{\Delta\Gamma} = \frac{\Delta\Gamma}{2\pi}\left(\tan^{-1}\frac{y}{x - X_0} - \tan^{-1}\frac{y}{x - \dfrac{b^2}{X_0}}\right) \qquad \text{(F.29)}$$

Defining the non-dimensional coordinates as:

$$\bar{X}_0 + \frac{1}{\bar{X}_0} = 2\bar{x}_0 \quad \text{or} \quad \bar{X}_0 = \bar{x}_0 + \sqrt{\bar{x}_0^2 - 1}$$

Then the induced potential due to the vortex pair can be reformulated as:

$$\phi_{\Delta\Gamma} = -\frac{\Delta\Gamma}{2\pi}\tan^{-1}\frac{\sqrt{1-\bar{x}^2}\sqrt{\bar{x}_0^2-1}}{1-\bar{x}\,\bar{x}_0} \tag{F.30}$$

The pressure difference generated due to this potential is the same as in equation (F.22). Theodorsen assumed that the vortices travel downstream with same velocity as the free stream. Then,

$$\frac{\partial\phi}{\partial t} = \frac{\partial\phi}{\partial x_0}U \tag{F.31}$$

Where $x_0 = b\bar{x}_0$.

Then the pressure difference at one point on the flat plate caused by one vortex is given by:

$$\Delta p = -2\rho U\left(\frac{\partial\phi}{\partial x}+\frac{\partial\phi}{\partial x_0}\right) = -2\rho\frac{U}{b}\left(\frac{\partial\phi}{\partial\bar{x}}+\frac{\partial\phi}{\partial\bar{x}_0}\right) \tag{F.32}$$

Using the non-dimensional coordinates, we get:

$$\Delta p(\bar{x},\bar{x}_0) = -\rho U\frac{\Delta\Gamma}{b\pi}\left(\frac{\bar{x}_0+\bar{x}}{\sqrt{1-\bar{x}^2}\sqrt{\bar{x}_0^2-1}}\right) \tag{F.33}$$

To obtain the full circulatory aerodynamic lift and moment, we need to integrate for all vortices over the wing and the wake.

Intergrading over the wing, we get:

$$L_c(\bar{x}_0) = \int_0^c \Delta p(\bar{x},\bar{x}_0)\,dx = b\int_{-1}^{1}\Delta p(\bar{x},\bar{x}_0)\,d\bar{x} \tag{F.34}$$

Substituting for the value of pressure difference from equation (F.33), we obtain:

$$L_c(\bar{x}_0) = -\frac{\rho U\Delta\Gamma}{\pi\sqrt{\bar{x}_0^2-1}}\int_{-1}^{1}\left(\frac{\bar{x}_0+\bar{x}}{\sqrt{1-\bar{x}^2}}\right)d\bar{x} \tag{F.35}$$

$$L_c(\bar{x}_0) = -\rho U \Delta\Gamma \frac{\bar{x}_0}{\sqrt{\bar{x}_0^2 - 1}} \tag{F.36}$$

Intergrading over the wake begins at the trailing edge and extends to infinity.

$$L_c(\bar{x}_0) = -\rho U \int_1^{\infty} \frac{\bar{x}_0}{\sqrt{\bar{x}_0^2 - 1}} \Delta\Gamma \tag{F.37}$$

The change in the circulation can be defined as

$$\Delta\Gamma = bV d\bar{x}_0 \tag{F.38}$$

Where V is a non-dimensional measure of vortex strength at a point x_0.

The circulatory lift becomes

$$L_c(\bar{x}_0) = -\rho U b \int_1^{\infty} \frac{\bar{x}_0}{\sqrt{\bar{x}_0^2 - 1}} V d\bar{x}_0 \tag{F.39}$$

The circulatory moment about the elastic axis is given by

$$M_c = \int_0^c \Delta p(\bar{x}, \bar{x}_0)(x - x_e)dx = b\int_{-1}^{1} \Delta p(\bar{x}, \bar{x}_0)\left[b(\bar{x}+1) - x_e\right]d\bar{x} \tag{F.40}$$

Substituting the value of the pressure difference from equation (F.33), and integrate, we obtain:

$$M_c = -\rho U b \int_1^{\infty} \left(\frac{b}{2} \sqrt{\frac{\bar{x}_0 + 1}{\bar{x}_0 - 1}} - ec \frac{\bar{x}_0}{\sqrt{\bar{x}_0^2 - 1}} \right) V d\bar{x}_0 \tag{F.41}$$

The value of V can be obtained by applying the Kutta condition which states that the velocity at the trailing edge is zero. This can be applied for the horizontal velocity component as the wing (flat plate) lies on the x-axis.

The Kutta condition is given by:

$$\left.\frac{\partial \phi_{total}}{\partial \bar{x}}\right|_{\bar{x}=1} = finite \tag{F.42}$$

ϕ_{total} is the total potential due to the sources and vortices.

From equations (F.16), (F.30) and (F.38), the total potential is:

$$\begin{aligned}\phi_{total}(\bar{x}) = b\left(U\alpha + \dot{h} - x_e\dot{\alpha}\right)\sqrt{1-\bar{x}^2} + \frac{b^2\dot{\alpha}}{2}(\bar{x}+2)\sqrt{1-\bar{x}^2} \\ -\frac{b}{2\pi}\int_1^{\infty}\tan^{-1}\frac{\sqrt{1-\bar{x}^2}\sqrt{\bar{x}_0^2-1}}{1-\bar{x}\,\bar{x}_0}V d\bar{x}_0\end{aligned} \tag{F.43}$$

The horizontal velocity component is produced by taking the derivative of the total potential along x-axis as in equation (F.44).

$$\begin{aligned}\frac{\partial \phi_{total}}{\partial \bar{x}} = -b\left(U\alpha + \dot{h} - x_e\dot{\alpha}\right)\frac{\bar{x}}{\sqrt{1-\bar{x}^2}} - \frac{b^2\dot{\alpha}}{2}\frac{2\bar{x}^2+2\bar{x}-1}{\sqrt{1-\bar{x}^2}} \\ +\frac{b}{2\pi}\int_1^{\infty}\frac{\sqrt{\bar{x}_0^2-1}}{\sqrt{1-\bar{x}^2}\,(\bar{x}-\bar{x}_0)}V d\bar{x}_0\end{aligned} \tag{F.44}$$

Rearranging the terms of equation (F.44), the velocity can be written as:

$$\frac{\partial \phi_{total}}{\partial \bar{x}} = \frac{1}{\sqrt{1-\bar{x}^2}}\left[\begin{array}{c} -b\left(U\alpha + \dot{h} - x_e\dot{\alpha}\right)\bar{x} - \frac{b^2\dot{\alpha}}{2}\left(2\bar{x}^2+2\bar{x}-1\right) \\ +\frac{b}{2\pi}\int_1^{\infty}\frac{\sqrt{\bar{x}_0^2-1}}{(\bar{x}-\bar{x}_0)}V d\bar{x}_0 \end{array}\right] \tag{F.45}$$

At the trailing edge $(\bar{x}=1)$, this makes the denominator to be zero. To have the velocity finite, the nominator must be zero to satisfy the Kutta condition at the trailing edge. Thus:

$$\left(U\alpha + \dot{h} - x_e\dot{\alpha}\right) + \frac{3b\dot{\alpha}}{2} = \frac{1}{2\pi}\int_1^{\infty}\frac{\sqrt{\bar{x}_0^2-1}}{(1-\bar{x}_0)}V d\bar{x}_0 \tag{F.46}$$

Rearranging terms, we get:

$$U\alpha + \dot{h} + \left(\frac{3c}{4} - x_e\right)\dot{\alpha} = -\frac{1}{2\pi}\int_1^\infty \frac{\sqrt{\bar{x}_0 + 1}}{\bar{x}_0 - 1} V d\bar{x}_0 \tag{F.47}$$

Dividing the circulatory lift in equation (F.39) and circulatory moment equation (F.41) by equation (F.47), we get:

$$L_c = \pi\rho UcC\left[U\alpha + \dot{h} + \left(\frac{3c}{4} - x_e\right)\dot{\alpha}\right] \tag{F.48}$$

$$M_c = -\pi\rho Uc\left(\frac{b}{2} - ecC\right)\left[U\alpha + \dot{h} + \left(\frac{3c}{4} - x_e\right)\dot{\alpha}\right] \tag{F.49}$$

Where *C* is the Theodorsen Function.

$$C = \frac{\int_1^\infty \frac{\bar{x}_0}{\bar{x}_0^2 - 1} V d\bar{x}_0}{\int_1^\infty \frac{\sqrt{\bar{x}_0 + 1}}{\bar{x}_0 - 1} V d\bar{x}_0} \tag{F.50}$$

Theodorsen function is very important quantity as it involves the effect of the wake in the aerodynamic loads for both lift and moment.

APPENDIX G

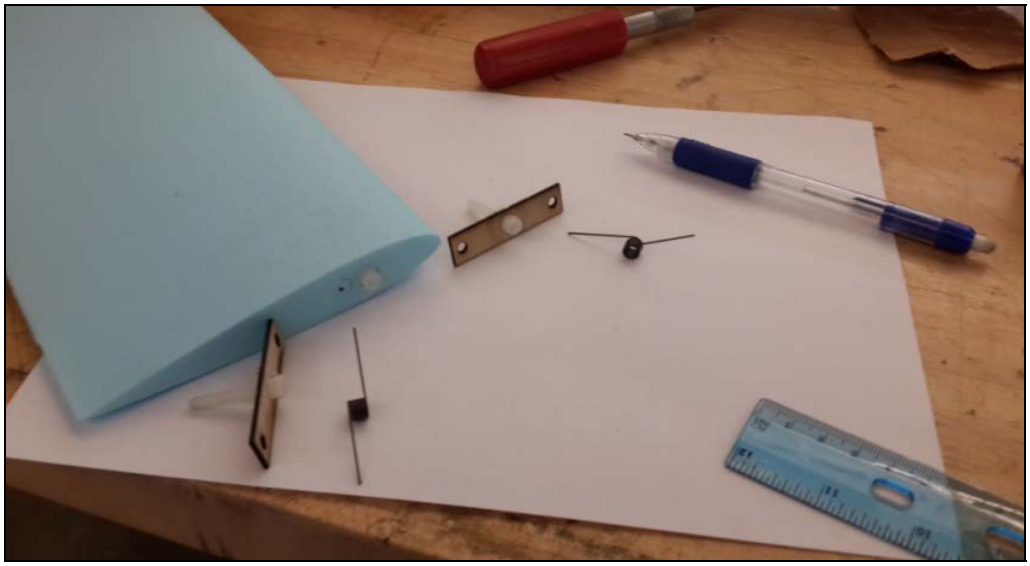

Figure G.1 Building the Blue wing model

Figure G.2 Building the other wing models

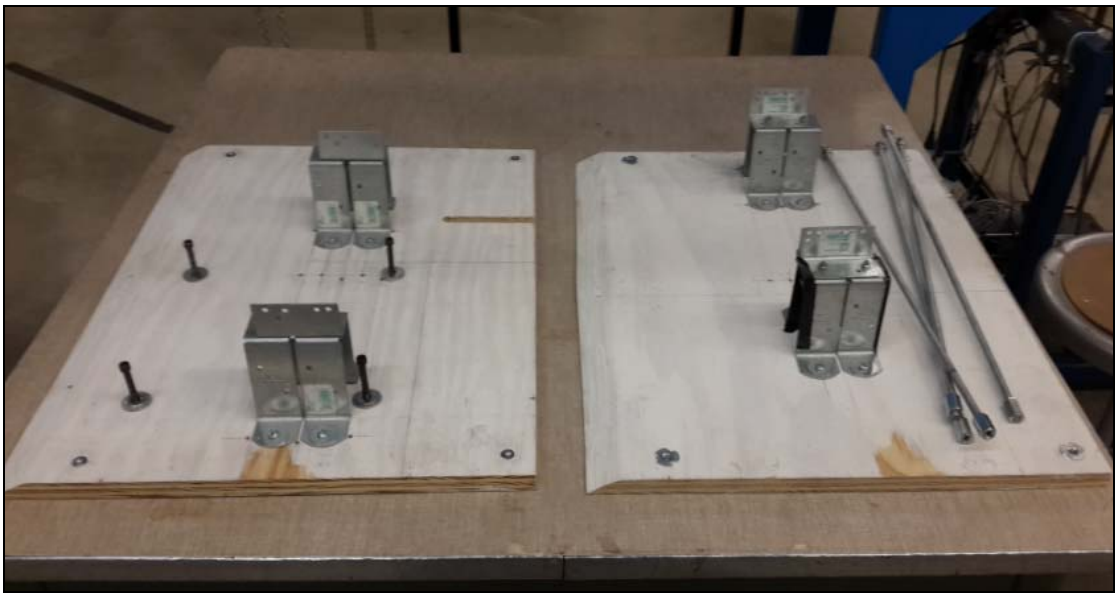

Figure G.3 Building the other fixture

Figure G.4 Wings ready for testing

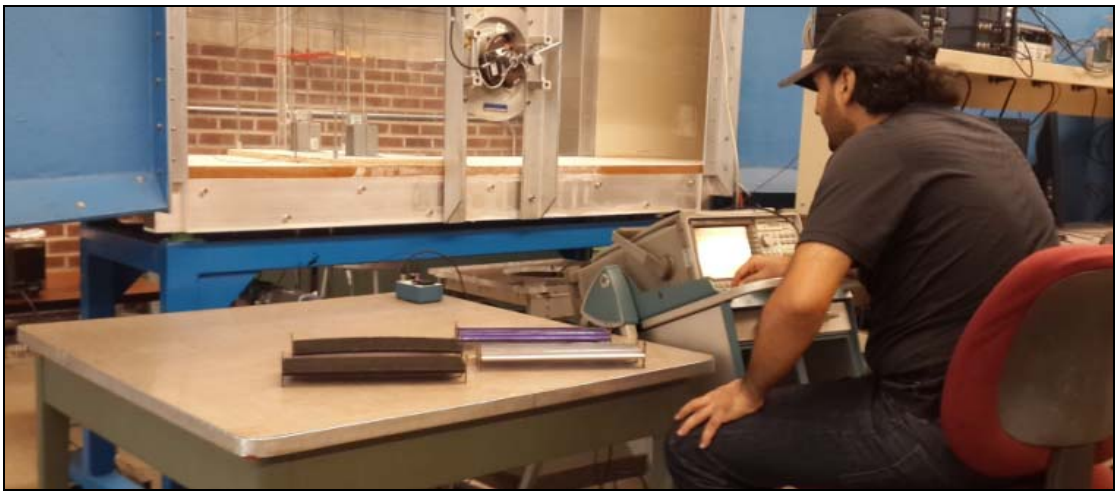

Figure G.5 Setting the signal analyzer to proper settings

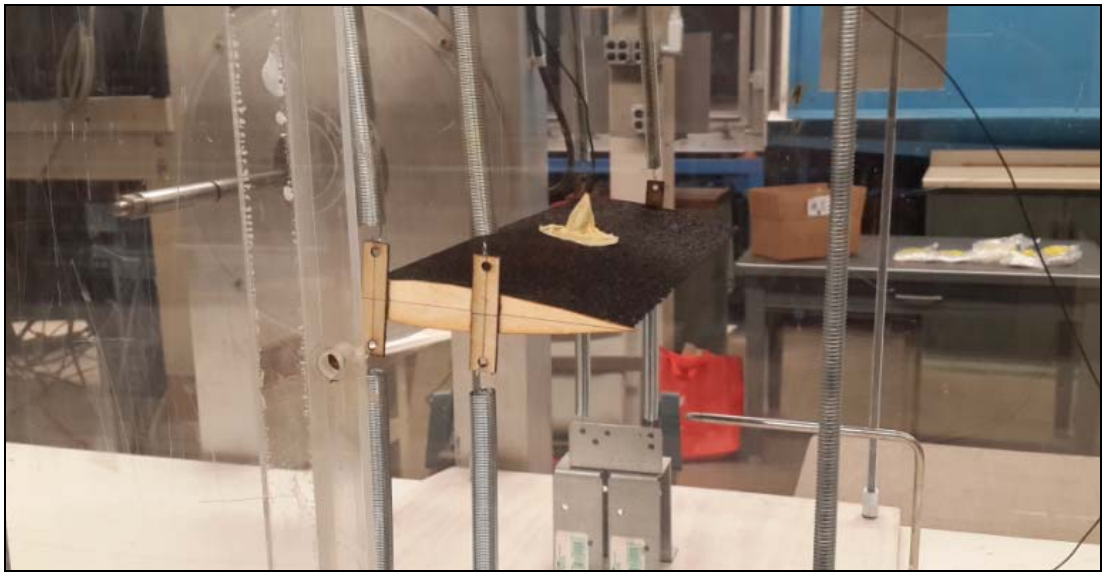

Figure G.6 Attaching the accelerometer sensor on the wing surface

Figure G.7 Taking measurements